

Resonance fluorescence and superfluorescence of intersubband transitions

Nathan Shammah

Supervisor: Dr Simone De Liberato

School of Physics and Astronomy
Faculty of Physical Sciences and Engineering
University of Southampton

This dissertation is submitted for the degree of
Doctor of Philosophy

July 2016

Declaration

I, Nathan Shammah, declare that the thesis entitled ‘Resonance fluorescence and superfluorescence of intersubband transitions’ and the work presented in it are both my own, and have been generated by me as the result of my own original research. I confirm that:

- this work was done wholly or mainly while in candidature for a research degree at this University;
- where any part of this thesis has previously been submitted for a degree or any other qualification at this University or any other institution, this has been clearly stated;
- where I have consulted the published work of others, this is always clearly attributed;
- where I have quoted from the work of others, the source is always given. With the exception of such quotations, this thesis is entirely my own work;
- I have acknowledged all main sources of help;
- where the thesis is based on work done by myself jointly with others, I have made clear exactly what was done by others and what I have contributed myself;
- Part of the results presented in this work have been published previously in Phys. Rev. B **89**, 235309 (2014), J. Phys. Conf. Ser. **619**, 012021 (2015), and Phys. Rev. B **92**, 201402(R) (2015).

Signed:

Nathan Shammah
July 2016

Abstract

UNIVERSITY OF SOUTHAMPTON

School of Physics and Astronomy, Faculty of Physical Sciences and Engineering

Doctor of Philosophy

RESONANCE FLUORESCENCE AND SUPERFLUORESCENCE OF
INTERSUBBAND TRANSITIONS

by Nathan Shammah

Intersubband transitions are unbound electronic transitions of doped quantum wells, semiconductors heterostructures with a planar symmetry. I theoretically studied the fluorescence of a strongly pumped intersubband transition, finding that the many-electron nature of such a system leads to a modification of the usual Mollow triplet. In particular, the intensity of the central peak in the fluorescence spectrum becomes a function of the electron coherence, allowing access to the coherence time of a quasi-two-dimensional electron gas through a fluorescence intensity measurement. Moreover, while transitions between the two states of the ac Stark-split doublet are forbidden in centrosymmetric systems, and thus almost impossible to observe in experiments performed with atoms they become allowed in asymmetric quantum wells, in which the wavefunction symmetry can be broken. I developed a many-body theory describing also this intradoublet emission, showing that by using doped asymmetry, the emission can be orders of magnitude higher than in previously studied systems. This opens the way to the realization of monolithic and tunable terahertz emitters since the Rabi frequency at which this emission occurs lies in the terahertz range and can be tuned by the pump power. Finally, I have investigated if superfluorescence can occur in intersubband transitions. In order to do so I used a general quantum master equation that includes dephasing and nonradiative emission to model the many-body system in solid state. Performing a second-order approximation allowed to obtain a closed system of equations that were studied analytically and numerically, verifying that in the regimes characteristic of intersubband transitions cooperative effects leading to powerful bursts of light could be observed experimentally.

Acknowledgements

I would like to thank my supervisor Simone De Liberato. He has been much more than a supervisor, I would dare to say a mentor. He has always encouraged every single proposal I have ever made to him, replying with enthusiasm. Learning physics from him is the best intellectual experience I have ever had.

From the department, I would like to thank especially Alexey Kavokin, Pavlos Lagoudakis, Alberto Politi, and Luca Sapienza. Thanks to Chris Phillips, Marco Genoni and Matteo Paris. I would like to thank for hospitality Franco Nori, Emanuele Dalla Torre, Alex Retzker, and Liron Gantz.

Many friends I have to thank that I will now forget. Really, thank you all, but in particular thanks to Giulia, Victor, Chiara, Simon and all of the other many friends made in Southampton. In the Quantum Light and Matter group I found a brother, Pasquale Cilibrizzi. I leave a full team at the Quantum Theory and Technology group: Erika Cortese, Chris Gubbin, Luigi Garziano, thanks to them all and also to all of the past members. Thanks to all of the players of the 'Light Club', including Alexis and Francesco. Thanks to Silvia for making Pint of Science happen. Thanks to the friends of the physics class in Milan, and in particular to Gabriele, Guido, Marta, Mattia, Simone and Pietro. In Milan, thanks to Davide, Vittorio and all of the usual suspects.

Thank you, Emanuel, really. Thanks to my cousins, Alessandra (x2), Alfonso, Giampiero, Fabio, Raffaele, Tancredi. Thank you Lina for all. I would like to thank my mother and my father for always supporting me—far away and yet so close. Thank you Diana and sorry for all this time apart.

I would like to dedicate this thesis to my grandfather.

Table of contents

1	Introduction	1
2	Basic concepts	7
2.1	Quantum two-level systems	7
2.1.1	Spontaneous emission	8
2.1.2	Purcell effect	11
2.1.3	ac Stark effect	11
2.1.4	Resonance fluorescence	13
2.1.4.1	Literature	15
2.1.5	Cooperative light emission	18
2.1.5.1	Collective coupling to light	19
2.1.5.2	Dicke states	20
2.1.5.3	Superradiant emission	21
2.1.5.4	State preparation	24
2.1.5.5	Superradiant master equation	25
2.1.5.6	Literature	28
2.2	Intersubband transitions of quantum wells	30
2.2.1	Line broadening	34
2.2.2	Terahertz technology	36
3	Intersubband resonance fluorescence	39
3.1	Introduction	39
3.2	Main theory	40
3.2.1	Driven Hamiltonian	40
3.2.2	State of the driven system	43
3.3	Visibility of Rabi oscillations	45
3.4	Experimental constraints	47
3.5	Conclusions	49

4 Terahertz light emission from the intersubband transitions of asymmetric systems	51
4.1 Introduction	51
4.2 Main theory	54
4.2.1 The light-matter coupling Hamiltonian	56
4.3 Emission rates	57
4.3.1 Numerical results	60
4.3.2 Free-space emission rate	61
4.3.3 Cavity emission rate	62
4.4 Conclusions	64
5 Cooperative light emission in presence of dephasing and nonradiative decay	65
5.1 Introduction	65
5.2 Main theory	68
5.2.1 Emission rates	69
5.2.2 Closed system dynamics	72
5.3 Numerical study of superfluorescence	74
5.4 Intersubband superfluorescence	76
5.5 Conclusions	79
6 Conclusions	81
Appendix A Second quantization for intersubband transitions	83
A.1 Intersubband commutation relations	83
A.2 Intersubband light-matter coupling	84
Appendix B Intersubband resonance fluorescence	87
B.1 Visibility of the collective Rabi oscillations	87
B.2 Photon emission rate	88
Appendix C Light-matter coupling in asymmetric systems	91
C.1 Polarizability in atomic systems	91
C.1.1 The static Stark effect	91
C.1.1.1 TLS approximation	92
C.1.1.2 General dipole term	93
C.1.1.3 Asymmetric dipole and magic wavelengths	94
C.1.1.4 Static and ac Stark shift: A comparison	95

C.2 Asymmetric artificial atom in a quantum well	96
C.2.1 General eigenstates	96
C.2.2 Numerical model of asymmetric quantum well	98
Appendix D N two-level systems: Further properties and dynamics	101
D.1 Dicke states and collective spin operators	101
D.1.1 Collective spin operators' algebra	101
D.1.2 Degeneracy of Dicke states	102
D.2 Cooperative dynamics	104
D.2.1 General superradiant master equation	104
D.2.1.1 Semiclassical limit	105
D.2.2 Collective dephasing term	106
D.2.3 Maxwell-Bloch Equations	107
D.2.4 Characteristic function	108
References	111

Chapter 1

Introduction

Resonance fluorescence and superfluorescence are two fundamental phenomena of quantum optics that historically have been described in terms of two-level systems. In this thesis we will explore what happens when the physical system in which they occur is a different one, given by the intersubband transitions of a semiconductor quantum well. This choice allows to study the interaction with light of a fundamental physical system, the quasi-two-dimensional electron gas, in a powerful experimental platform, as a semiconductor heterostructure can be fabricated with precise characteristics and can find various solid-state applications.

In the standard theory of resonance fluorescence, an electronic two-level system is strongly driven by a classical electromagnetic field, such as that of a laser. The two-level system can be pictured performing Rabi oscillations between the ground state and the excited state at a frequency controlled by the strength of the field. Just like an excited two-level system can emit a photon by spontaneous emission, also in this dynamical setting light can be re-emitted incoherently due to the coupling with the free photonic field. This incoherent fluorescence spectrum not only has a peak centred at resonance, as one would expect in a classical theory of light scattering, but displays two additional symmetrically-displaced peaks. The distinctive fluorescence profile, predicted by B. R. Mollow in 1969 [1] and now known as the Mollow triplet, is a hallmark of quantum optics theory, as it has since been detected in very different physical implementations—atoms, molecules, superconducting circuits, semiconductor nanostructures—that can all be described as a two-level system driven at resonance. Moreover, since the satellite peaks occur at frequencies displaced from the resonance frequency by an amount proportional to the Rabi frequency, the Mollow triplet can be “squeezed” or “stretched” by tuning the power of the pumping laser.

Superfluorescence is possibly an even more puzzling quantum phenomenon. Consider now *two* excited two-level systems. We assume that the two two-level systems cannot interact between them, and they can couple only to the electromagnetic field. At first sight, one would expect, even in the quantum picture, that the ensemble eventually ends up in its ground state, by spontaneous emission according to the characteristic time of the two-level system. Yet as R. H. Dicke showed in a simple *gedankenexperiment* in 1954 [2], if the two two-level systems are contained in a portion of space smaller than the wavelength of the electromagnetic field, the rate of photon emission is doubled. He observed that the mechanism becomes particularly significant if the number of two-level systems grows, as the ensemble thus releases its energy cooperatively much more rapidly—*superradiantly*—with the intensity of light emission proportional not to N but $\propto N^2$. Moreover, the pulse of the emitted light is a coherent light pulse. These features are quite striking, as there is no driving field or cavity—such as for a laser—that can actively lock in coherence in the system nor initially the system is found in a superposition state, whose imprint could be converted in the coherence of the emitted light. What happens instead is that, although initially no superposition is present in the system, as soon as a single photon is emitted the full system is cast into a maximally entangled superposition state, as there is no way to know which single emitter flipped—a beautiful example of the emergence of coherence from incoherence.

A rather different story, one could say, is that of intersubband transitions, a particular kind of optical excitations occurring in doped semiconductor quantum wells. A quantum well is a nanometric heterostructure in which thin layers of different semiconductors are used to precisely design an electronic potential to effectively trap electrons in two dimensions. Its strong, but finite, quantum confinement resolves the discrete nature of the electronic momentum, introducing a finer energy splitting of the valence and conduction bands. If dopants are included in the fabrication process, such as Silicon impurities for GaAs, it is possible to further change the optoelectronic properties of the heterostructure. The effect of doping is that of releasing free electronic carriers, raising the Fermi energy of the material above the valence-conduction bandgap. The quasi-two-dimensional electron gas is then trapped in the discrete levels in which the conduction band has been split due to confinement. These discrete energy levels are known as subbands, and by populating the lower one(s) with the electron gas, *intersubband* transitions between different conduction subband levels can be engineered. An optical excitation then does not create electron-hole *bound* pairs (excitons), but rather *unbound* intersubband transitions. Moreover, as conduction subbands are quasi-parallel, many electrons (of the order of 10^{12} per cm^2) can be excited around a

single resonance frequency, with a very small width in the photon absorption peak. Recently the possibility of embedding quantum wells in photonic microcavities has allowed to explore new regimes of cavity quantum electrodynamics (cQED) in which the light-matter interaction becomes strong, an example of the versatility of this physical system to explore the fundamental properties of the interaction of light with matter. It is important to point out that while in this thesis the light-matter coupling between intersubband transitions and the photonic vacuum is always in the weak regime, interesting new effects arise. While the coherent properties of driven intersubband transitions can be explained in terms of the interaction with light of an ensemble of two-level systems, the quasi-two-dimensional electron gas trapped in a doped quantum well is a much more complex system, from both a fundamental and a practical point of view. Indeed the fact that intersubband transitions are unbound means that upon light emission, electrons can be scattered in diagonal transitions that make the system “messier” than a collection of two-level systems (such as a collection of atoms), in which one rightly assumes that some kind of quantum confinement prevents electron exchange between different sites. This condition can be relaxed, or controlled, for intersubband transitions, as it will be shown. Moreover for intersubband transitions dephasing times are extremely short, typically hundreds of femtoseconds, because nonradiative scattering channels can be particularly important. We will thus need to account for this dephasing constraint in our study of the light-emission mechanisms.

A drive for the investigations that have been performed in this thesis has been how to exploit the peculiar properties of intersubband transitions with reference to light-emission processes for applications. Indeed this physical system has very interesting technological properties: Quantum wells can be used in portable solid-state optoelectronic devices, and they emit light at infrared and terahertz frequencies. Finding new sources of terahertz emission is a very active field of research, which merges the photonics and the electronics community. Terahertz applications span from contactless and non-ionizing radiation diagnostics to airport security to ultrafast short-range data transfer beyond tera-bit per second rates. As it will be shown, we have proposed new schemes to obtain tunable terahertz light emission channels. The structure of the thesis is as follows.

In Chapter 2 an overview of light-matter interactions, further described in the subsequent Chapters, is given with reference to two-level systems. Specific attention is devoted to cooperative phenomena, as we find that a comprehensive description is not found from a single source in the literature. Then the optoelectronic properties

of semiconductor quantum wells will be introduced, together with their potential for terahertz application, as well as their limitations.

In Chapter 3 we will describe the theory of resonance fluorescence of intersubband transitions, showing how the assumption that each oscillating electron is an independent dipole, as for a collection of two-level systems, can break down. Diagonal transitions between different electronic states are possible, affecting the final state of two electrons, as the relative state of the two electronic dipoles determines the strength of the transition. This affects the intensity of the central peak of the Mollow triplet and can be exploited for a novel measure of the coherence of the collective Rabi oscillations of the quasi-two-dimensional electron gas simply from a time integrated fluorescence measure.

In Chapter 4 we will show how asymmetric quantum wells can be used to open up a new tunable light emission channel. When an asymmetric potential confines the quasi-two-dimensional electron gas, the electronic wavefunctions do not have a well-defined inversion symmetry. For this reason otherwise dipole-forbidden transitions become allowed. We will show how such a mechanism can be engineered when the intersubband transitions are driven at resonance, exploiting the tunability given by the Mollow triplet's satellite peaks. The driven dynamics and the rates of photon emission for the new peak are estimated upon calculating second quantization matrix elements. A numerical study in the parameter space of a quantum well design is used to optimize light emission at terahertz frequencies. The quantum efficiency of a realistic device based on this mechanism is calculated.

In Chapter 5 we assess the physics of cooperative light emission from a collection of N two-level systems embedded in the solid state, in presence of strong dephasing and nonradiative decay. Since in the solid state incoherent mechanisms can be extremely fast, we include the description of dephasing and nonradiative decay mechanisms in a superradiant master equation treatment by adding two different sets of Lindbladian terms. We find a closed set of equations beyond the semiclassical approximation to study the dynamical properties of the system, exploring the parameter space for $N \gg 1$ and for a wider range of dephasing and scattering rates. We show that this general treatment, which applies to the interband and intersublevel transitions of a collection of quantum dots, can describe, within some limits, also the superfluorescence of intersubband transitions in a doped quantum well. Numerical simulations show that characteristic times typical of intersubband transitions meet the critical parameters for the onset of superfluorescence.

Finally, in Chapter 6 the general conclusions of this research project are given and perspectives delineated. The interested reader can find detailed calculations as well as additional information in the Appendices that accompany the next four Chapters.

Chapter 2

Basic concepts

In the first Section of this Chapter, some basic concepts on the interaction of quantum two-level systems with light are given. Since for both resonance fluorescence and superfluorescence the coupling of the two-level systems to the free electromagnetic field is the key element, this is introduced in its basic formulation, the spontaneous emission of a single two-level system. Then the characteristics of a strongly driven two-level system will be used to illustrate resonance fluorescence. Following this, the cooperative light emission from an ensemble of identical two-level systems will be discussed. In the second Section of this chapter, the fundamental characteristics of a semiconductor quantum well will be given and the Hamiltonian of light-matter coupling for intersubband and intrasubband transitions introduced. Some considerations on experimental limitations and technological applications to terahertz science are given.

2.1 Quantum two-level systems

The two-level system (TLS) represents the simplest model of an atom that one can imagine: It can accommodate one and only one electron, either in the lower state or in the upper state. And yet the interaction with light of this simple system has been used to describe almost all of the striking quantum effects that characterize light-matter coupling—spontaneous emission, anti-bunching—leading to the birth of the fruitful field of quantum optics (see the Introduction to Ref. [3] for a brief historical perspective.) Moreover since the paradigmatic building block of quantum information theory, the qubit, can be exactly encoded onto a TLS, the control of the light-matter interaction of a TLS in a cavity is considered an important requirement for the full development of hybrid quantum technologies [4].

From a mathematical point of view, a TLS belongs to a Hilbert space of dimension two, and it is equivalent to a spin- $\frac{1}{2}$ particle. For this reason much of the early physics describing the interaction of light with a TLS inherited concepts from the earlier study of a spin in a magnetic field, such as the Bloch's sphere formalism, Rabi oscillations and Pauli's matrices.

One of the most interesting characteristics of a TLS is that it possesses an intrinsic quantum nonlinearity, due to the fact that it saturates after only one excitation, differently from the quantum harmonic oscillator. Imagine an experiment in which the system under study is unknown, and one can investigate it only by sending n photons into a black box. Only for $n > N$ one can discern if the unknown system is a collection of N TLSs or a quantum harmonic oscillator, because the former becomes transparent while the latter can in theory indefinitely absorb excitations. At low excitation numbers, $n \ll N$, thus the physics of TLSs can be described in terms of bosonic operators. In such diluted regime, also intersubband transitions can be studied in terms of bosonic operators [5]. In this thesis we will explore regimes in which this condition is not always fulfilled and the nonlinearity is relevant.

2.1.1 Spontaneous emission

In order to describe spontaneous light emission from a TLS, let us describe the Hamiltonian of the TLS, that of the free photonic field and then that of the relative light matter interaction. A TLS can be only in the state $|1\rangle$ or $|2\rangle$ and its Hilbert space is of dimension 2, $\mathcal{H}_{\text{TLS}} = \{|1\rangle, |2\rangle\}$. Its non-interacting Hamiltonian can be written as

$$H_{\text{TLS}} = \frac{\hbar\omega_0}{2}\sigma_z, \quad (2.1)$$

where $\sigma_z = |2\rangle\langle 2| - |1\rangle\langle 1|$ is one of the three unitary and traceless Pauli matrices, whose algebra is defined by $[\sigma_\alpha, \sigma_\beta] = 2i\epsilon_{\alpha\beta\gamma}\sigma_\gamma$, with $\alpha, \beta, \gamma = \{x, y, z\}$. The energy gap is $\hbar\omega_0$, with \hbar Planck's constant and ω_0 the bare frequency of the system.

With regard to the photonic degrees of freedom, the Hamiltonian of the free photonic field is

$$H_{\text{phot}} = \hbar \sum_{\mathbf{q}, q_z} \omega_{\mathbf{q}, q_z} a_{\mathbf{q}, q_z}^\dagger a_{\mathbf{q}, q_z} \quad (2.2)$$

where $[a_{\mathbf{q}, q_z}, a_{\mathbf{q}', q'_z}^\dagger] = \delta(\mathbf{q} - \mathbf{q}')\delta_{q_z, q'_z}$ and the photonic wavevector is $\mathbf{q}_{\text{tot}} = (\mathbf{q}, q_z)^T$, already divided into its in-plane component \mathbf{q} and out-of-plane component q_z as this distinction will prove useful with regard to intersubband transitions, and is made here

only for homogeneity of notation. The frequency of each mode is

$$\omega_{q,q_z} = c \sqrt{\frac{\mathbf{q}^2 + q_z^2}{\epsilon_r}} \quad (2.3)$$

where c is the speed of light in vacuum and ϵ_r the relative permittivity of the homogenous medium in which light propagates. H_{phot} of Eq. (2.2) belongs to an infinite-dimension Hilbert space and its eigenstates are Fock states $|n_{\text{phot}}(\mathbf{q}, q_z)\rangle$, where $n_{\text{phot}}(\mathbf{q}, q_z)$ gives the number of photons of the mode $(\mathbf{q}, q_z)^T$. In the dipole approximation, the TLS interacts with the electric field associated to the free photonic field according to

$$H_{\text{int}} = \hbar \sum_{\mathbf{q}, q_z} \Omega_{0,q,q_z} (a_{\mathbf{q}, q_z} + a_{\mathbf{q}, q_z}^\dagger) (\sigma^+ + \sigma^-) \quad (2.4)$$

where σ^\pm are Pauli's ladder operators, $\sigma^+ = |2\rangle\langle 1|$, $\sigma^- = (\sigma^+)^\dagger$ and we have introduced the modal vacuum Rabi frequency Ω_{0,q,q_z} . If Eq. (2.4) can be considered as a perturbation of Eq. (2.1), that is if $\frac{\Omega_{0,q,q_z}}{\omega_0} \ll 1$ for any \mathbf{q}, q_z , the rate of photon emission can be calculated with Fermi's Golden Rule, that is to first order in perturbation. Since first order approximations will be applied extensively to different Hamiltonians to estimate photon rates in the following Chapters, it is instructive to derive Fermi's Golden Rule in a general way. Consider

$$H = H_0 + V, \quad (2.5)$$

where H_0 is an Hamiltonian whose eigenstates and eigenenergies are known. V is a light-matter interaction Hamiltonian inducing only a small displacement on the eigenenergies and eigenstates of the bare Hamiltonian H_0 . For this reason it can be treated as a perturbation, and up to first order it affects the time evolution of a generic state $|\psi\rangle$ according to

$$|\psi_I(t)\rangle \simeq |\psi\rangle - \frac{i}{\hbar} \int_{t_0}^t dt' V_I(t') |\psi\rangle, \quad (2.6)$$

where we used the interaction picture formalism, that is $|\psi_I(t)\rangle = e^{iH_0 t/\hbar} |\psi(t)\rangle$ for the Schrödinger state and

$$A_I(t) = e^{iH_0 t/\hbar} A_S e^{-iH_0 t/\hbar} \quad (2.7)$$

for and operator A_S in the Schrödinger picture. t_0 is the time at which the interaction is turned on, or generally a distant moment in the past. The probability of transition $p(t)$ of a system that is initially in the state $|i\rangle$ into a final state $|f\rangle$ is given by the square

of the braket between the two states. The rate of transition is the time derivative of the probability of transition that can be written, using Eq. (2.6) and Eq. (2.7), as

$$\gamma = \frac{d}{dt} p(t) = \frac{d}{dt} \sum_f |\langle f_I | i_I(t) \rangle|^2 = \frac{1}{\hbar^2} \frac{d}{dt} \sum_f \left| \int_{t_0}^t dt' \langle f | V_I(t') | i \rangle \right|^2 \quad (2.8)$$

$$= \frac{1}{\hbar^2} \sum_f |V_{fi}|^2 \frac{d}{dt} \left| \int_{t_0}^t dt' e^{i(\omega_f - \omega_i)t} \right|^2 = \frac{2\pi}{\hbar^2} \sum_f |V_{fi}|^2 \delta(\omega_f - \omega_i) \quad (2.9)$$

where $V_{fi} = \langle f | V | i \rangle$ is the matrix element of the interaction Hamiltonian V . Note that in Eq. (2.8) it has been assumed that the initial and final states are orthogonal to each other and in the l.h.s. of Eq. (2.9) it was assumed that they were two eigenstates of energies $\hbar\omega_i$ and $\hbar\omega_f$, respectively. Finally, in Eq. (2.9) the time integration is performed taking the limits to infinity, leading to Dirac's delta.

In the specific case of spontaneous emission of a TLS in free space,

$$H_{\text{free}} = H_{\text{phot}} + H_{\text{TLS}}, \quad (2.10)$$

we can identify $H = H_0 + V$ of Eq. (3.1) with $H_0 = H_{\text{free}}$ and $V = H_{\text{int}}$ and use as initial state $|i\rangle = |2\rangle |0_{\text{phot}}\rangle$, which represents an excited TLS and no photon. The sum over the final states in Eq. (2.9) can be performed explicitly as

$$\sum_f = \sum_{\mathbf{q}, q_z} \rightarrow \frac{\mathcal{V}}{(2\pi)^3} \frac{\epsilon_0 \epsilon_r}{c^2} \int_0^\infty \omega_{q,q_z}^2 d\omega_{q,q_z} \int_0^\pi \sin \theta \int_0^{2\pi} d\varphi \quad (2.11)$$

where ϵ_0 is the vacuum permittivity and we used Eq. (2.3) to convert the discrete sum over the wavevectors into one over frequency, taking the continuous limit of an integral. \mathcal{V} is the quantization volume and the integral in space is performed over the solid angle with standard polar coordinates θ and φ . Since the energy difference between the initial and final state is $\omega_f - \omega_i = \omega_0 - \omega_{q,q_z}$, using the explicit formula for the modal Rabi frequency $\Omega_{0,q,q_z} = d_{12} (\hbar\omega_{q,q_z}/2\epsilon_0\epsilon_r\mathcal{V})^{1/2}$, determined from the quantization of the electromagnetic field in a portion of space of volume \mathcal{V} [3], the rate of spontaneous photon emission in free space for a TLS is

$$\gamma_0 = \frac{\sqrt{\epsilon_r} d_{12}^2}{3\pi\epsilon_0\hbar c^3} \omega_0^3, \quad (2.12)$$

where $\mathbf{d}_{12} = \langle 1 | \mathbf{d} | 2 \rangle$ is the dipole matrix element associated to the TLS, which is for generality assumed to be inserted in a uniform medium of relative dielectric permittivity ϵ_r .

2.1.2 Purcell effect

It was first noted in 1946 by Purcell in Ref. [6] while studying radio waves, that if an electromagnetic emitter is placed in a resonant cavity modifying the boundary conditions of the free electromagnetic field, the decay rate of the excited emitter can be altered. For a TLS contained in a planar cavity of length L_{cav} , assuming a very sharp resonance of the cavity, the modal density can be well approximated by a delta function centered at ω_0 , the sum over final states of Eq. (2.11) becomes

$$\sum_f = \sum_{\mathbf{q}, q_z} \rightarrow \frac{S}{(2\pi)^2} \frac{\sqrt{\epsilon_0 \epsilon_r}}{c} \int_0^\infty \omega_{q, q_z} d\omega_{q, q_z} \int_0^\pi \sin \theta d\theta \int_0^{2\pi} d\varphi, \quad (2.13)$$

where the quantizing volume is $\mathcal{V} = SL_{\text{cav}}$. The rate of spontaneous emission in such resonant cavity is then given by

$$\gamma_{\text{cav}} = \frac{d_{12}^2}{4L_{\text{cav}}\epsilon_0\hbar c^2} \omega_0^2 \quad (2.14)$$

with now a quadratic—instead of cubic—dependence on the resonance frequency due to the modification of the photonic environment introduced by the boundary conditions of the cavity. The ratio between the free-space and cavity emission rate is quantified by the Purcell factor, $F_P = \gamma_{\text{cav}}/\gamma_0$, as

$$F_P = \frac{3\pi c}{4\omega_0\sqrt{\epsilon_r}L_{\text{cav}}} = \frac{3}{2} \frac{(\lambda_0/2)}{L_{\text{cav}}}, \quad (2.15)$$

which shows that a sub-wavelength cavity is required to accelerate the spontaneous emission process, and already for $L_{\text{cav}} = \lambda_0/2$, where λ_0 is the resonance wavelength in the material, the rate can be enhanced by a factor $\frac{3}{2}$. The use of cavities with extremely high quality factors Q to enhance the coupling to the vacuum of the photonic field has been pioneered with atoms and trapped ions and the use of subwavelength microcavities is currently undertaken in many artificial atoms in solid state, as quantum wells and quantum dots. The smaller volume effectively “squeezes” the vacuum photonic field, enhancing the light-matter coupling.

2.1.3 ac Stark effect

Let us now consider the experimental condition in which a TLS is driven at resonance by an external optical pump. We assume that the optical pump is a laser of frequency $\omega_L \simeq \omega_0$ and electric field's amplitude maximum value is \mathcal{E} . The Hamiltonian can be

written as

$$H_{\text{pump}} = \hbar\Omega(e^{-i\omega_L t}\sigma^+ + e^{i\omega_L t}\sigma^-), \quad (2.16)$$

where

$$\Omega = \mathbf{\mathcal{E}} \cdot \mathbf{d}_{12}/\hbar \quad (2.17)$$

is the pump-induced Rabi frequency (not to be confused with the vacuum Rabi frequency Ω_0), which can be controlled by the pump's power, $P = \mathcal{I}\pi w^2 = \frac{1}{2}\epsilon_0\epsilon_r\mathbf{\mathcal{E}}^2$, where w is the laser waist and \mathcal{I} the field's intensity in the medium of propagation. The interaction of Eq. (2.16) is in the rotating wave approximation (RWA), which drops terms counter-rotating at frequencies of the order of the bare frequency. This is a good approximation as long as $\frac{\Omega}{\omega_0} \ll 1$ and $\omega_L \simeq \omega_0$, which is the case for the physical conditions treated here and in most of the literature, as we will show in Subsection 2.1.4.1. Both choices simplify the treatment of the problem while retaining the fundamental physics. Regarding the approximation to a classical field, there are different motivations that can be given. Firstly, a quantitative one. In an intense laser beam it is hardly possible to distill the effect of adding or subtracting a single photon. To grasp the quantities at play, a laser beam of power $P = 0.01$ W and $\hbar\omega_L = 125$ meV is a source of more than 10^{18} photons per second. Secondly, another way of looking at this approximation is through the very formalism of quantum coherence, developed by R. J. Glauber [7] in terms of single-mode coherent states, $|\alpha\rangle$. By definition

$$a|\alpha\rangle = \alpha|\alpha\rangle, \quad (2.18)$$

where α is a *c*-number such that $|\alpha|^2 = \bar{n}_{\text{phot}}$ gives the average number of photons of the single-mode field defined by the standard bosonic commutation relations $[a, a^\dagger] = 1$. In Eq. (2.18) the considered mode is the pump mode, which elsewhere in the thesis is indicated with $(\bar{\mathbf{q}}, \bar{q}_z)^T$. So what Eq. (2.18) shows is that the coherent state is robust against photon subtraction, as $|\alpha\rangle$ remains the eigenstate of the pump mode even if single photons are absorbed from the beam.

Taking H_{free} from Eq. (2.10) we obtain the Hamiltonian $H_0 = H_{\text{free}} + H_{\text{pump}}$, which depends on time. It is possible to eliminate the time dependency by choosing a frame rotating with respect to H_{free} ,

$$H'_0 = e^{iH_{\text{free}}t/\hbar}H_0e^{-iH_{\text{free}}t/\hbar} = \frac{\hbar\Omega}{2}(\sigma^+ + \sigma^-), \quad (2.19)$$

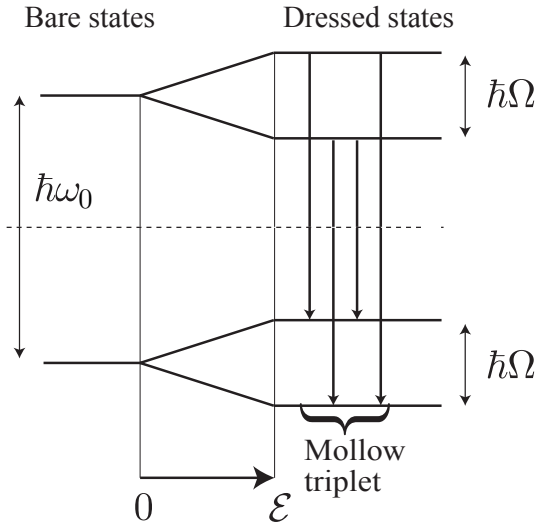


Fig. 2.1 At strong pump intensities, the ac Stark effect splits the bare energies into that of dressed states, with a Rabi splitting $\hbar\Omega$ linear with the pump amplitude \mathcal{E} . The dipole-allowed transitions that can occur between two doublets give rise to the Mollow triplet in the resonance fluorescence spectrum, since two transitions occur at a frequency ω_0 and the other two at the satellite frequencies $\omega_0 \pm \Omega$. Already in this simple picture the ratio of the three peaks is 1:2:1.

whose eigenstates (always in the rotating frame) are

$$|\pm\rangle = \frac{1}{\sqrt{2}}(|2\rangle \pm |1\rangle), \quad (2.20)$$

with eigenenergies $\pm \frac{\hbar\Omega}{2}$, respectively. The effect on the TLS of the strong resonant and coherent pump is that of inducing a split proportional to Ω of the eigenenergies. This is known as the dynamical or ac (alternated current) Stark effect for it is an extension of the static Stark effect [8]. In terms of the undressed basis in the non-rotating frame, the electron can be pictured as oscillating between the states $|1\rangle$ and $|2\rangle$ at the Rabi frequency Ω . As it will be shown in the next section, the possibility of transitions among the dressed eigenstates of Eq. (2.20) gives rise to the characteristic Mollow triplet profile in the resonance fluorescence of the TLS.

2.1.4 Resonance fluorescence

The resonance fluorescence spectrum corresponds to the light scattered by a system that is driven at resonance. Under strong driving, the resolution of a three-peaked profile was derived by Mollow by calculating the full spectrum and the second-order

correlation functions giving the photon statistics using the quantum regression theorem [1, 9, 10]. This method allows to calculate two-time averages of operators using the same dynamical equations of the time evolution of the TLS density matrix. The emission mechanism can be pictured either with a fully quantum Hamiltonian, in which the light field is described in terms of bosonic operators, or with the semiclassical Hamiltonian of Eq. (2.16). In the fully quantum picture, also the Fock state of the photonic field is considered, and the eigenstates equivalent to Eq. (2.20) are then superpositions of the product states of the coupled light-matter system, in which the lower and upper TLS states are coupled to Fock photon states [11].

At resonance the driven system couples the spectrum of free photonic field to that of the TLS, and each energy level of the quantum harmonic oscillator is then split in a Rabi doublet whose splitting at high excitation numbers can be well approximated by $\hbar\Omega$. Of the four possible spontaneous emission channels between two Rabi doublets, two are resonant with the bare frequency of the TLS, ω_0 , and the other two are at frequency $\omega_0 \pm \Omega$ (see Figure 2.1 for a scheme of the emission channels and frequencies.)

The three peaks of the spectrum, which can be derived with this and other refined theoretical approaches [1, 11–14], can also be estimated simply using H_{pump} , Eq. (2.16), which leads to the transitions depicted in Figure 2.2 (a). In the frame rotating according to H_{free} of Eq. (2.10), the interaction with the photonic vacuum of Eq. (2.4) has the expression, in the RWA,

$$V'(t) = \sum_{\mathbf{q}, q_z} \Omega_{0,q,q_z} (e^{i(\omega_{q,q_z} - \omega_0)t} a_{\mathbf{q},q_z}^\dagger \sigma^+ + e^{-i(\omega_{q,q_z} - \omega_0)t} a_{\mathbf{q},q_z} \sigma^-) \quad (2.21)$$

where $\Omega_{0,q,q_z} = \mathcal{E}_0(q, q_z) d_{12}$, $\mathcal{E}_0(q, q_z) = \sqrt{\hbar\omega_{q,q_z}/(2\epsilon_0\epsilon_r\mathcal{V})}$.

To calculate the value of the number of photons incoherently emitted in the scattered field,

$$N_{\text{phot}} = \sum_{\mathbf{q}, q_z} a_{\mathbf{q},q_z}^\dagger a_{\mathbf{q},q_z}, \quad (2.22)$$

we use the perturbative expansion to first order of $|\psi\rangle$, Eq. (2.6),

$$\begin{aligned} \langle N_{\text{phot}}(t) \rangle &= \langle \psi | N_I(t) | \psi \rangle - \frac{i}{\hbar} \int_{t_0}^t dt' \langle \psi | N_I(t) V_I(t') | \psi \rangle \\ &\quad + \frac{i}{\hbar} \int_{t_0}^t dt' \langle \psi | V_I(t') N_I(t) | \psi \rangle \\ &\quad + \frac{1}{\hbar^2} \int_{t_0}^t dt' dt'' \langle \psi | V_I(t'') N_I(t) V_I(t') | \psi \rangle, \end{aligned} \quad (2.23)$$

where in the interaction picture $N_I(t) = e^{iH'_0 t/\hbar} N_{\text{phot}}(t) e^{iH'_0 t/\hbar}$. Explicitly,

$$\begin{aligned} \langle N_{\text{phot}}(t) \rangle &= \frac{1}{\hbar^2} \sum_{\mathbf{q}, q_z} |\Omega_{0,q,q_z}|^2 \int_{t_0}^t dt' dt'' e^{i(\omega_{q,q_z} - \omega_0)(t' - t'')} \frac{1}{8} \times \\ &\quad \times (2 + e^{-i\Omega(t' - t'')} + e^{i\Omega(t' - t'')}), \end{aligned} \quad (2.24)$$

and taking the time integrals to infinity around a symmetrical domain we obtain

$$\begin{aligned} \langle N_{\text{phot}} \rangle &= \frac{1}{8\hbar^2} \sum_{\mathbf{q}, q_z} |\Omega_{0,q,q_z}|^2 4\pi^2 (2\delta^2(\omega_{q,q_z} - \omega_0) \\ &\quad + \delta^2(\omega_{q,q_z} - \omega_1) + \delta^2(\omega_{q,q_z} - \omega_2)), \end{aligned} \quad (2.25)$$

where we introduced the two satellite frequencies $\omega_1 = \omega_0 - \Omega$ and $\omega_2 = \omega_0 + \Omega$. Using $\delta(\omega)^2 = \delta(0)\delta(\omega) = \frac{t\delta(\omega)}{2\pi}$ and the sum on the final states of Eq. (2.11), the expression for the time derivative in the limit $t \rightarrow \infty$ simplifies to

$$\frac{d}{dt} \langle N_{\text{phot}}(t) \rangle = \frac{d^2 \sqrt{\epsilon_r \pi}}{6\hbar\epsilon_0 c^3} \int_0^\infty d\omega \omega^3 (2\delta(\omega - \omega_0) + \delta(\omega - \omega_1) + \delta(\omega - \omega_2)) \quad (2.26)$$

$$= \frac{d^2 \sqrt{\epsilon_r \pi}}{12\hbar\epsilon_0 c^3} (2\omega_0^3 + \omega_1^3 + \omega_2^3) = \frac{\gamma_0}{4\omega_0^3} (2\omega_0^3 + \omega_1^3 + \omega_2^3), \quad (2.27)$$

which gives the 1:2:1 structure of the Mollow triplet, as depicted in Figure 2.2 (b).

2.1.4.1 Literature

After Mollow's seminal work the theory of resonance fluorescence has been further extended, as the general theory of open quantum systems had become better formalised[11, 15–18]. Recently, in the context of solid-state cQED, the Mollow triplet of a quantum dot has been studied in the case of incoherent pumping, including the interaction with other quantum systems and phononic effects [19, 13, 20, 14].

The first experiments validating Mollow's 1969 inelastic spectrum prediction were made in the 1970s on hot, collimated, atomic beams of sodium atoms illuminated with resonant single-mode dye laser operated in continuous wave [21–23]. The experiments provide beautiful data, with recorded spectra matching very nicely the theoretical prediction. In the 1980s and 1990s the quantum optics community has been mainly involved in testing the coherent and incoherent properties of the light field and in harnessing coherent control of atoms, trapped ions and their degrees of freedom [24]. Two examples for all are given by the exquisite experimental results obtained by the groups lead by Serge Haroche in Paris and David Wineland in Boulder, Colorado. Their experiments pioneered research on the coupling between the vacuum of the

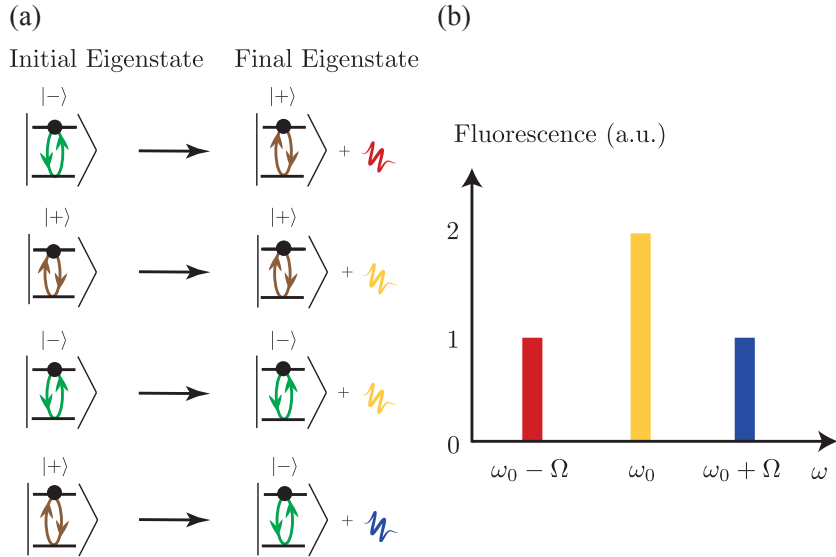


Fig. 2.2 (a) Scheme of the electron transitions giving rise to the Mollow triplet in the resonance fluorescence spectrum of a strongly pumped TLS. The only eigenstates coupling to the photonic field are $|\pm\rangle$, the horizontal arrows indicate the interaction with the free electromagnetic field and the emission of a photon at the frequency $\omega_0 - \Omega$ (photon depicted in red), ω_0 (yellow), $\omega_0 + \Omega$ (blue). (b) In this simple picture, the relative weight of the three emission lines give rise to the typical ratio 1:2:1 in the Mollow triplet.

photonic field and matter excitations. The interest for the application to quantum optics and quantum information of solid-state artificial atoms increased along with the improvement of fabrication and characterization techniques. The first resonance spectrum coming from a single quantum dot individually addressed in solid state were achieved only in 2007 [25, 26] but since then the quality and features investigated (including control of the quantum dot spin) have considerably increased [27–36]. The Mollow triplet has also been observed in the resonance fluorescence of a single molecule embedded in a solid-state matrix [37]. At the same time an important platform has emerged for the engineering of artificial atoms: Superconducting qubits in a circuit quantum electrodynamics system, on which the physics of cQED can be simulated [38–40]. Finally, the Mollow triplet has been also observed in quantum wells embedded in a microcavity, where the strong coupling of the cavity mode and the interband exciton transition [41] forms quasiparticles known as exciton-polaritons [42, 43]. Table 2.1 is an attempt at reporting comprehensively the significant parameters of the several different observations of the resonance fluorescence of a strongly pumped TLS or similar

Table 2.1 Experiments with strongly driven quantum systems. For experiments performed at a detuning Δ , Ω is derived from $\Omega' = \sqrt{\Omega^2 + \Delta^2}$. d_{12} can be derived from the linear relation $d_{12} = \hbar\Omega/\mathcal{E}$. Since $\mathcal{E} \propto \sqrt{P}$, standard laser waist beams are sometime assumed to derive \mathcal{E} . For atoms, the transition is the Sodium hyperfine transition $D_2, 3P_{3/2} \rightarrow 3S_{1/2}$. QDs are made of InAs/GaAs. QWs experiments refer to the ac Stark effect only.

Year	Ref.	Emitter	Pump	T (K)	$\frac{\omega_0}{2\pi}$ (THz)	max $\frac{\Omega}{2\pi}$ (THz)	max $\frac{\Omega}{\omega_0}$	d_{12} (ea_0)
1974	[21–23]	Atoms	CW	800	509	10^{-4}	10^{-7}	1
2008	[37]	Molecule	CW	1	508	10^{-4}	10^{-7}	1
2007	[25]	QD	CW	5	522	10^{-3}	10^{-6}	10
2007	[26]	QD	CW	10	327	10^{-3}	10^{-5}	-
2009	[29]	QD	pulse (ps)	24	328	10^{-3}	10^{-5}	-
2009	[27]	QD	CW	4	380	10^{-3}	10^{-5}	10
2009	[28]	QD	CW	10	320	10^{-2}	10^{-5}	-
2011	[30–33]	QD	CW	5	-	10^{-1}	-	-
2014	[36]	QD	CW	4–14	10^{-1}	10^{-2}	10^{-1}	10
2009	[38]	SC loop	electric	10^{-3}	10^{-3}	10^{-3}	10^{-2}	-
2010	[39]	SC loop	electric	-	10^{-2}	-	10^{-4}	10^{-2}
2013	[40]	SC loop	electric	10^{-2}	-	10^{-7}	10^{-5}	
2000	[41]	QW exciton	pulse (ps)	-	360	1	10^{-3}	10^{-2}
1998	[42]	QW polariton	pulse (ps)	10	-	4	-	-
2012	[43]	QW polariton	pulse (ps)	10	60	10^{-1}	10^{-3}	10^{-1}
2005	[44]	QW ISBT	pulse (ns)	300	30	3	10^{-3}	4

quantum systems. Reports of indirect evidence of the Mollow triplet, that is ac Stark splitting or Rabi oscillations are also included to provide information on Rabi splitting and dipole moment magnitudes. These have indeed been observed in the intersubband transitions of a doped quantum well [44, 45], while the theory of resonance fluorescence is developed in Chapter 3.

2.1.5 Cooperative light emission

In this Subsection the physics of cooperative (also called superradiant) light emission is described. We begin by considering the properties of the non-interacting Hamiltonian of N TLSs and the degeneracy of its eigenvalues. Then we will describe the coupling to the light field, §2.1.5.1, and introduce the Dicke states, §2.1.5.2, making an estimate of the superradiant light emission, §2.1.5.3. The different properties of the initial states, which determine a superradiant, superfluorescent or subradiant light emission, are illustrated in §2.1.5.4. The standard superradiant master equation is used to calculate the time evolution of the system in §2.1.5.5, and finally a historical overview on the literature is given in §2.1.5.6. In Chapter 5 we will use these concepts to describe superradiant light emission, and in particular superfluorescence – the cooperative light emission from an initially totally inverted ensemble of TLSs –, in a more general setting in which both dephasing and nonradiative decay are included, and a mapping to the case of intersubband transitions is given. More details both regarding the physical system, its algebra and symmetries, and the dynamics are given in Appendix D.

Cooperative light emission can arise from a collection of N identical TLSs contained in a portion of space with linear dimension L smaller than the resonance wavelength $\lambda_0 = \frac{2\pi c}{\sqrt{\epsilon_r}\omega_0}$, $L < \lambda_0$, and possibly $L \ll \lambda_0$. At visible frequencies or above this is a requirement that is hardly met, but at microwave and Terahertz frequencies, as we will show, there are solutions that can satisfy this condition. Each TLS is counted by an index i that generalizes the notation of the previous subsections. The bare Hamiltonian for a collection of N TLSs is

$$H_0 = \sum_{i=1}^N \frac{\hbar\omega_0}{2} \sigma_{z_i} = \hbar\omega_0 J_z, \quad (2.28)$$

which is indeed just a sum of the single TLS Hamiltonians, Eq. (2.1), rewritten in terms of the collective spin operator J_z . The states $|1\rangle_i$ and $|2\rangle_i$ of the i th TLS have all the same eigenenergies $\pm \frac{\hbar\omega_0}{2}$. From the algebra of Pauli's matrices one gets $[J_\alpha, J_\beta] = i\epsilon_{\alpha\beta\gamma}J_\gamma$ for $\alpha, \beta, \gamma = \{x, y, z\}$, and we define $J_\pm = \sum_i^N J_{\pm_i}$, with the identity $J_{\pm_i} = \sigma_i^\pm$ (see Appendix D.1.1 for further algebraic relations.) Before describing the interaction of light with this ensemble and introduce the proper Dicke states, let us focus on Eq. (2.28) and the properties of the collective eigenstates. It is possible to quantify the total excitation of the ensemble by applying the Hamiltonian Eq. (2.28) to a general state $|\{m\}\rangle$ describing any microscopic configuration such that there are n_2 “spins up”

and n_1 “spins down”, with $m = \frac{1}{2}(n_2 - n_1)$,

$$H_0 |\{m\}\rangle = \hbar\omega_0 m |\{m\}\rangle. \quad (2.29)$$

For N even, $m = 0, \pm 1, \pm 2, \dots, \pm \frac{N}{2}$, while if N is odd, $m = \pm \frac{1}{2}, \pm \frac{3}{2}, \dots, \pm \frac{N}{2}$, and always $|m| \leq \frac{N}{2}$. For $N = 2$, $m = \{-1, 0, 1\}$ and both the configurations $|2\rangle_1 |1\rangle_2$ and $|1\rangle_1 |2\rangle_2$, or their superpositions, can be represented by the state $|\{m\}\rangle = |\{0\}\rangle$ and have energy equal to zero. The degeneracy of the eigenvalue of Eq. (2.28) is thus the number of possible reshuffling of different configurations with the same number of spins up, n_2 , and of spins down, n_1 ,

$$d_m = \binom{N}{n_2} = \binom{N}{\frac{N}{2} + m} = \frac{N!}{(\frac{N}{2} + m)! (\frac{N}{2} - m)!}. \quad (2.30)$$

d_m grows quickly with N , for fixed m , while for fixed N it increases with decreasing $|m|$ —it is 1 for $m = \pm \frac{N}{2}$ and is greatest for $m = 0$, $d_0 = \binom{N}{\frac{N}{2}} \sim \sqrt{\frac{2}{\pi}} \frac{2^N}{\sqrt{N}}$ for $N \rightarrow \infty$. This degeneracy is partly lifted by considering the coupling with light and introducing the Dicke states, as we will show in the following two Subsections.

2.1.5.1 Collective coupling to light

If the ensemble of the N TLSs is coupled with the electromagnetic field, then when one of the spins “flips up”, it means that it has absorbed one quantum of the external field, while when one of the TLSs in the upper level “flips down”, it releases a quantum of excitation into the environment. Assuming that the TLSs are identically coupled to a single mode of the field, one obtains the single-mode Dicke model Hamiltonian,

$$H_{\text{Dicke}} = \hbar\Omega_0 \sum_{i=1}^N (\sigma_i^+ + \sigma_i^-)(a + a^\dagger) = \hbar\Omega_0 (J_+ + J_-)(a + a^\dagger), \quad (2.31)$$

where Ω_0 is the vacuum Rabi frequency for the single resonant photonic mode that couples to the TLSs. The Dicke model is known to be difficult to unravel, and ascertaining the properties of the system as the ratio $\frac{\Omega_0}{\omega_0}$ is continuously increased is a fruitful field of study, especially with regard to the quantum phase transition of the ground state [46].

When the ratio $\frac{\Omega_0}{\omega_0}$ is negligible (typically less than 0.001), the RWA can be performed by assuming that bare-energy conserving processes are dominant, and Eq.

(2.31) becomes

$$H_{lm} = \hbar\Omega_0(J_+a + J_-a^\dagger), \quad (2.32)$$

which is the light-matter coupling that will be studied in the following. We point out that a generalisation of either Eq. (2.31) or Eq. (2.32) can be made in the inhomogeneous case, in which terms $\Omega_{0,i}$ appear inside the sum over the N TLSs. If the coupling is dependent only on the position of the TLSs up to phase factors $e^{i\mathbf{q}_0 \cdot \mathbf{x}_i}$, where \mathbf{q}_0 is the wavevector of the field at the position \mathbf{x}_i of the i th TLS, the collective raising and lowering operators can be redefined accordingly and the spirit of Eq. (2.32) is preserved.

2.1.5.2 Dicke states

As in Eq. (2.32) above the collective raising and lowering operators have been introduced, it is even more evident the fact that the N TLSs interacting with light can be studied with the tools employed for a collection of spin- $\frac{1}{2}$ particles, the collective spin operators J_x, J_y, J_z and J_+, J_- . If the operator J_+ is applied only once to the collective state containing no atomic excitations (ground state), it takes the system into a symmetrical superposition with only one excitation. Iterative application of the collective raising operator leads to subsequent jumps up in the energy spectrum given by Eq. (2.28), until the most excited state is reached, in which all “spins are up” and the system saturates, as anticipated in the Introduction, §1. Notice that as one can expect, both the atomic ground state and most excited state have no degeneracy, as one can check also from Eq. (2.30), $d_{\frac{N}{2}} = d_{-\frac{N}{2}} = 1$. The eigenstates of Eq. (2.28) can be expressed in a way relevant to Eq. (2.32) as it is possible to define a total collective spin $\mathbf{J}^2 = J_x^2 + J_y^2 + J_z^2$ and since $[\mathbf{J}^2, J_\alpha] = 0$, for $\alpha = \{x, y, z\}$, we can choose a common basis of eigenstates of both \mathbf{J}^2 and J_z ,

$$\mathbf{J}^2 |j, m\rangle = j(j+1) |j, m\rangle, \quad (2.33)$$

$$J_z |j, m\rangle = m |j, m\rangle, \quad (2.34)$$

where $j \leq \frac{N}{2}$ and $|m| \leq j$, with j either a positive integer or a positive half-integer, whether N is even or odd, respectively. That is $j = \frac{N}{2}, \frac{N}{2}-1, \frac{N}{2}-2, \dots, j_{\min}+1, j_{\min}$ with $j_{\min} = 0$ for N even and $j_{\min} = \frac{1}{2}$ for N odd. The states $|j, m\rangle$ are called *Dicke states* and their relevance to Eq. (2.32) can be better understood by the fact that the

action of the ladder operators gives

$$J_+ |j, m\rangle = \alpha_{j,m}^+ |j, m+1\rangle = \sqrt{(j-m)(j+m+1)} |j, m+1\rangle \quad (2.35a)$$

$$J_- |j, m\rangle = \alpha_{j,m}^- |j, m-1\rangle = \sqrt{(j+m)(j-m+1)} |j, m-1\rangle, \quad (2.35b)$$

where the coefficients $\alpha_{j,m}^\pm$ are set by normalization, with $\alpha_{j,j}^+ = \alpha_{j,-j}^- = 0$ and $\alpha_{j,m}^- = \alpha_{j,m-1}^+$. A key property of the Dicke state $|j, m\rangle$ is that, by construction, the interaction with the light field, Eq. (2.32), does not change the quantum number j . As it will be shown, since the greater the value of j the greater the possibility of accelerating light emission, j is commonly called *cooperativity* or cooperative number in this context. A scheme of the Dicke states in the (j, m) plane is shown in Figure 2.3 for $N = 6$ in panel (a) and for $N = 7$ in panel (b). States characterized by the same j

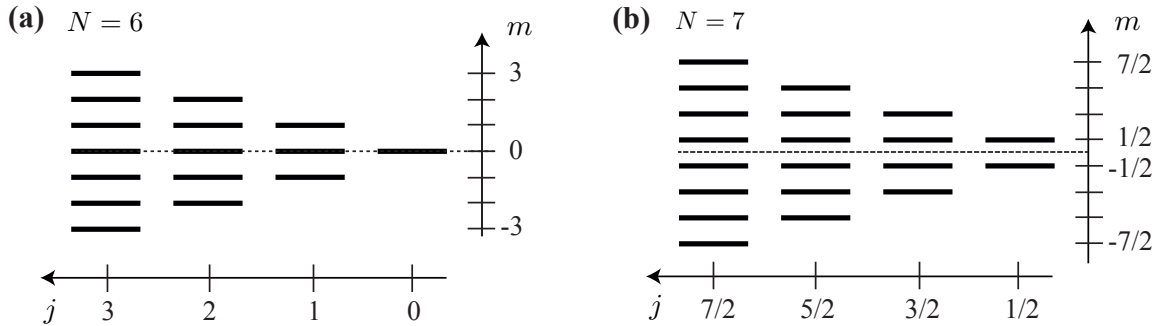


Fig. 2.3 Scheme of the Dicke phase space (j, m) for (a) $N = 6$ and (b) $N = 7$. Each rung represents a Dicke state $|j, m\rangle$ in a Dicke ladder with cooperativity number j . The Dicke ladder $j = \frac{N}{2}$ is formed of symmetrical Dicke states $|\frac{N}{2}, m\rangle$. As shown in panel (a), in case of an even number of states there is a dark (or subradiant) state completely decoupled from the light interaction, $|0, 0\rangle$. We point out that the degeneracy of the Dicke states is not evident in the (j, m) phase space: See the main text and Appendix D for details.

can be collected in a multiplet called *Dicke ladder*, whose rungs increase with j , as visible in Figure 2.3.

2.1.5.3 Superradiant emission

The light-matter interaction of Eq. (2.32) can be studied in terms of a perturbation of the atomic Hamiltonian Eq. (2.28) if $\Omega_0 \ll \omega_0$. The rate of photon emission for an

initial state $|i\rangle = |j, m\rangle |0_{\text{phot}}\rangle$ can then be derived using Fermi's golden rule, Eq. (2.9),

$$\gamma_{jm} = (j+m)(j-m+1)\gamma, \quad (2.36)$$

where γ equals the spontaneous emission from a single isolated atom. Eq. (2.35) selects as only non-zero matrix element that of the $|j, m\rangle \rightarrow |j, m-1\rangle$ transition.

The simplest example to study light emission from Dicke states is for $N = 2$. For $j = 1$ there is a triplet configuration of eigenstates, $|1, 1\rangle = |2\rangle_1 |2\rangle_2$, $|1, 0\rangle = \frac{1}{\sqrt{2}}(|2\rangle_1 |1\rangle_2 + |1\rangle_1 |2\rangle_2)$, $|1, -1\rangle = |1\rangle_1 |1\rangle_2$, which are connected by the ladder operators J_{\pm} . The two possible transitions involving $|1, 0\rangle$ either as initial or as final state occur at an enhanced rate 2γ . In general the state $|\frac{N}{2}, 0\rangle$ is called *superradiant* state. The singlet state $|0, 0\rangle = \frac{1}{\sqrt{2}}(|2\rangle_1 |1\rangle_2 - |1\rangle_1 |2\rangle_2)$ instead is uncoupled from light and is thus called dark or *subradiant*. How this energy scheme for the Dicke states is generalised to $N > 2$ can be seen in Figure 2.3 (a), by noting that this structure is preserved and that these four energy levels can be individuated at $j = 1, 0$.

When the system is initially prepared into the state $|\frac{N}{2}, \frac{N}{2}\rangle$ its dynamics is limited to the Dicke ladder with $j = \frac{N}{2}$, that is the one on the far left in Figure 2.3 (a) and (b). The states $|\frac{N}{2}, m\rangle$ are called symmetrical Dicke states. The first jump to $|\frac{N}{2}, \frac{N}{2}-1\rangle$ occurs at a rate equal to $N\gamma$. The rate of emission Eq. (2.36) progressively increases and becomes maximum for $|\frac{N}{2}, 0\rangle$,

$$\gamma_{\text{sr}} = \frac{N}{2} \left(\frac{N}{2} + 1 \right) \gamma \simeq \frac{N^2}{4} \gamma, \quad (2.37)$$

which shows the superradiant feature as the rate of photon emission scales as the square of the size of the ensemble.

In general for any j , the superradiant nature of light emission increases as the state climbs down the rungs of the Dicke ladder near to the rung $m = 0$. All of the states at the bottom of the Dicke ladders $|j, -j\rangle$ are *dark states* completely decoupled from the light field. Apart for the ground state, they all trap some excitation and are thus also called subradiant. The intensity of light emitted from the system can be calculated by [47]

$$I = \gamma \langle J_+ J_- \rangle, \quad (2.38)$$

where for an operator A , $\langle A \rangle = \text{Tr}[\rho A]$ is the average performed projecting onto a state or more generally making the trace over a density matrix ρ . Notably, we can single out two qualitatively different contributions in Eq. (2.38) by expanding the collective

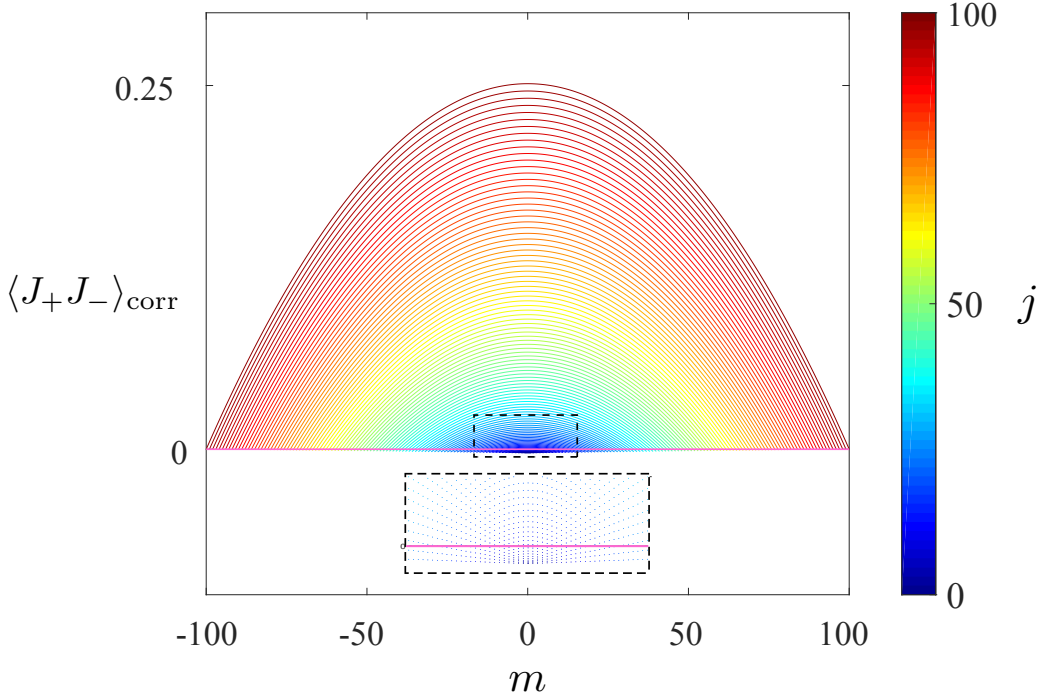


Fig. 2.4 The plot shows the portion of radiation emitted from a state $|j, m\rangle$ that is associated to the correlations between the single TLSs. This is given by $\langle J_+ J_- \rangle_{\text{corr}}$ of Eq. (2.40) and is plotted as a function of m (horizontal axis) and j (value encoded in the color). The number of TLSs is fixed, $N = 200$. $\langle J_+ J_- \rangle_{\text{corr}}$ is maximum for $m = 0$ and decreases as $|m|$ increases. The inset highlights an interesting feature, that is that there are Dicke states $|j, m\rangle$ for which $\langle J_+ J_- \rangle_{\text{corr}} < 0$, as shown by points corresponding to $\langle J_+ J_- \rangle_{\text{corr}}$ below horizontal solid pink line marks $\langle J_+ J_- \rangle_{\text{corr}} = 0$.

spin operators in terms of the single TLS ones,

$$I = \gamma \left\langle \sum_i J_{+i} \sum_j J_{-j} \right\rangle = \gamma \left(\left\langle \sum_i^N J_{+i} J_{-i} \right\rangle + \left\langle \sum_{i \neq j}^{N(N-1)} J_{+i} J_{-j} \right\rangle \right), \quad (2.39)$$

where on the r.h.s. of Eq. (2.39), the first term gives the portion of radiated emission from uncorrelated TLSs and the second term the one from correlated TLSs. Using the properties of the algebra, the first term on the r.h.s. of Eq. (2.39) can be rewritten as $\sum_i J_{+i} J_{-i} = J_z + \frac{N}{2}$, while the permutational symmetry of any term $J_{+i} J_{-j}$ with $i \neq j$ allows us to define the second term on the r.h.s of Eq. (2.39) as $N(N-1)\langle J_+ J_- \rangle_{\text{corr}}$. Eq. (2.39) can then be rearranged to obtain, starting from a Dicke state $|j, m\rangle$, a

quantity proportional to the light emission coming from correlated TLSs

$$\langle J_+ J_- \rangle_{\text{corr}} = \frac{1}{N(N-1)} (j(j+1) - m^2 - \frac{N}{2}). \quad (2.40)$$

A plot of Eq. (2.40) is given in Fig. 2.4 as a function of m for fixed $N = 200$ and the value of j encoded in the color of the lines that join each state. The maximum intensity of light emitted from correlated TLSs is at $m = 0$, as the maxima of each curved line show. In order to picture the superradiant dynamics, the plot can be interpreted as follows: If the system is initially prepared in a Dicke state $|j, j\rangle$, at $t = 0$, the state is at the right end of the curved line with corresponding j . The state will emit light, as a function of time, following the corresponding curved line, going over it from the right end to the left end, until the system ends in a point corresponding to a subradiant state $|j, -j\rangle$. We point out that dephasing, as well as spontaneous emission in modes other than the superradiant one, is a process that diminishes j , hence prompting a decrease in the system *cooperativity*. In the plot of Fig. 2.4 the action of pure dephasing can be visualised as prompting jumps tangent to the considered curved line towards curved lines with a lower value of j (toward the inner part of the “rainbow”), thus drastically reducing the amount of radiation coming from correlated dipoles. The pink line traced for $\langle J_+ J_- \rangle_{\text{corr}} = 0$ highlights the fact that Eq. (2.40) has also negative values, and in the closeup at the bottom of Figure 2.4 the discrete states—instead of joined lines—are shown to let appreciate their increasing density as $m \rightarrow 0$. Usually instead this fact is not appreciated as Eq. (2.40) is written assuming that $j \equiv \frac{N}{2}$ only, as the study of the system is restricted to the symmetrical Dicke states [47, 48]. Another interesting feature of Eq. (2.40) is that it gives information on the value of a quantity that depends on TLS operators in terms of collective spin eigenvalues j and m , which is something we will exploit also in Chapter 5 with regard to incoherent phenomena, as pure dephasing, occurring at the single TLS level.

2.1.5.4 State preparation

As shown in Eq. (2.36) each Dicke state has its own decay rate. The time evolution of the system, depending on its initial preparation, experiences very different evolutions. If the system is initialised in the maximally excited Dicke state, $|\frac{N}{2}, \frac{N}{2}\rangle$, the subsequent light emission is called *superfluorescence*. This initial state can be obtained for example by exciting with a π -pulse the ground state. If the dynamics is set only by Eq. (2.32), the system will emit a cascade of N photons down the Dicke ladder with maximum cooperativity, $j = \frac{N}{2}$, accelerating towards $m \rightarrow 0$, and then decelerating as $m \rightarrow -\frac{N}{2}$.

It is possible to estimate the delay time, t_D , with which the system reaches the superradiant state $|\frac{N}{2}, 0\rangle$ and that corresponds to the instant at which the intensity of the emitted light reaches its maximum. By linearising Eq. (2.36) and summing over all contributing states $m < \frac{N}{2}$ [47], one obtains an estimate for the delay time

$$t_D = \frac{\log(N)}{\gamma N}. \quad (2.41)$$

In order to obtain superradiant light emission on the fastest possible time scale, instead of having the fully excited state $|\frac{N}{2}, \frac{N}{2}\rangle$ trickle down the middle of the Dicke ladder from the top rung, it would be desirable to initialise the system already in the *superradiant state* $|\frac{N}{2}, 0\rangle$. This initialisation requires coherent control on the ensemble TLS and it is usually beyond experimental reach. A more feasible preparation is obtained instead by applying an external $\frac{\pi}{2}$ -pulse onto the ground state of the system, which gives a pure state that is the product state of Eq. (2.20),

$$|+\rangle_N = \bigotimes_{i=1}^N \frac{1}{\sqrt{2}} (|2\rangle_i + |1\rangle_i) = \sum_{m=-N/2}^{N/2} w_m |\frac{N}{2}, m\rangle, \quad (2.42)$$

which in the r.h.s. of Eq. (2.42) has been expressed in terms of Dicke states, with $w_m = \left(\frac{1}{2}\right)^{\frac{N}{2}} d_m^{\frac{1}{2}}$, with d_m given by Eq. (2.30) and thus symmetrical in $|m|$. The weight $|w_0|^2$ of the superradiant state $|\frac{N}{2}, 0\rangle$ slowly decreases with the number of TLSs N , as shown in Fig. (2.5) up to $N = 1000$. In the inset the full decomposition $|w_m|^2$ is shown for $N = 100$. Notice that the superposition Eq. (2.42) consists only of a sum of all of the symmetrical Dicke states with relative weight. As shown in Figure 2.5 the weight of $|\frac{N}{2}, 0\rangle$ into $|+\rangle_N$, given by $|w_0|^2$, decreases slowly for large N and it remains the single dominant weight, compared to all other $|w_m|^2$ weights with $m \neq 0$, as shown in the inset of Figure 2.5. For completeness we also give the formula of $|-\rangle_N$ derived as a product state of single TLS states of Eq. (2.20) in the Dicke state basis,

$$|-\rangle = \prod_{i=1}^N \frac{1}{\sqrt{2}} (|2\rangle_i - |1\rangle_i) = \sum_{m=-\frac{N}{2}}^{N/2} \left(\frac{1}{2}\right)^{\frac{N}{2}} (-1)^{m+\frac{N}{2}} d_m^{\frac{1}{2}} |\frac{N}{2}, m\rangle. \quad (2.43)$$

2.1.5.5 Superradiant master equation

Although Eq. (2.36) and Eq. (2.41) give some estimates on the time evolution of a state, it would be desirable to obtain a more comprehensive dynamics. A master equation can be derived using Eq. (2.28) for H_0 and Eq. (2.32) as a perturbation, valid in the limit $\frac{\Omega_0}{\omega_0} \ll 1$. Tracing over the photonic degrees of freedom, a master

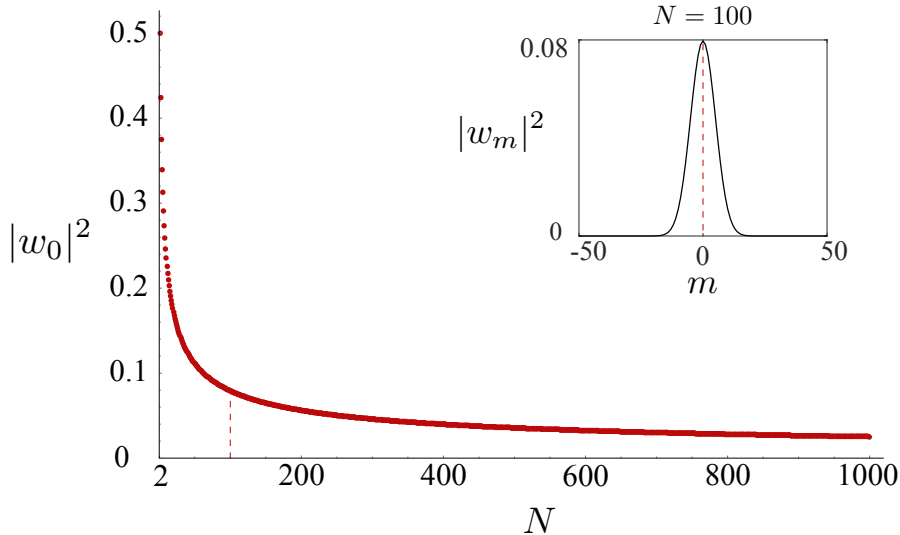


Fig. 2.5 Weight of the maximally superradiant Dicke state, $|\frac{N}{2}, 0\rangle$, in the decomposition of the pure state $|+\rangle_N$, as a function of N TLSs. Inset: Decomposition of the pure state $|+\rangle_N$ onto the symmetrical Dicke states for $N = 100$.

equation for the reduced density matrix of the TLSs can be written in the Linblad form using a Louivillian superoperator. The derivation requires the Born and Markov approximations, so that the *superradiant master equation* [47, 49] can be written as

$$\begin{aligned} \dot{\rho} &= -\frac{i}{\hbar}[H_0, \rho] + \gamma \mathcal{L}_{\text{lm}}[\rho] \\ &= -i\omega_0[J_z, \rho] + \gamma \left(J_- \rho J_+ - \frac{1}{2} J_+ J_- \rho - \frac{1}{2} \rho J_+ J_- \right). \end{aligned} \quad (2.44)$$

The braket $\langle j', m' | \dot{\rho} | j, m \rangle$ applied to Eq. (2.44) is non-zero only for $j' = j$ and $m' = m, m + 1$, giving the following sets of coupled equations

$$\dot{p}_{j,m} = \gamma (p_{j,m+1}(t)(j-m)(j+m+1) - p_{j,m}(t)(j+m)(j-m+1)). \quad (2.45)$$

The time evolution of the matrix element depends only on states in the same Dicke ladder j , which gives $\frac{N}{2}$ sets of $2j + 1$ coupled equations for each Dicke ladder. The time evolution of $p_{j,m}(t)$ are plotted in Figure 2.6 for $N = 10$ (left column) and $N = 100$ (right column) for different initial conditions: In panels (a)-(b) we consider a system initialised in $|\frac{N}{2}, \frac{N}{2}\rangle$, in panels (c)-(d) $|+\rangle_N$, and in panels (e)-(f) $|\frac{N}{2}, 0\rangle$. All initialisation conditions show that the system evolves irreversibly into the ground state ($p_{\frac{N}{2}, -\frac{N}{2}}(t) \rightarrow 1$) in a time that is of the order of t_D , a manifestation of cooperative dynamics. Moreover, a comparison of the dynamics from the two similar initial

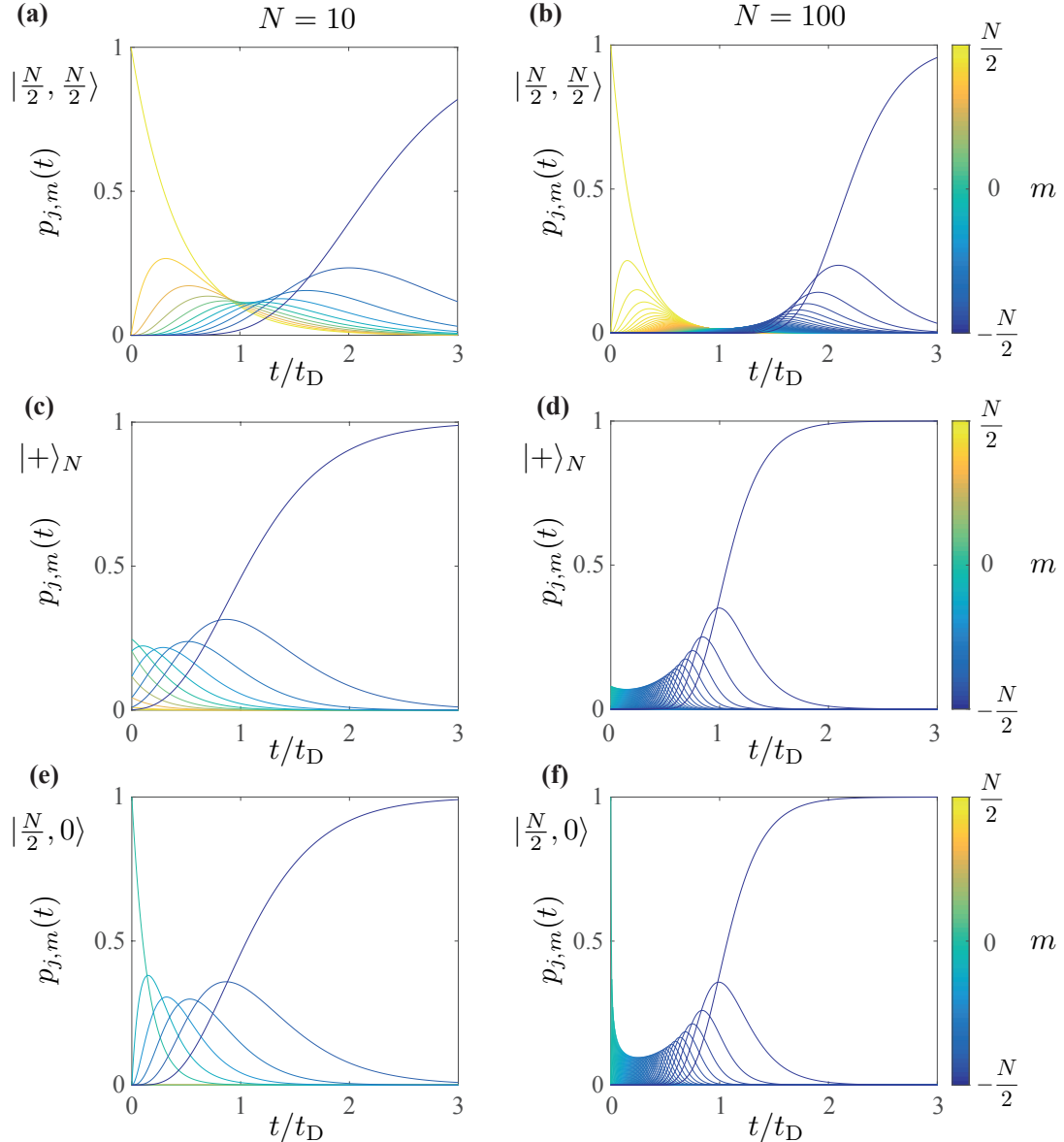


Fig. 2.6 Time evolution of $p_{j,m}(t)$ according to Eq. (2.45), for $N = 10$ (panels in the left column) and $N = 100$ (right column) when at $t = 0$ the system is prepared in different states: (a)-(b), $|\frac{N}{2}, \frac{N}{2}\rangle$ as with an optical π -pulse applied to the ground state; (c)-(d), $|+\rangle_N$ as with an optical $\frac{\pi}{2}$ -pulse applied to the ground state; (e)-(f), $|\frac{N}{2}, 0\rangle$ the superradiant state. The dynamics of each $p_{j,m}(t)$ is set by Eq. (2.45) and in all panels the initial cooperativity $j = \frac{N}{2}$ is conserved, while the color of the curves allows to find the value of m . In panels (a)-(b) (superfluorescence) the density matrix becomes maximally delocalised over many states around the delay time $t = t_D$, while for (c)-(f) the system performs a cascade between subsequent Dicke states.

conditions $|+\rangle_N$ in panels (c)-(d), and $|\frac{N}{2}, 0\rangle$ in panels (e)-(f) show that there is little difference in the subsequent dynamics, and that this difference becomes more attenuated for growing N , as visible by comparing panels (d) and (f) that refer to $N = 100$. Finally, with regard to superfluorescence, the $p_{j,m}(t)$ in panels (a)-(b) are “squeezed” around $t = t_D$ much more than the $p_{j,m}(t)$ for the other two initial conditions (c)-(e). Indeed for superfluorescence, around the delay time t_D , the state of the system becomes maximally delocalised over a superposition of several Dicke states, while in the two other cases – when the system is initialised in the superradiant state or with a $\frac{\pi}{2}$ -state – the system performs a cascade between subsequent Dicke states. This shows that when the dynamics starts from full inversion, if superfluorescence is described in the semiclassical limit, for which $\langle J_z^2 \rangle \simeq \langle J_z \rangle^2$, it will fail to describe such peculiar characteristic of the exact superfluorescent dynamics. See Appendix D for the semiclassical solution to Eq. (2.44). In Chapter 5 we will describe a dynamics more general than the one given by Eq. (2.44) and we will do so beyond the semiclassical approximation, thus in a good position to study the evolution of superfluorescence.

2.1.5.6 Literature

Here we give an historical perspective on theoretical and experimental research on cooperative light emission, while at the same time clarifying some points on the terminology that can be found in the broad literature on the topic. Superradiance is not treated in some of the most popular quantum optics textbooks [3, 50, 51], with the exception of Refs. [48, 24] and the handbooks by H. J. Carmichael [10, 52]. This makes the 1982 review by M. Gross and S. Haroche still one of the most comprehensive introductory reference to the topic [47]. Other reviews include a collection of essays edited by R. Bonifacio [53]; a review by L. I. Men’shikov that includes classical counterparts of superradiance [54], one by T. Brandes focusing on mesoscopic systems [55], a review on cooperative effects in various systems [56], and a very recent review paper by K. Cong *et al.* on their novel solid-state experimental results [57]. Already in 1954 R. H. Dicke developed the main part of the concepts introduced in this Section [2]—based on the use of collective spin operators and states—but further research on cooperative light emission by other authors intensified only in the 1970s and 1980s [49, 58–80], with important contributions made in Milano, Essen, and at Harvard by R. Bonifacio, F. Haake, and R. J. Glauber, with their collaborators. In particular R. Bonifacio and collaborators [49, 60, 67] highlighted the distinctive features of cooperative light emission when it originates from a completely inverted ensemble—already first described by Dicke—and coined for it the term superfluorescence [72–76], so that when

instead the term superradiance is used in the same context, one refers to light emission from an ensemble initialised in the state $|\frac{N}{2}, 0\rangle$. More generally though, superradiance not only is used as a synonym for cooperative light emission but it can also refer to the study of the phase transition of a state whose Hamiltonian is given by the Dicke model, Eq. (2.31). This problem is generally not concerned with mechanisms for light emission and focuses on entanglement and the properties of light matter coupling or the symmetry of the Dicke states [46]. Let us also mention then that symmetrical Dicke states $|\frac{N}{2}, m\rangle$ find applications beyond the study of superradiant light emission, and have been generated on photonic degrees of freedom as an important class of robust multi-particle states for the study of entanglement [81–86]. With reference to cooperative light emission, the term *Dicke's superradiance* has been coined to refer to a system in which the small sample condition is valid [87] with recent research focused mainly on the regime of single-photon excitation [88–92], proposed also as a tool in schemes that aim at obtaining a light-harvesting enhancement through quantum effects [93]. Indeed with regard to light harvesting, the mechanism of *superabsorbance* has been proposed, which could be implemented by engineering the photonic environment to favor light absorption over light emission [94]. Regarding the solid state, recent studies have assessed the specific dynamics of excitons in quantum dots or undoped quantum wells [95–98]. When the small sample limit is not valid, with regard to superfluorescence, the propagation of the emitted light can induce a ringing regime of several pulses, which are damped by decoherence mechanisms. When decoherence is even stronger, it can prevent the onset of a proper superfluorescence burst but an *amplified spontaneous emission* can still occur [99–101]. Investigations of cooperative effects in presence of a driving field have been performed [77, 102–104] and when the atomic system is contained in a resonant cavity, optical bistability can be observed, that is the radiated field shows an hysteresis cycle with respect to the driving field [70, 71, 78–80]. Recently, optical bistability and pumped superradiance have been studied theoretically with regard to quantum well excitonic transitions strongly coupled to photonic microcavity modes [105–108].

With reference to experiments, cooperative light emission has been observed in the optical transition of a gas of diatomic molecules [109] and in vibronic spectra of molecules in a solid-state matrix [110]. As already mentioned in §2.1.4.1, from the mid 2000s, nano-fabrication techniques improved and allowed more intense exploration of quantum optics phenomena in the solid state. Accelerated emission rates, but not properly superfluorescent peaks, have been observed from small ensembles of TLSs—as little as two—encoded on superconducting qubits by Walrapp's group [111, 112]

on quantum dots [113] and even on a single large quantum dot containing many excitations [114]. Russian scholars predicted the occurrence of collective effects in dense optical media, anticipating the polariton spectrum, the superradiant decay of cyclotron resonance, and classical analogues of superradiance [115–117]. These predictions have been recently observed experimentally in undoped quantum wells under a strong magnetic field [118–122], as also discussed in Ref. [57]. Finally, superradiant emission from single-photons has been recently observed in heavily doped quantum wells whose excitations are multisubband plasmons [123].

2.2 Intersubband transitions of quantum wells

In the following we will describe the optoelectronic properties of semiconductor quantum wells (QWs). These are only one type of nanometric structures that, together with quantum wires and quantum dots, are used in solid state as an implementation of lower dimensional quantum systems—respectively 2D, 1D, and 0D—that until a few decades ago were only conceptual paradigms. Improved fabrication techniques, creativity and skilfully-exploited self-assembly constraints have incredibly widened this classification while at the same time expanding the scope of their applications.

A QW is a heterostructure with a planar symmetry whose fundamental property is the strong spatial confinement in one direction—assumed to be z , also called growth direction for the way the device is fabricated, layer by layer. The other two linear dimensions are much greater than the third one, $L_x, L_y \gg L_z$ and the structure is considered isotropic in the plane, which can be a good approximation used also in experimental studies, thanks to the improvements made with regard to the nanometric control on the growth of the heterostructure. For this reason the notation $S = L_x L_y$ and $L_{\text{QW}} = L_z$ will equally be used throughout the thesis. The different layers are alternated in order to obtain a well potential due to the offset in the characteristic bandgap energies at the interface of the different semiconductor materials. We will focus on the case in which the material used as a barrier has a bigger bandgap than the material used to create the QW (known as type I heterojunction.) This basic concept of bandgap engineering is shown in panel (a) of Figure 2.7. For more details on materials properties, see the next subsection. Due to the tight quantum confinement along the growth direction, the energy dispersion is modified from that of the bulk semiconductor, shown in the scheme in panel (a) of Figure 2.7. In both the valence and conduction band, discrete subbands are resolved, as shown in panels (b) and (c)

of Figure 2.7, as the resolution of discrete energy levels in real space corresponds to quasi-parallel parabolic subbands in the valence and conduction band.

In an undoped semiconductor QW, typically the Fermi energy $\hbar\omega_F$ lies in the bandgap dividing valence subbands to conduction subbands. Optical excitation of the system creates electron-hole pairs known as excitons. These are bound quasiparticles that annihilate upon recombination.

If the semiconductor QW is doped, usually with Silicon, which is a *n*-type donor, the Fermi energy can be raised while otherwise not affecting too much the overall band structure of the undoped QW. It is then possible to trap a quasi-two-dimensional electron gas (2DEG) in the first conduction subbands. This particular physical system will be investigated in the following chapters. It is worth mentioning that besides from doping, the first conduction subbands can be populated with a 2DEG also with other methods applied to undoped QWs, for example by applying short optical pulses [124] or by raising the temperature [124–126].

The many-body Hamiltonian giving the energy of the conduction subbands is

$$H_{\text{el}} = \hbar \sum_{j,\mathbf{k}} \omega_{j,k} c_{j\mathbf{k}}^\dagger c_{j\mathbf{k}} \quad (2.46)$$

where $c_{j,\mathbf{k}}^\dagger$ is the second quantization operator creating an electron in subband $j = \{1, 2, \dots\}$ with in-plane wavevector \mathbf{k} and energy $\hbar\omega_{j,k}$, $\{c_{i,\mathbf{k}}^\dagger, c_{j,\mathbf{k}'}\} = \delta(\mathbf{k} - \mathbf{k}')\delta_{ij}$. In the following we will always limit our analysis to the light-matter coupling between the first two conduction subbands, as this model holds important similarities with the light-matter interaction of a collection of TLSs. Thus in Eq. (2.46) we limit to $j = \{1, 2\}$ only and consider structures in which a 2DEG partially fills the first conduction subband only. These assumptions can be precisely fulfilled by tailored experimental conditions in the growth process of the sample. We also point out that in Eq. (2.46) and in the following all the sums over electronic wavevector run until the Fermi wavevector, k_F , and since all the interactions considered are spin conserving, they implicitly sum also over spin. The ground state of the electronic system is

$$|G\rangle = \prod_{|\mathbf{k}| < k_F} c_{1,\mathbf{k}}^\dagger |0_{el}\rangle, \quad (2.47)$$

where $|0_{el}\rangle$ is the empty conduction band and k_F the Fermi wavevector setting level of occupied states in the first conduction subband.

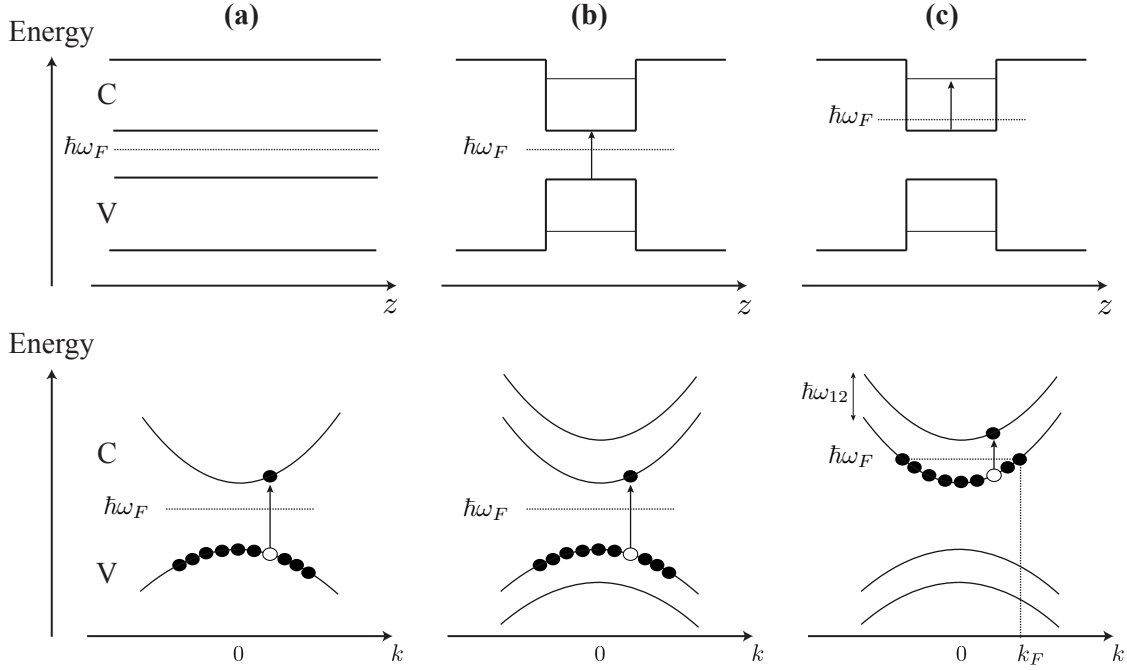


Fig. 2.7 Scheme representing the band structure of (a) a bulk semiconductor; (b) an undoped quantum well; (c) a doped quantum well. The effect of spatial confinement on the valence (V) and conduction (C) bands is shown in real space in the top part of the panels, while the corresponding in-plane wavevector dispersion is shown in the bottom part of the panels. The horizontal dashed line indicates the Fermi energy, $\hbar\omega_F$, while k_F the Fermi wavevector. Notice that while in panels (a) and (b) a bound electron-hole pair is formed upon photon absorption, in panel (c) an unbound intersubband transition is excited, and due to the fact that the conduction subbands are quasi-parallel, the 2DEG can be excited around a thin resonance centered at the single intersubband gap $\hbar\omega_{12}$.

Intersubband transitions (ISBTs) occurring between the two conduction subbands due to the interaction with the free electromagnetic field are given by the Hamiltonian

$$H_{\text{int}} = \hbar \sum_{\mathbf{k}, \mathbf{q}, q_z} \chi_{12, q, q_z} (a_{\mathbf{q}, q_z}^\dagger + a_{\mathbf{q}, q_z})(c_{2\mathbf{k}+\mathbf{q}}^\dagger c_{1\mathbf{k}} + c_{1\mathbf{k}}^\dagger c_{2\mathbf{k}+\mathbf{q}}), \quad (2.48)$$

where here and in the following we adopt the formalism of using \mathbf{q} and q_z for the photonic momentum and \mathbf{k} for the electronic momentum since they are on very different orders of magnitude, $\mathbf{k} \gg \mathbf{q}, q_z$. For the explicit derivation of Eq. (2.48) and the relation with first quantization variables, look at Appendix A.2. Also, in Eq. (2.48) we introduced the ISBT modal vacuum Rabi frequency χ_{12, q, q_z} corresponding to Ω_{0, q, q_z} of

Eq. (2.4) for a TLS. As only transverse magnetic modes couple to ISBTs, we neglect photon polarization [127].

Being the photonic wavevector much smaller than the typical electronic one, and given that the conduction subbands are to a good approximation parallel, we can consider $\omega_{12} \simeq \omega_{2,|\mathbf{k}+\bar{\mathbf{q}}|} - \omega_{1,k}$. This is a flat band approximation, which allows to apply the results that will be obtained with reference to intersubband transitions, also to other physical systems with flat-band dispersion. One of the most important features for technological applications and for a simplified theoretical treatment is that, due to the fact that the conduction subbands are quasi-parallel [128, 129], ISBTs have a narrow absorption line. Notice that though, differently from interband excitations, ISBTs do not create bound quasiparticles. Since the coupling terms belong to sums which run over $\mathbf{k}, \mathbf{q}, q_z$, this means that Eq. (2.48) cannot always be mapped into an ensemble of TLSs.

In Chapter 3 it will be shown how a pump with fixed photonic momentum can effectively map the driven dynamics of ISBTs to that of a collection of N TLSs. The resonance fluorescence spectrum of this system can differ from the usual Mollow triplet because also 'diagonal' transitions in \mathbf{k} -space coupling different TLSs can occur.

In Chapter 4 the possibility of designing asymmetric QWs will be exploited to allow transitions that are forbidden in a centrosymmetric system. The Hamiltonian that needs to be considered is then a more general one than Eq. (2.48) and includes also intrasubband transitions that are otherwise parity-forbidden,

$$\begin{aligned} H_{\text{asym}} = & \sum_{\mathbf{k}, \mathbf{q}, q_z} \chi_{12, q, q_z} (c_{2, \mathbf{k}+\mathbf{q}}^\dagger c_{1, \mathbf{k}} + c_{1, \mathbf{k}}^\dagger c_{2, \mathbf{k}-\mathbf{q}}) (a_{-\mathbf{q}, q_z}^\dagger + a_{\mathbf{q}, q_z}) \\ & + \sum_{\mathbf{k}, \mathbf{q}, q_z} [\chi_{11, q, q_z} c_{1, \mathbf{k}+\mathbf{q}}^\dagger c_{1, \mathbf{k}} + \chi_{22, q, q_z} c_{2, \mathbf{k}+\mathbf{q}}^\dagger c_{2, \mathbf{k}}] (a_{-\mathbf{q}, q_z}^\dagger + a_{\mathbf{q}, q_z}), \end{aligned} \quad (2.49)$$

where the coupling coefficient χ_{12, q, q_z} has been generalised to the four possible couplings

$$\chi_{ij, q, q_z} = \mathcal{E}_0 \frac{q}{\sqrt{q^2 + q_z^2}} z_{ij} \quad (2.50)$$

with $i, j \in \{1, 2\}$ where \mathcal{E}_0 is the maximum amplitude of the vacuum photonic field,

$$z_{ij} = \int \psi_i^*(z) \psi_j(z) z dz, \quad (2.51)$$

with $i, j \in \{1, 2\}$ and $\psi_j(z)$ is the envelope function of an electron in the j th subband. See Appendix A for details of the general definition of envelope functions in second quantization.

2.2.1 Line broadening

Several mechanisms lead to line broadening, $\Delta\omega$, in ISBTs and to first approximation we can differentiate, just like for a TLS, between decay time T_1 and a pure dephasing time T_2^* ,

$$\Delta\omega = \hbar \left(\frac{1}{T_1} + \frac{2}{T_2^*} \right). \quad (2.52)$$

At the microscopic level, T_1 and T_2^* can be induced by different mechanisms, mainly longitudinal optical (LO) and acoustic (LA) phonon emission, interface roughness scattering, ionized impurities scattering, electron-electron interaction, and radiative decay by spontaneous photon emission. Starting with phonon scattering, we can individuate two different regimes depending on whether the optical phonon energy, which in GaAs is 37 meV at cryogenic temperatures, is detuned from or near to the ISB gap. In the former case, LO emission can be strongly suppressed, while in the latter it can contribute significantly to line broadening, especially at resonance. When the rate of LO emission is not negligible, it is several orders of magnitude greater than LA phonon emission mechanisms, which for this reason is then neglected. Ionized impurities and alloy disorder depend on the characteristics of the sample, as the chosen materials and the magnitude (and technique) of doping. Electron-electron Coulomb interactions usually dominate intrasubband scattering. Finally, the contribution of interface roughness scattering is dependent on mainly two factors. The first one is the growth technique: The effect is generally greater in case of metal-organic chemical vapour deposition (MOCVD) than for molecular beam epitaxy (MBE). The second one is the length of the quantum well L_{QW} , with the interface roughness scattering rate increasing strongly for short quantum wells, as a function of L_{QW}^{-6} [130]. It becomes very large for thin QWs as those in Nitride-based systems that are only a few monolayer-thick and that exploit their wide bandgap to engineer large ISBTs that cover up to the telecom range, 1.33-1.55 μm [131].

Incoherent mechanisms can also alternatively be divided in two groups depending on their effects on the final shape of the emission line. For homogenous scattering, the lifetime gives rise to a Lorentzian lineshape, while for inhomogenous scattering, to a Gaussian one. A given mechanism can contribute to homogenous or inhomogeneous

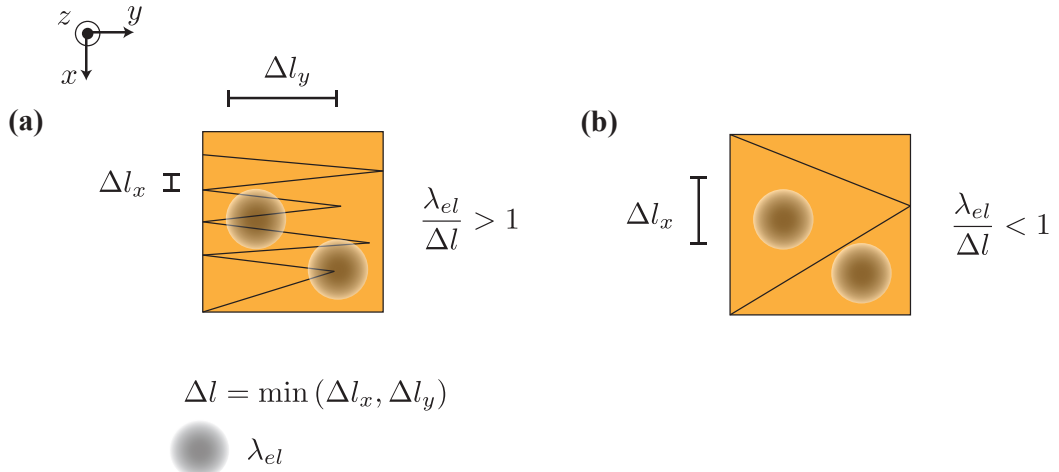


Fig. 2.8 An illustration depicting two regimes of interface roughness scattering. (a) For $\lambda_{el} > \Delta l$ the inhomogeneities are on a length scale shorter than the electron's wavelength and electrons experience on average similar potential landscapes; the mechanism leads to homogeneous broadening. (b) For $\lambda_{el} < \Delta l$ different electrons experience different potentials; the mechanism leads to inhomogeneous broadening.

line broadening depending on the characteristics of the system. For example interface roughness scattering gives rise to inhomogeneous broadening when the typical length of the uneven terrace, Δl , is greater than the electron De Broglie's wavelength, $\lambda_{el} < \Delta l$, while it corresponds to homogeneous line broadening when the length is smaller, $\lambda_{el} > \Delta l$; the two scenarios are schematised in Figure 2.8, see Ref. [127] and [132] for more details.

Most of the literature reports on the fact that overall line broadening is homogeneous and some claim that this is a hint of collective phenomena occurring in the 2DEG. Faist *et al.*, 1993 and 1994 [133, 134] report homogeneous broadening. They also estimate that at low temperature the minimum wavelength of the electron is given not by the de Broglie but by the Fermi wavelength, which can be estimated from $\lambda_F = 2\pi/k_F$, with $k_F^2 = 2\pi n_{2\text{DEG}}$, where $n_{2\text{DEG}}$ is the surface electron density. In a double asymmetric QW structure with a central barrier, similar to the one studied in Chapter 4, for which $L_{\text{QW}} = L_a + L_b + L_c = 6 \text{ nm} + 2 \text{ nm} + 7 \text{ nm}$, they estimate an electron wavelength $\lambda_{el} = 40 \text{ nm}$ that is greater than the interface roughness scattering terraces length, $\Delta l = 6 \text{ nm}$. Heyman *et al.* [135] report a homogeneous lineshape with $\text{FWHM} = \hbar\Delta\omega = 0.8 \text{ meV}$, $\hbar\omega_{12} = 11 \text{ meV}$. Craig *et al.* [136] assume homogeneous broadening and Vodopyanov, 1997 [137] give a discussion for this mechanism. Kaindl *et al.* [138] also

measure a homogeneous linewidth and estimate that the contribution is mainly due to intrasubband Coulomb scattering, with $T_1 = 550$ fs, $T_2 = 320$ fs and pump intensities up to 7 MW/cm 2 . They are able to suppress LO and LA phonon emission by using 50 QWs with resonances off-tuned from the phononic resonances, with $L_{\text{QW}} = 10$ nm and $n_{\text{2DEG}} = 6 \cdot 10^{11}$ cm $^{-2}$. Williams *et al.* [139] and Unuma *et al.* [132], report a dominant interface roughness scattering contribution to line broadening, in wide QWs with $L_{\text{QW}} = 40$ nm.

The theory of the 2DEG, developed mainly for the interest in its peculiar conduction properties, can be found in Ref. [140], by T. Ando *et al.* The response function $\mathbf{Re}[\sigma(\omega)]$, the electrical conductivity tensor, is calculated from many-body condensed matter theory. A similar approach has been taken recently [141] with reference to ISBTs. R. Ferreira and G. Bastard account for a sum over fixed Coulomb scatterers [142]. C. A. Ullrich and G. Vignale use the functional density theory within (and beyond) the low density approximation, a standard method in condensed matter calculations [143]. C. Ciuti and S. De Liberato diagonalize second quantization Hamiltonians to calculate the eigenmodes and explore the collective phenomena [144–147].

The most used materials for the QW fabrication are III-V alloys that, as direct bandgap materials, are the most suitable for optoelectronic applications, such as AlGaAs/GaAs [44, 45]. Also Nitride-based structures, such as AlN/GaN, have been recently explored, for their large bandgap [131]. Another alloy with a large bandgap that has been recently used for ISBTs is ZnO [148]. Other options include non-polar materials with a single element, such as in Ge/SiGe QWs [149, 141]. In Figure 2.9 the bandgap of several materials used for QW structures are shown against the lattice constant, a critical parameter to ensure the minimisation of strain and impurities at the interfaces and thus a precise nanometric confinement.

Summarizing, in ISBTs it is generally valid the rule $T_2 \ll T_1$, that is intrasubband mechanisms dominate in limiting the coherence of the system, with typical times of $T_2 \simeq 0.01\text{-}1$ ps, while $T_1 \simeq 1\text{-}100$ ps. LO and LA phonons are mainly responsible for the limit on T_1 , while T_2 depends strongly on interface roughness scattering, especially in short QWs (wider ISB gaps).

2.2.2 Terahertz technology

Terahertz (THz) technology is a term that is broadly used with reference to technological solutions that advance our capabilities in emitting and detecting light at THz frequencies [150]. This is currently a technological challenge and is referred to as the “THz gap”, a portion of the electromagnetic field spanning 0.3 - 30 THz (or 1.24 - 124 meV or

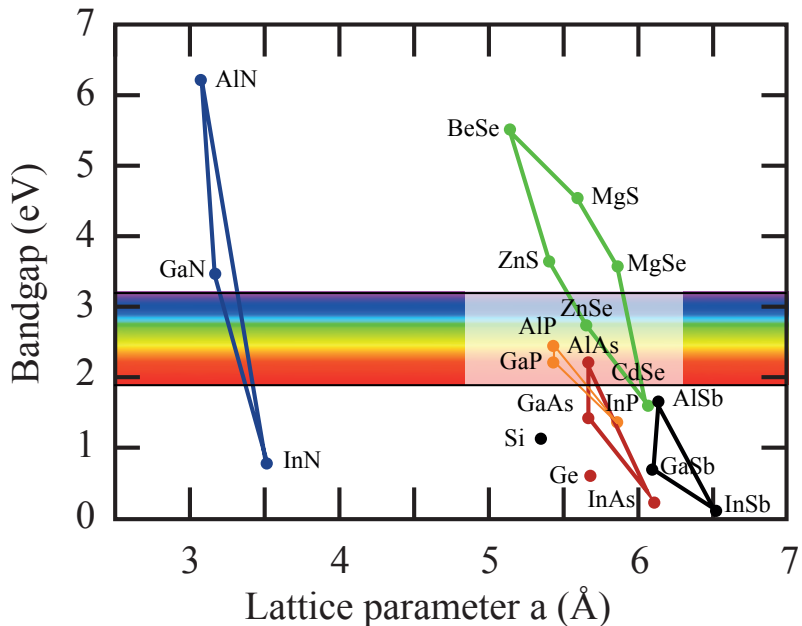


Fig. 2.9 Scheme of the bandgap energies vs. lattice parameter at room temperature for typical materials used in the fabrication of quantum well structures. Lines connect commonly used alloys. The frequency range of the visible spectrum is shown. Data from [131, 149].

1 mm - 10 μ m in vacuum, respectively) that partially overlaps with the far infrared in its upper bound and is lower bounded by the microwave region. The THz portion of the electromagnetic spectrum is well above radio frequencies and well below the visible range: Its waves are non-ionizing, so that they can be safely used for medical applications, such as imaging, providing sub-millimiter resolution. They also find applications in short-distance ultrafast wireless data transfer and fields that require imaging or sensing, from airport security to homeland defence, from environmental studies of the upper atmosphere's composition to industrial product-quality control [150–152]. THz technology is one of the fastest growing research topics in the fields of photonics and electronics. Since at THz frequencies both electronic and photonic systems can resonate, THz technology is emerging as a bridge between these two fields. For all these reasons, a technological aspect that guided the research performed in this thesis has been the possibility to find new paths to emit light at THz frequencies. With respect to THz emission, ISBTs in doped QWs possess many interesting properties. QWs are a solid-state system that can be integrated in portable devices, as it has been done for QW infrared photodetectors, commonly called with their acronym, QWIPs

[127]. For QWs of several nanometers of length, the bare resonance of the ISBT is in the infrared range, just above the THz range. The major technological breakthrough for THz technology came when the infrared quantum cascade laser was adapted to emit THz light [153, 154]. The mechanism of the quantum cascade laser is based on the fact that even a single electron, injected at the top of the potential in an upper subband, can emit many photons—hence the cascade. First a photon is emitted upon transition to the lower subband of the QW. Then, upon tunnelling of the QW barrier, the electron enters in the next QW, whose potential is tuned so that the electron once again occupies the upper level. Several repetition of QWs are employed in a single device to maximize the efficiency.

Moreover, typically the vacuum Rabi splitting of doped QWs in microcavities lies within the THz range, generally a few meV. For this reason several proposals use strongly-coupled light-matter systems for THz light emission. The exciton bare frequencies of undoped QWs can be changed in embedded microcavities to the point that the eigenmodes of the systems are light-matter quasiparticles, known as exciton polaritons [155]. In particular, one scheme recently proposed involves superradiant light emission at THz frequencies from dipolaritons, which arise from coupled double QWs [106]. Similarly to exciton polaritons, light-matter quasiparticles form also when ISBTs strongly couple to the mode of the photonic vacuum, and this can be achieved by embedding the doped QW structure in a microcavity. Recently mechanisms based on polariton scattering that exploit the asymmetry of a QW to achieve THz lasing have been proposed for intersubband [156] and excitonic systems [157]. Indeed the possibility of using the asymmetric QW to open up new emission mechanisms has recently been explored [158–161]. In Chapter 4 we will illustrate the possibility of exploiting a new emission channel based on the broken inversion symmetry of a QW to obtain tunable light emission at the pump Rabi frequency Ω [162].

Chapter 3

Intersubband resonance fluorescence

3.1 Introduction

In the precedent Chapter the physics of resonance fluorescence has been described for a physical system well described by a TLS. In this Chapter, the resonance fluorescence of intersubband transitions is described [163]. When a strong pump excites the 2DEG, almost all the electrons that lie in the first subband are promoted to the second subband at the same time [44]. While the characteristics of the coherent phenomena are very similar to that of a collection of TLSs driven in Rabi oscillations, the physics can be quite different with regard to the coupling to the free electromagnetic field, and thus to the resonance fluorescence spectrum. The main difference is that ISBTs are not bound to occur among well-separated electronic sites. We can thus expect that the TLS approximation, used to derive the usual theory of the Mollow triplet, can break down in certain regimes. One of the main consequences with regard to the calculation of the resonance fluorescence emission is that, differently from the case of a resonantly driven single TLS, here the quantum regression theorem cannot be applied and thus higher-order correlations in the emitted photon flux are not calculated. This is somehow the price to pay in order to treat such a complex many-body system and its unbound transitions.

In this Chapter we will develop a predictive many-electron theory describing resonant fluorescence emission from ISBTs and other similar systems beyond the TLS approximation [147, 122]. Yet the physical picture can be rather different from the TLS case and, while the three-peaked structure is conserved, the relative intensity of the peaks becomes a function of the coherence of the electron gas. This feature

thus hints at the intriguing possibility of measuring the coherence time of a 2DEG through a measure of its resonance fluorescence. In the following we introduce the theoretical description of a resonantly pumped ISBT and develop a perturbative theory of fluorescence emission in order to estimate the intensity of the emitted radiation. By considering the limitations of the theory here developed, the experimental constraints required to observe such interference effects are delineated.

3.2 Main theory

3.2.1 Driven Hamiltonian

We consider two conduction subbands, the lower one containing a 2DEG, pumped by a coherent source resonant at the ISBT transition frequency between the two subbands, ω_{12} . The Hamiltonian of the pumped electronic system can be written as

$$H_0 = \sum_{j,\mathbf{k}} \hbar\omega_{j,\mathbf{k}} c_{j,\mathbf{k}}^\dagger c_{j,\mathbf{k}} + \frac{\hbar\Omega}{2} \sum_{\mathbf{k}} \left(c_{2,\mathbf{k}+\bar{\mathbf{q}}}^\dagger c_{1,\mathbf{k}} e^{-i\omega_L t} + c_{1,\mathbf{k}}^\dagger c_{2,\mathbf{k}+\bar{\mathbf{q}}} e^{i\omega_L t} \right), \quad (3.1)$$

where Ω is the Rabi frequency proportional to the pump field amplitude, and ω_L is the pump frequency, whose in-plane wavevector is $\bar{\mathbf{q}}$ and out-of-plane wavevector is \bar{q}_z . In Eq. (3.1) the strong driving field is classical, as discussed in §2.1.3, and the RWA is applied since still the Rabi frequency induced by the pump is much smaller than the intersubband gap frequency, $\frac{\Omega}{\omega_{12}} \ll 1$. Moreover we are assuming that no resonant microcavity is (strongly) coupled to the ISBT bare frequency, so photons that are pumped into the system are continuously scattered. Passing in the frame rotating at the pump frequency, in the resonant case $\omega_L = \omega_{12}$, the Hamiltonian can be reduced to the time-independent form, equivalent to Eq. (2.19)

$$H'_0 = \frac{\hbar\Omega}{2} \sum_{\mathbf{k}} \left(c_{2,\mathbf{k}+\bar{\mathbf{q}}}^\dagger c_{1,\mathbf{k}} + c_{1,\mathbf{k}}^\dagger c_{2,\mathbf{k}+\bar{\mathbf{q}}} \right). \quad (3.2)$$

Being the in-plane wavevector conserved in a planar structure, the pump, which has a fixed wavevector $\bar{\mathbf{q}}$, couples each electronic state of the first subband with wavevector \mathbf{k} , to a single state in the second one with wavevector $\mathbf{k} + \bar{\mathbf{q}}$, and vice versa. The set of all the electron levels in the two subbands is divided into coupled pairs, and the Hilbert space of the electronic system is consequently partitioned into four-dimensional subspaces. If only one of each pair of levels is occupied by an electron, then we can

consider only two states in each of these subspaces and the eigenstates are

$$|\pm, \mathbf{k}\rangle = \frac{1}{\sqrt{2}} (c_{2,\mathbf{k}+\bar{\mathbf{q}}}^\dagger \pm c_{1,\mathbf{k}}^\dagger) |0_{\text{el}}\rangle, \quad (3.3)$$

corresponding to those of Eq. (2.20), as the system maps exactly onto a set of pumped TLSs, each one having eigenvalues $\hbar\omega_{\pm,k} = \pm \frac{\hbar\Omega}{2}$ in the referential frame rotating at the pump frequency, where Ω is the Rabi frequency proportional to the pump amplitude, similarly to the one defined for a TLS in Eq. (2.17). Yet in order to span the whole Hilbert space of the system, we also have to include the states in which neither or both levels of the pair are occupied,

$$|E, \mathbf{k}\rangle = |0_{\text{el}}\rangle, \quad (3.4a)$$

$$|F, \mathbf{k}\rangle = c_{2,\mathbf{k}+\bar{\mathbf{q}}}^\dagger c_{1,\mathbf{k}}^\dagger |0_{\text{el}}\rangle, \quad (3.4b)$$

and as these states are either empty or Pauli blocked, they do not couple with the pump, and have eigenvalue zero in the rotating frame [162, 164], as shown in Fig. 3.1 (a). To each \mathbf{k} value we can thus associate a four-dimensional Hilbert space: $\mathcal{H}_k \equiv \{|-, \mathbf{k}\rangle, |F, \mathbf{k}\rangle, |E, \mathbf{k}\rangle, |+, \mathbf{k}\rangle\}$. Now that the Hamiltonian for the closed system is solved, in order to describe resonance fluorescence, we need to couple it to the free electromagnetic field. This light-matter interaction, already introduced in Eq. (2.48), in the RWA takes the form

$$V = \sum_{\mathbf{k}, \mathbf{q}, q_z} \chi_{12,q,q_z} (c_{2,\mathbf{k}+\mathbf{q}}^\dagger c_{1,\mathbf{k}} a_{\mathbf{q},q_z} + c_{1,\mathbf{k}}^\dagger c_{2,\mathbf{k}+\mathbf{q}} a_{\mathbf{q},q_z}^\dagger), \quad (3.5)$$

where χ_{12,q,q_z} has been introduced in Eq. (2.48), and is the light-matter coupling term, directly proportional to the ISBT dipole moment. Contrary to the TLS case, the interaction in Eq. (3.5) causes scattering between two-electron eigenvectors, i.e. involving in general states belonging to $\mathcal{H}_k \otimes \mathcal{H}_{k+\mathbf{q}}$. These processes are shown in Fig. 3.1 (b), for the two-electron initial state in Fig. 3.1 (c).

There are four different scattering channels, two emitting at frequency ω_{12} and the other two at $\omega_{12} \pm \Omega$. While this could seem to lead to a result analogous to that obtained with standard TLS Mollow theory, there is a fundamental difference: Here the final state of all the emission channels is the same, which is the product of a fully occupied and an empty state, $|F, \mathbf{k}\rangle \otimes |E, \mathbf{k} + \mathbf{q}\rangle$. This two-wavevector state reflects the fundamental difference of ISBTs with respect to bound transitions: upon emitting a photon of wavevector \mathbf{q} , the electron scatters to a different final state. The total final electron state for the single photon-emission process is composed of the electronic

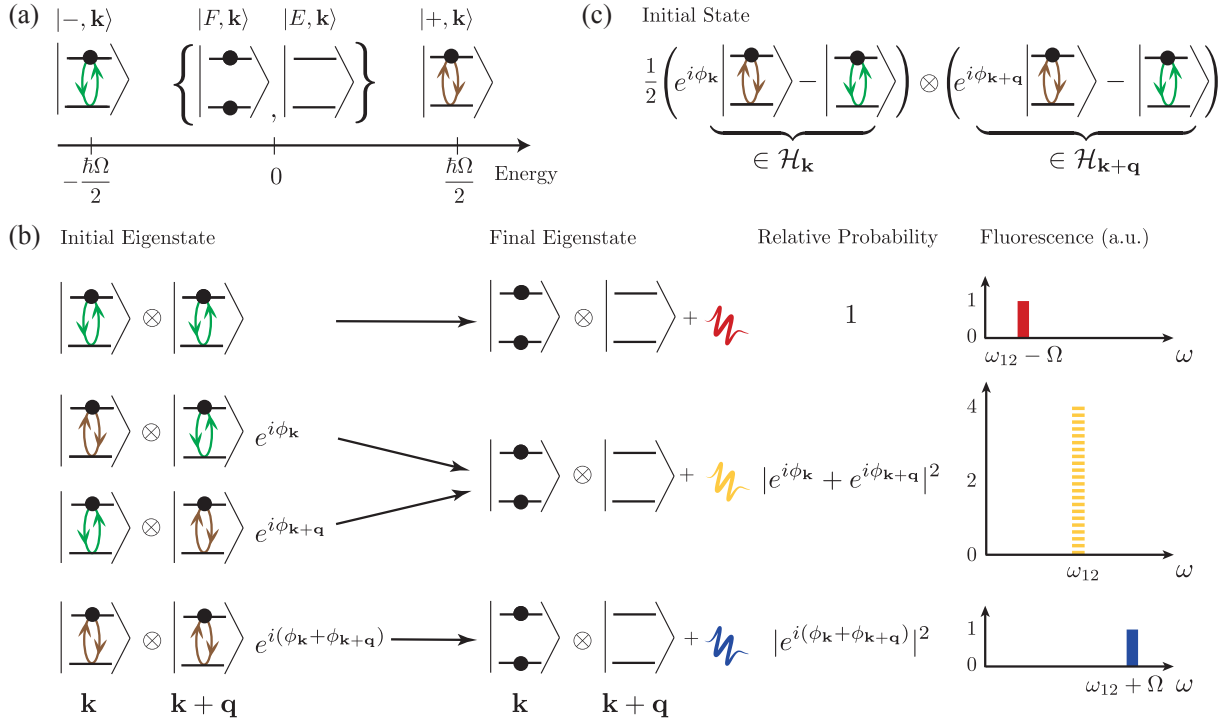


Fig. 3.1 (a) Eigenvectors and eigenenergies relative to the partition into the subspace \mathcal{H}_k of the bare Hamiltonian H'_0 . (b) Transitions in intersubband resonance fluorescence, with the black arrows depicting the scattering of the initial states into the final states under the action of the interaction Hamiltonian V . There are four different transitions, corresponding to the emission of light at three different frequencies, ω_{12} and $\omega_{12} \pm \Omega$. At ω_{12} , two different scattering processes interfere and the intensity of the emitted light is given by their relative phases, $4 \cos^2 \left(\frac{\phi_k - \phi_{k+q}}{2} \right)$. (c) Two-electron state in which the electrons oscillate between the two subbands with phases ϕ_k and ϕ_{k+q} .

states relative to two subbands at values k and $k + q$. This opens up the possibility of having *interference* for the emission of the central peak, with its intensity depending on the relative phases between the two electrons involved. A simple understanding of the phase-dependence of the emission intensity can be gained by considering the semiclassical picture of the two electrons cycling between the two subbands, driven by the pump. The interaction Hamiltonian in Eq. (3.5) can lead to a diagonal process in which one of the electrons scatters from its own upper state to the other electron's lower state. This transition is Pauli blocked unless both electrons are at the same time in their upper state. The emission intensity will thus depend on the relative phase of the two cycling electrons.

In order to make quantitative such a handwaving discussion, we need to describe the full many-body state of the system undergoing the Rabi oscillations, taking care of the relative phases of the electrons, $\phi_{\mathbf{k}}$, which will have a paramount role in the following.

3.2.2 State of the driven system

Let us assume that initially the pump is “off” and that the ground state of the system thus describes a 2DEG in the lower subband, the Fermi state of Eq. (2.47),

$$|\psi_{\text{el}}(0)\rangle = |G\rangle. \quad (3.6)$$

The state in Eq. (3.6) can be rewritten in terms of the two eigenstates of H' in Eq. (3.4) as

$$|\psi_{\text{el}}(0)\rangle = \bigotimes_{\mathbf{k}} \frac{1}{\sqrt{2}} \left(e^{i\phi_{\mathbf{k}}} |+, \mathbf{k}\rangle - |-, \mathbf{k}\rangle \right), \quad (3.7)$$

where a relative phase of each oscillating electron $\phi_{\mathbf{k}}$ has been added. These phases are all zero at $t = 0$, in order to recover Eq. (3.6), but they can evolve in time due to dephasing processes, which cannot be accounted for in the Hamiltonian dynamics we considered. This is a cruder approximation than a treatment that embodies the incoherent processes in a microscopic description of the dynamics e.g., with a master equation for a single TLS or a collection of TLSs, but the choice is determined in order to treat more generally the *unbound* transitions given by the action of V of Eq. (3.5).

When the optical pump is “switched on” the electrons start oscillating under the action of H' . The state in Eq. (3.7) can be evolved using Eq. (3.2) and Eq. (3.4) as

$$\begin{aligned} |\psi_{\text{el}}(t)\rangle &= e^{-iH't/\hbar} |\psi\rangle \\ &= \bigotimes_{\mathbf{k}} \frac{1}{\sqrt{2}} \left(e^{i(\phi_{\mathbf{k}} - \frac{\Omega}{2}t)} |+, \mathbf{k}\rangle - e^{i\frac{\Omega}{2}t} |-, \mathbf{k}\rangle \right) \\ &= \prod_{\mathbf{k}} e^{i\frac{\phi_{\mathbf{k}}}{2}} [i \sin(\frac{\phi_{\mathbf{k}} - \Omega t}{2}) c_{2,\mathbf{k}+\bar{\mathbf{q}}}^\dagger + \cos(\frac{\phi_{\mathbf{k}} - \Omega t}{2}) c_{1,\mathbf{k}}^\dagger] |0_{\text{el}}\rangle, \end{aligned} \quad (3.8)$$

where in the second line of Eq. (3.8) we expressed the state in terms of the fermionic operators acting on the empty subbands, which makes it evident that the electrons are oscillating between the two subbands.

This state is not stationary and as such it cannot be used in the standard formulation of the Fermi’s golden rule to calculate the photon emission. An equivalent formulation can be obtained by calculating, to the first order in V , the total number of emitted

photons per unit time, leading to [165],

$$\gamma_{\text{Mol}} = \frac{1}{4\hbar^2 t} \sum_{\mathbf{k}, \mathbf{q}, q_z} |\chi_{12, q, q_z} \int_{-t/2}^{t/2} e^{i(\omega_{12} - \omega_{q, q_z})\tau} f_{\mathbf{k}, \mathbf{q}}(\tau) d\tau|^2, \quad (3.9)$$

with

$$f_{\mathbf{k}, \mathbf{q}}(t) = \cos\left(\frac{\phi_{\mathbf{k}} + \phi_{\mathbf{k}+\mathbf{q}}}{2} - \Omega t\right) - \cos\left(\frac{\phi_{\mathbf{k}} - \phi_{\mathbf{k}+\mathbf{q}}}{2}\right). \quad (3.10)$$

The integrand in Eq. (3.9) contains only phase factors linear in τ and as such, for long enough times, Eq. (3.9) will be given by a sum of squared Dirac delta-like functions. Using the usual trick of formally transforming $\delta(\omega)^2 = \delta(0)\delta(\omega) = \frac{t\delta(\omega)}{2\pi}$, we obtain

$$\begin{aligned} \gamma_{\text{Mol}} = & \frac{\pi}{8\hbar^2} \sum_{\mathbf{k}, \mathbf{q}, q_z} |\chi_{q, q_z}|^2 [4 \cos^2\left(\frac{\phi_{\mathbf{k}} - \phi_{\mathbf{k}+\mathbf{q}}}{2}\right) \delta(\omega_{q, q_z} - \omega_{12}) \\ & + \delta(\omega_{q, q_z} - (\omega_{12} + \Omega)) + \delta(\omega_{q, q_z} - (\omega_{12} - \Omega))]. \end{aligned} \quad (3.11)$$

In order to calculate the sums in Eq. (3.9) we neglect specific correlations between the phases, considering them as independent and identically distributed (IID) random variables. This is a mean-field approximation that allows us to replace the sum over \mathbf{k} with an average over the phase distribution, multiplied by the total number of electrons N . While an exact investigation of the phase dynamics is beyond our scope, we can give a qualitative description of phase diffusion. In a typical experiment the phases will be initially all equal, as all the electrons lie in the lower conduction subband. Once the continuous drive of the pump is turned on, the electrons will eventually diffuse with a coherence time τ_{coh} , leading to the experimentally observed wash-out of the Rabi oscillations [166–168], see Figure 3.2 for an illustration of the process. Under this approximation, and for times long enough to be able to resolve the peaks ($t > \frac{2\pi}{\Omega}$), we can calculate the emission rate as We assume that the phases are IID random variables. The sum over \mathbf{k} of the only term depending on \mathbf{k} in Eq. (3.9) thus becomes

$$\begin{aligned} \frac{1}{N} \sum_{\mathbf{k}} 4 \cos^2\left(\frac{\phi_{\mathbf{k}} - \phi_{\mathbf{k}+\mathbf{q}}}{2}\right) &= \frac{1}{N} \sum_{\mathbf{k}} 2(1 + \cos \phi_{\mathbf{k}} \cos \phi_{\mathbf{k}+\mathbf{q}} + \sin \phi_{\mathbf{k}} \sin \phi_{\mathbf{k}+\mathbf{q}}) \\ &\stackrel{IID}{=} 2(1 + \langle \cos \phi \rangle^2 + \langle \sin \phi \rangle^2), \end{aligned} \quad (3.12)$$

and then we can write

$$\gamma_{\text{Mol}} = \frac{1}{8} (1 + \langle \cos \phi \rangle^2 + \langle \sin \phi \rangle^2) \gamma_0(\omega_{12}) + \frac{1}{16} \gamma_0(\omega_{12} + \Omega) + \frac{1}{16} \gamma_0(\omega_{12} - \Omega), \quad (3.13)$$

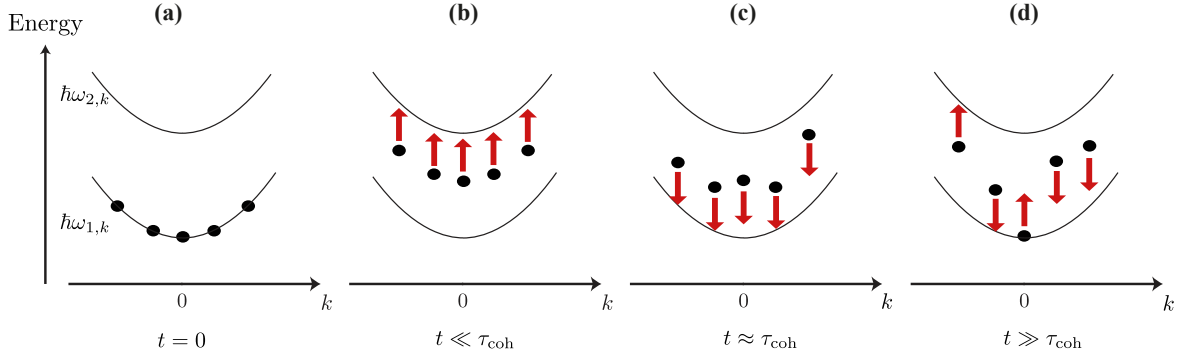


Fig. 3.2 An illustration of phase diffusion over time. (a) At $t = 0$, all electrons lie in the first subband and the state is well described by Eq. (3.6), that is Eq. (3.7) with all $\phi_{\mathbf{k}} = 0$. (b) For $t \ll \tau_{coh}$ the electrons oscillate coherently. (c) For $t \approx \tau_{coh}$ the electrons start dephasing. (d) At $t \gg \tau_{coh}$ coherence between electrons is lost and Rabi oscillations are averaged out.

where $\gamma_0(\omega)$ is the spontaneous emission in free space at frequency ω and the angular bracket is the average over the phase ϕ . While electrons are fully coherent, the phase distribution will be strongly peaked around a well defined value $\bar{\phi}$, and in Eq. (3.13) we obtain $\langle \cos \bar{\phi} \rangle^2 + \langle \sin \bar{\phi} \rangle^2 = 1$, independently of the specific value of $\bar{\phi}$. By assuming a flat photonic spectrum, if we approximate $\gamma_0(\omega_{12} \pm \Omega) \simeq \gamma_0(\omega_{12})$, the intensity of the central peak is in a ratio 1:4:1 with respect to the satellites. For $t \gg \tau_{coh}$ instead, the electron coherence is lost. The phases can in this case be considered as uniformly distributed and we have $\langle \cos \phi \rangle = \langle \sin \phi \rangle = 0$, recovering the usual ratio 1:2:1 for the area of the three peaks and the expected asymptotic value for the total incoherent emission rate $\gamma_{eq} = \frac{\gamma_0}{4}$ [162] [see Appendix B.2].

3.3 Visibility of Rabi oscillations

A clear way to present this result is in terms of the many-electron Rabi oscillations. The fraction of electrons in the second subband can be calculated as [see Appendix B.1]

$$n_2(t) = \langle \psi_{el}(t) | \frac{\sum_{\mathbf{k}} c_{2,\mathbf{k}}^\dagger c_{2,\mathbf{k}}}{N} | \psi_{el}(t) \rangle = \langle \sin^2(\frac{\phi - \Omega t}{2}) \rangle, \quad (3.14)$$

which have a visibility decreasing exponentially in time due to decoherence (see the inset of Fig. 3.3), given by an envelope function normalized between 0 and 1,

$$C = 2 \max_t n_2(t) - 1 = \sqrt{\langle \cos \phi \rangle^2 + \langle \sin \phi \rangle^2}. \quad (3.15)$$

Remarkably, Eq. (3.13) can be recast as a simple function of C ,

$$\gamma_{\text{Mol}} = \frac{1}{8}(1 + C^2)\gamma_0(\omega_{12}) + \frac{1}{16}\gamma_0(\omega_{12} + \Omega) + \frac{1}{16}\gamma_0(\omega_{12} - \Omega), \quad (3.16)$$

which is plotted in Fig. 3.3, assuming that $\gamma_0(\omega_{12} \pm \Omega) \simeq \gamma_0(\omega_{12})$, valid for $\omega_{12} \gg \Omega$. From Eq. (3.16) we can clearly see how the relative intensity of the central peak decreases from 4 to 2 with dephasing.

Notice that, while the coherence time can be measured by four-wave mixing [169], or by the populations, through Eq. (3.14) [168], this requires one to perform either a pump and probe measurement, or to have an appositely crafted system with a shelving level [44]. Through γ_{Mol} instead, the same information can be acquired via a time-resolved fluorescence measurement. A main experimental challenge will be to discriminate the weak fluorescence signal from the pump. While polarization cannot be used to this aim, due to ISBTs selection rules, it is possible to exploit the broad angular distribution of the fluorescence. Similarly to what was done in Ref. [26], the sample can be engineered for the pump beam to be confined in a waveguided mode, while part of the fluorescence is emitted in non-guided modes, and collected outside of the sample.

Above we implicitly assumed that the visibility C can be considered almost constant over a few Rabi oscillations, in order to neglect the time dependency of Eq. (3.15) in Eq. (3.9). Such a condition, which can be expressed as $\Omega\tau_{\text{coh}} \gg 1$, can be fulfilled by present-day technology. The main contributions to τ_{coh} generally come from interface roughness scattering (IRS) and longitudinal optical phonon emission, which are both suppressed in wide QWs [142, 127, 138, 132, 149]. Since IRS scales as the inverse sixth power of the QW length [127, 130] and the phonon emission is forbidden when the intersubband gap becomes smaller than the optical phonon frequency [170], coherence times of the order of a picosecond are achievable in wide QWs. Regarding phonon coupling, it should be noted that excitation-induced dephasing can be considerable due to the fact that a change in charge configuration of the system can dynamically couple to phonons.

In GaAs/AlGaAs QWs similar to the ones investigated in Ref. [171], of bare frequency $\hbar\omega_{12} = 100$ meV, at $T = 4.2$ K, linewidths of 2.5 meV, corresponding

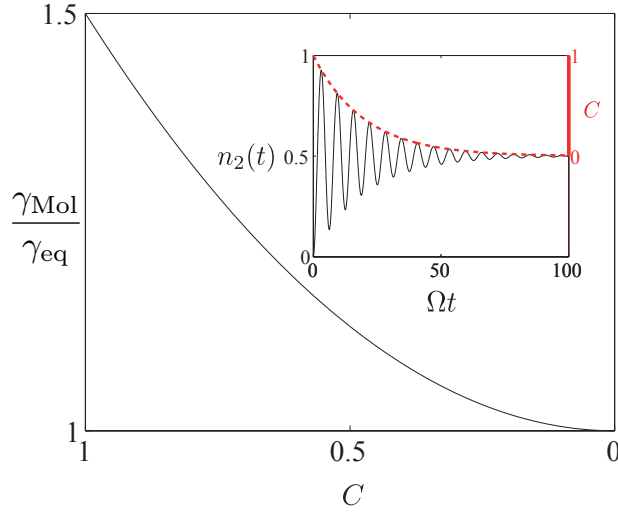


Fig. 3.3 The integrated intensity of fluorescence, plotted normalized to the fully incoherent value γ_{eq} , decreases as the visibility C goes to zero. Inset: The collective Rabi oscillations of the second subband, $n_2(t)$ (black solid line, left axis) are washed out in a time τ_{coh} . The visibility C (red dashed line, right axis) decreases accordingly in time. Here $\Omega\tau_{\text{coh}} = 20$.

to $\tau_{\text{coh}} = 0.5$ ps, can be obtained even under intense pumping [44, 45, 172]. In such structures, Rabi splittings in excess of 10 meV are achievable for internal pump intensities of the order of $\sim \text{MW/cm}^2$ [138, 44], leading to $\Omega\tau_{\text{coh}} \simeq 10$. In Ge/SiGe QWs, the non-polarity of the Ge lattice inhibits Fröhlich-mediated phonon emission and removes the constraint of performing measurements at cryogenic temperatures. While no observation of Rabi oscillations has been made in these systems, recent results with linewidths of a few meV have been obtained up to $T = 300$ K for the bare frequencies, so $\tau_{\text{coh}} = 1$ ps or longer is reachable by current technology [141]. For a structure with $\hbar\omega_{12} = 50$ meV and $L_{\text{QW}} = 10$ nm as in Ref. [141], we expect $\Omega\tau_{\text{coh}} \simeq 20$.

3.4 Experimental constraints

We developed our theory neglecting the Coulomb interaction. While it is well known that in the case of parallel subbands its effects usually reduce to a renormalization of the intersubband transition energy [128] (the so-called depolarization shift, vanishing for parabolic wells [173, 174]), Coulomb interaction could have a non-negligible impact in our case, as the presence of collective excitations [175, 146, 176–178] could spoil

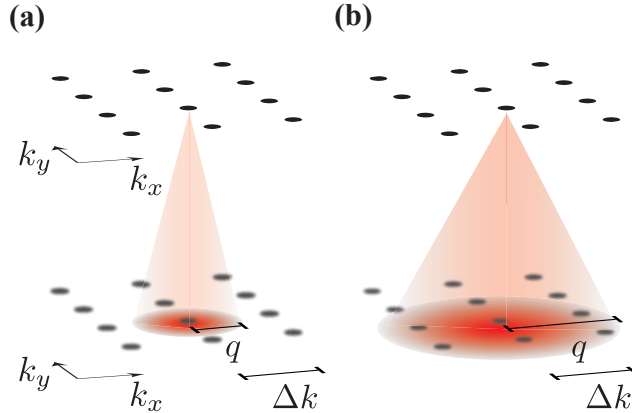


Fig. 3.4 Energy dispersion of the first two conduction subbands in a doped QW as a function of the in-plane wavevector $k = (k_x, k_y)^T$ in the flat-band approximation. The ratio between the emitted photon wavevector, q , and the electron wavevector uncertainty Δk , determines how many final states are accessible for a photonic emission. The TLS approximation is valid in the case shown in panel (a) $q < \Delta k$, while more complex scattering processes occur in the case of panel (b), $q > \Delta k$.

the independent electron picture we used [179]. For this reason we can consider our analysis as rigorous only in the limit in which the depolarization shift is much smaller than the Rabi frequency, and plasmonic effects can be ignored. In both structures from Refs. [171] and [141] we estimated a depolarization shift of less than 0.8 meV for a carrier concentration of $n_{2\text{DEG}} = 10^{11} \text{ cm}^{-2}$ [127, 180, 181, 124]. Our hypothesis of a depolarization shift much smaller than the Rabi frequency is thus fulfilled for all but the most heavily doped structures.

A last point worth stressing is that we considered a planar infinite 2DEG. While this is usually a very good approximation for high mobility samples, we still have to consider that the oscillating electrons are localized in the laser spot. If we call Δk the electron wavevector uncertainty due to such a confinement, the observation of interference of multi-electron scattering will require that the in-plane momentum of the emitted photon, q , obeys the relation

$$q \gg \Delta k, \quad (3.17)$$

see Figure 3.4 for a scheme of the emission process. For a typical waist $w \simeq 50 \mu\text{m}$ [44], this condition is well fulfilled already for $\hbar\omega_{12} > 7 \text{ meV}$, but attention should be paid when applying our theory to narrow waists and THz QWs.

3.5 Conclusions

In conclusion, we have shown that when ISBTs are strongly driven at resonance by an optical pump, the fluorescence has peculiar features that are not found in that of a collection of non-interacting TLSs. Although the TLS approximation is useful to describe Rabi oscillations, the richer dynamics introduced by incoherent emission processes requires a more sophisticated approach. In ISBTs the ratio between the three resonance fluorescence peaks deviates from the Mollow triplet due to interference effects that enhance the emission from the central peak. Thanks to this effect, the coherence time of a 2DEG could be accessed directly from a measure of the time resolved fluorescence intensity.

Chapter 4

Terahertz light emission from the intersubband transitions of asymmetric systems

4.1 Introduction

The theory of resonance fluorescence of a TLS has been summarised in Chapter 2. The Mollow triplet [1, 13] arises from transitions between states of neighbouring Rabi doublets (thick black arrows in Figure 4.1). The transitions between states belonging to the same Rabi doublet (thick red arrows in Figure 4.1) were not considered so far since they are dipole-forbidden in centro-symmetric systems. Yet by breaking the symmetry of the potential that confines the electrons, this selection rule can be lifted [182], allowing new emission lines centred at the Rabi frequency Ω . The description of the full dynamics of this system and a quantification of this source is the topic of this Chapter. A more intuitive understanding of such an emission channel can be gained reasoning in the time domain, in which the electrons undergo Rabi oscillations at frequency Ω between the initial and final bare states under the effect of the pump. In a centro-symmetric system, the average electron position is the same for both these states, and Rabi oscillations do not result in a net charge oscillation. If the symmetry of the electronic wavefunctions is broken instead, the electronic charge oscillates back and forth, and we expect the system to radiate as a dipole oscillating at frequency Ω (see Figure 4.2 (a) for a pictorial representation.)

Interband transitions in quantum dots have been proposed as candidates for observing this emission channel [183], but the magnitude of their asymmetric dipole is small

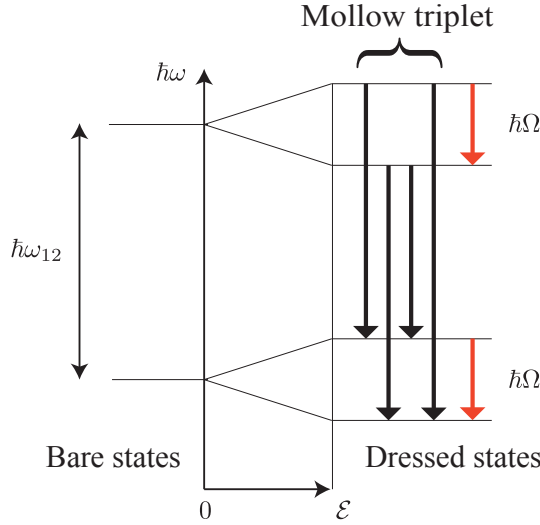


Fig. 4.1 Spectrum of a two-level system resonantly driven with amplitude \mathcal{E} . Inter-doublet transitions (thick black arrows) give rise to the Mollow triplet with emission centred at frequencies ω_{12} and $(\omega_{12} \pm \Omega)$. Intra-doublet transitions (thick red arrows) at frequency Ω , are forbidden in centro-symmetric systems.

and difficult to control, as it relies on the intrinsic anisotropy of the crystal lattice. ISBTs in doped QWs appear to be a better candidate, thanks to the possibility of tailoring their asymmetry by engineering the confining structure [173]. Moreover, for these systems, the Rabi splitting lies in the THz domain [44], and it depends on the intensity of the pump beam, as shown by Eq. (2.17). Symmetry-forbidden transitions in ISBTs, apart from their fundamental interest in quantum optics, could thus empower a new generation of tunable monolithic THz emitters.

The possibility obtaining THz lasing from polariton microcavities was recently explored in Ref. [156] in the polaritonic case, where the splitting is not due to the high intensity of the pump laser, but to the strong coupling of ISBTs to the vacuum field of a photonic microcavity. In that case, in the dilute excitation regime, the spectrum of the system is composed of quasi-bosonic excitations called intersubband polaritons [184–187, 145, 175]. In Ref. [156], it was shown that an asymmetric QW structure can give rise to scattering between different polaritonic branches, leading to the possibility of designing an efficient THz laser, whose emission frequency could be partially tuned by modifying the electron density in the QWs [188, 126]. Related works, that also use symmetry breaking to observe otherwise forbidden emissions, have also recently been proposed [155, 159–161, 189, 190].

Compared with these existing works, the scheme here presented offers the advantages of an extreme tunability of the emission frequency, and of a comparatively simple and flexible design, because it does not rely on a resonant photonic cavity coupled to the ISBT. From a theoretical point of view, a major difference between this scheme and all the others cited above, is that here we are interested in the full electron dynamics, and so we cannot limit ourselves to the bosonic or quasi-bosonic regime. We will have to work in a fermionic basis, without any bosonization approximation. Moreover, in this non-bosonic, nonlinear regime, the electrons in ISBTs do not generally behave as independent dipoles (as it has been recently proved in Ref. [147]) and thus we cannot a priori rely on the single dipole theory developed in Ref. [182].

In the following we will develop a general theory of the spontaneous emission from the resonantly driven ISBT of a 2DEG. After developing the general formalism to calculate the emission efficiency, we will perform a numerical study of the magnitude of the asymmetric dipole achievable in a QW structure. This will allow us to quantify the experimentally achievable emission efficiency, and to address future experiments toward the best sample geometry.

The Chapter is structured as follows: In Section 4.2 we develop a theory describing optically pumped ISBTs and the light-matter coupling in an asymmetric structure. Such a theory will then be used to calculate the photon emission rate in Section 4.3, in which estimates are made of the THz emission efficiency for a realistic asymmetric device. Finally, conclusions and perspectives are drawn in Section 4.4.

Before proceeding with our study of THz emission in asymmetric QWs, we stress that symmetry-forbidden emission channels have never been observed in atomic systems [24], which are usually an ideal testbed to observe quantum optics phenomena. Although atoms are intrinsically symmetric, their symmetry can be broken applying a static electric field [191]. But even in Alkali atoms, which possess the strongest polarizabilities of both the ground state ($n = S_{1/2}$) and of the first excited states ($m = P_J$, with $J = \{1/2, 3/2\}$), and were for this reason a testbed for the Mollow triplet [21, 23], we estimated [162] from available experimental data and theoretical calculations of the literature [192], that even considering extremely strong electric field ($\mathcal{E}_{\text{stat}} = 10^7$ V/m [193]) any effect due to the asymmetric dipole will be very challenging to observe. More details are given in Appendix C.1.

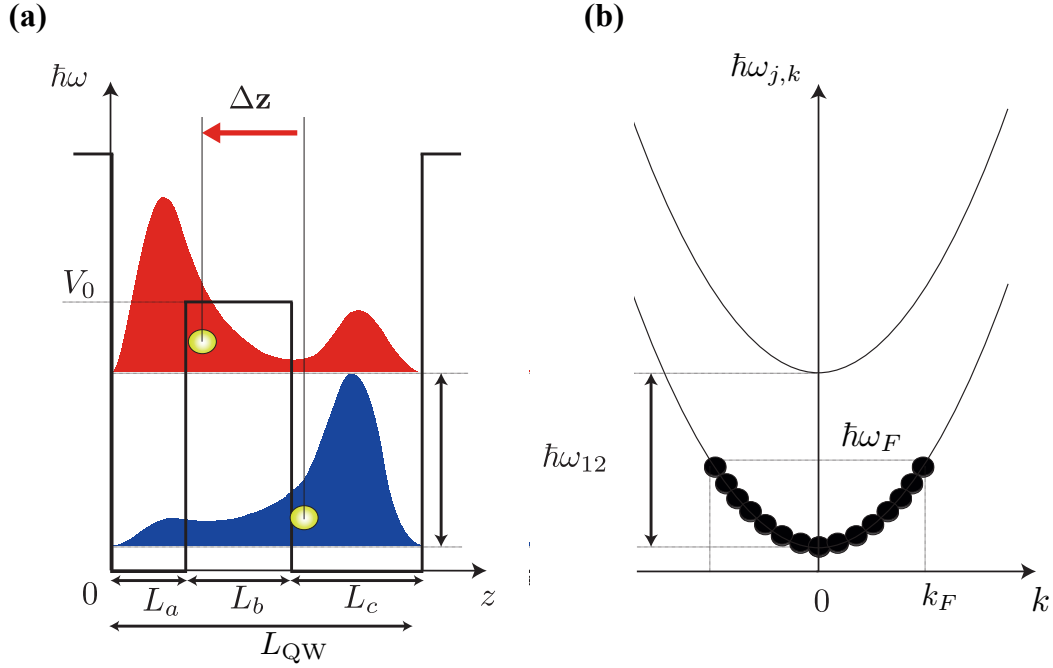


Fig. 4.2 Panel (a): An asymmetric quantum well and the wavefunctions of its first two conduction subbands. Due to the asymmetry, the average charge position in the two subbands is different. Electrons cycling between them under the effect of a resonant pump generate a radiating dipole of length Δz , oscillating at the Rabi frequency Ω . Panel (b): The parabolic dispersion in \mathbf{k} -space of the first two conduction subbands, $j = \{1, 2\}$.

4.2 Main theory

The Hamiltonian describing the effect of a pump driving the ISBT between the first two conduction subbands is still H_0 from Eq. (3.1) and the strength of this light-matter coupling is quantified by the Rabi frequency, Eq. (2.17), $\Omega = ez_{12}\mathcal{E}/\hbar$, where z_{12} is given by Eq. (2.51). In order to be able to calculate the THz emission due to the presence of an asymmetric dipole, we will start by finding the full many-body eigenstates of Eq. (3.2), in order to be then able to perturbatively calculate emission using Fermi's Golden Rule.

From the decomposition of H'_0 in a sum of commuting Hamiltonians in Eq. (3.2), a general eigenvector of H'_0 , can be put in the form

$$|\psi\rangle = \bigotimes_{\mathbf{k} \in S_+} |+, \mathbf{k}\rangle \bigotimes_{\mathbf{k} \in S_-} |-, \mathbf{k}\rangle \bigotimes_{\mathbf{k} \in S_F} |F, \mathbf{k}\rangle \bigotimes_{\mathbf{k} \in S_E} |E, \mathbf{k}\rangle \quad (4.1)$$

$$= \prod_{\mathbf{k} \in S_+} M_{\mathbf{k}}^+ \prod_{\mathbf{k} \in S_-} M_{\mathbf{k}}^- \prod_{\mathbf{k} \in S_F} F_{\mathbf{k}} \prod_{\mathbf{k} \in S_E} E_{\mathbf{k}} |G\rangle, \quad (4.2)$$

where the four sets S_+ , S_- , S_F , and S_E are a partition of the Fermi sphere, with cardinalities N_+ , N_- , N_F , and N_E , respectively, which are constrained by the fact that the total electron number is conserved

$$N = N_+ + N_- + 2N_F. \quad (4.3)$$

In Eq. (4.2) we introduced new operators,

$$E_{\mathbf{k}} |G\rangle = c_{1,\mathbf{k}} |G\rangle \quad (4.4a)$$

$$F_{\mathbf{k}} |G\rangle = c_{2,\mathbf{k}+\bar{\mathbf{q}}}^\dagger |G\rangle \quad (4.4b)$$

$$M_{\mathbf{k}}^\pm |G\rangle = \frac{1}{\sqrt{2}}(c_{2,\mathbf{k}+\bar{\mathbf{q}}}^\dagger c_{1,\mathbf{k}} \pm 1) |G\rangle, \quad (4.4c)$$

which will be used equivalently to Eq. (3.3) and Eq. (3.4) of Chapter 3. By introducing in Eq. (4.4) operators acting directly onto the Fermi ground state $|G\rangle$, we can derive an algebra that will prove useful to calculate more easily the matrix elements relative to the asymmetric light-matter interaction. The eigenvalue of a given many-body state $|\psi\rangle$ in Eq. (4.1) is thus given by

$$\hbar\omega_\psi = \frac{\hbar\Omega}{2}(N_+ - N_-). \quad (4.5)$$

For further reference, it is useful to calculate the following operator products,

$$F_{\mathbf{k}} E_{\mathbf{k}} = \frac{M_{\mathbf{k}}^+ + M_{\mathbf{k}}^-}{\sqrt{2}}, \quad (4.6)$$

$$F_{\mathbf{k}} M_{\mathbf{k}}^\pm = \pm \frac{F_{\mathbf{k}}}{\sqrt{2}},$$

$$E_{\mathbf{k}} M_{\mathbf{k}}^\pm = \pm \frac{E_{\mathbf{k}}}{\sqrt{2}},$$

$$E_{\mathbf{k}} E_{\mathbf{k}} = F_{\mathbf{k}} F_{\mathbf{k}} = 0.$$

4.2.1 The light-matter coupling Hamiltonian

In order to calculate the photonic emission rate from dipolar transitions between the states of the pumped electronic system, we need to couple it to the electromagnetic field continuum. This can be accomplished by considering the full version of the Hamiltonian considered in Eq. (3.5), without any assumption on the symmetry of the dipole coupling,

$$\begin{aligned} H'_{\text{asym}} = & \sum_{\mathbf{k}, \mathbf{q}, q_z} (a_{-\mathbf{q}, q_z}^\dagger + a_{\mathbf{q}, q_z}) [\chi_{11, q, q_z} c_{1, \mathbf{k}+\mathbf{q}}^\dagger c_{1, \mathbf{k}} + \chi_{22, q, q_z} c_{2, \mathbf{k}+\mathbf{q}}^\dagger c_{2, \mathbf{k}} \\ & + \chi_{12, q, q_z} (e^{-i\omega_{12}t} c_{2, \mathbf{k}+\mathbf{q}}^\dagger c_{1, \mathbf{k}} + e^{i\omega_{12}t} c_{1, \mathbf{k}}^\dagger c_{2, \mathbf{k}-\mathbf{q}})], \end{aligned} \quad (4.7)$$

which is just the interaction introduced in Eq. (2.49) expressed in the frame rotating at the bare intersubband frequency, given by H_{el} in Eq. (2.46), for which the explicit expressions for the coupling coefficients are given in Eq. (2.50) and Eq. (2.51). An inspection of Eq. (4.7) reveals that, for $q \neq \bar{q}$, V couples subspaces corresponding to different values of \mathbf{k} in Eq. (3.2). Therefore, we cannot limit ourselves to treat each subspace independently and we must calculate the transition matrix elements while taking into account the full many-body nature of the problem.

There are two qualitatively different kinds of terms that can be identified in Eq. (4.7). The last two terms, whose coupling is proportional to the intersubband dipole, $e z_{12}$, where considered in Eq. (3.5) and give the emission centred on the unperturbed frequency ω_{12} , with the two satellite peaks at $\omega_{12} \pm \Omega$. In the following, we disregard these Mollow-like emission, which has been the subject of Chapter 3, and focus instead on the remaining part of the interaction Hamiltonian, that we rename V_{THz} ,

$$V_{\text{THz}} = \sum_{\mathbf{k}, \mathbf{q}, q_z} (\chi_{11, q, q_z} c_{1, \mathbf{k}+\mathbf{q}}^\dagger c_{1, \mathbf{k}} + \chi_{22, q, q_z} c_{2, \mathbf{k}+\mathbf{q}}^\dagger c_{2, \mathbf{k}})(a_{-\mathbf{q}, q_z}^\dagger + a_{\mathbf{q}, q_z}), \quad (4.8)$$

which is responsible for the asymmetry-induced THz emission. Notice that, using Eqs. (2.51) and (2.50), by a simple shift in the origin of the z axis, we can shift both χ_{11, q, q_z} and χ_{22, q, q_z} by the same amount, while keeping χ_{12, q, q_z} constant. We can thus simplify Eq. (4.8) into

$$V_{\text{THz}} = \sum_{\mathbf{k}, \mathbf{q}, q_z} \Delta \chi_{q, q_z} c_{2, \mathbf{k}+\mathbf{q}}^\dagger c_{2, \mathbf{k}} (a_{-\mathbf{q}, q_z}^\dagger + a_{\mathbf{q}, q_z}), \quad (4.9)$$

where $\Delta\chi_{q,q_z} = \chi_{22,q,q_z} - \chi_{11,q,q_z}$. Thanks to the fact that V_{THz} annihilates the ground state

$$V_{\text{THz}} |G\rangle |0_{\text{phot}}\rangle = 0, \quad (4.10)$$

matrix elements of V_{THz} between the different eigenstates of Eq. (4.1) can be easily calculated from the commutators of V_{THz} . Straightforward algebra gives

$$\begin{aligned} [V_{\text{THz}}, M_{\mathbf{k}}^{\pm}] &= \frac{1}{\sqrt{2}} \sum_{\mathbf{q}, q_z} \Delta\chi_{q,q_z} F_{\mathbf{k}+\mathbf{q}} E_{\mathbf{k}} (a_{-\mathbf{q}, q_z}^{\dagger} + a_{\mathbf{q}, q_z}), \\ [V_{\text{THz}}, F_{\mathbf{k}}] &= \sum_{\mathbf{q}, q_z} \Delta\chi_{q,q_z} F_{\mathbf{k}+\mathbf{q}} (a_{-\mathbf{q}, q_z}^{\dagger} + a_{\mathbf{q}, q_z}), \\ [V_{\text{THz}}, E_{\mathbf{k}}] &= 0. \end{aligned} \quad (4.11)$$

4.3 Emission rates

We have now all the tools we need to calculate the THz emission due to the asymmetric dipole. To this aim we employ Fermi's Golden Rule, Eq. (2.9),

$$\gamma^{\text{THz}} = \frac{2\pi}{\hbar^2} \sum_f |\langle \psi_f | V_{\text{THz}} | \psi_i \rangle|^2 \delta(\omega_i - \omega_f), \quad (4.12)$$

where the electronic part of the initial and final states, $|\psi_i\rangle$ and $|\psi_f\rangle$, are eigenstates of H'_0 with energies $\hbar\omega_i$ and $\hbar\omega_f$, respectively. We start by calculating the emission induced by V_{THz} in the simplest case in which all the electrons are cycling between the two subbands under the effect of the pump, and no electrons are blocked in double excitation states ($N_F = 0$). This assumption is supported by previous experiments, with limited asymmetry samples [45, 44, 194], where the fraction of electrons participating in the coherent Rabi oscillation has been estimated to be up to 90%. Although this assumption neglects the electrons that end up in blocked states due to the THz emission, including the latter does not alter the results significantly. Proving this, however, requires a rather cumbersome algebraic calculation which has been relegated to Appendix C.2.1 for the sake of simplicity. Using the notation of Eq. (4.1), we are thus considering emission starting from states of the form

$$|\psi_i\rangle = \prod_{\mathbf{k} \in S_+} M_{\mathbf{k}}^+ \prod_{\mathbf{k} \in S_-} M_{\mathbf{k}}^- |G\rangle |0_{\text{phot}}\rangle, \quad (4.13)$$

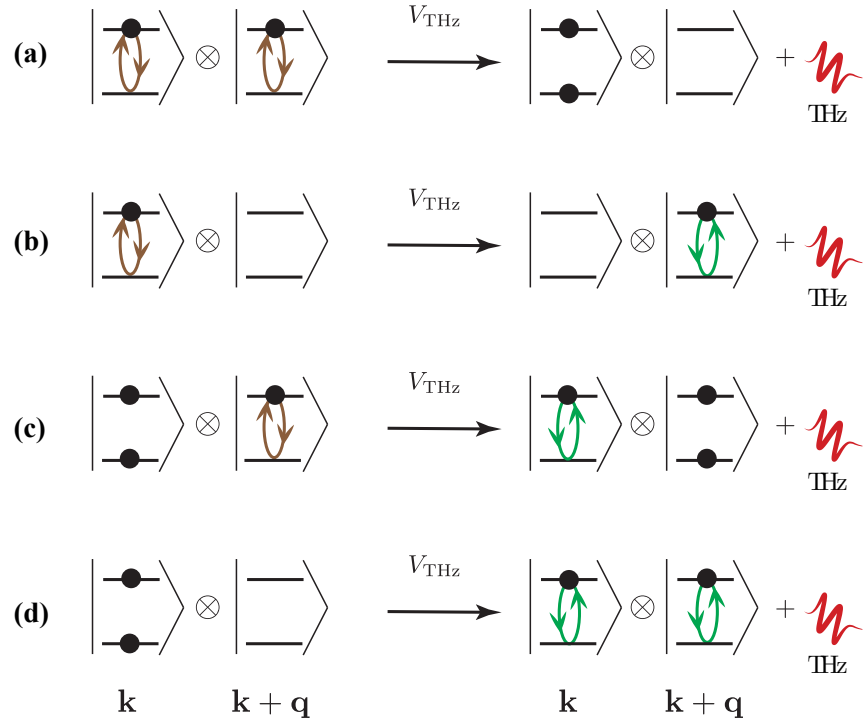


Fig. 4.3 (a)-(d): Scheme for the four resonant processes involved in the emission of THz photons. The two-site electronic states shown on the left, upon action of the Hamiltonian V_{THz} scatter in to the states on the right column and emit a photon of frequency Ω . All of the four processes contribute to the THz light emission of the resonantly pumped 2DEG. The processes in (a)-(c) involve, as starting state, at least one bright state (in which an electron is driven by the pump). The contribution to the last process, shown in (d), includes in the initial state a Pauli-blocked dark state $|F_{\mathbf{k}}\rangle$. As mentioned in the main text and shown in Appendix C.2.1, the contribution to γ_{THz} of this last process can be neglected.

whose energy we will call $\hbar\omega_i$. The effect of V_{THz} can be calculated by commuting it all the way to the right and using Eqs. (4.6), (4.10), and (4.11),

$$\begin{aligned}
 V_{\text{THz}} |\psi_i\rangle &= \frac{1}{\sqrt{2}} \sum_{\substack{\mathbf{k}, \mathbf{q}, q_z \\ \mathbf{k} \in S_+ + S_-}} \Delta \chi_{q, q_z} F_{\mathbf{k} + \mathbf{q}} E_{\mathbf{k}} \prod_{\mathbf{k}' \neq \mathbf{k}} M_{\mathbf{k}'}^{j_{\mathbf{k}'}} a_{-\mathbf{q}, q_z}^\dagger |G\rangle |0_{\text{phot}}\rangle \\
 &= \sum_{\substack{\mathbf{k}, \mathbf{q}, q_z \\ \mathbf{k}, \mathbf{k} + \mathbf{q} \in S_+ + S_-}} \frac{j_{\mathbf{k} + \mathbf{q}}}{2} \Delta \chi_{q, q_z} F_{\mathbf{k} + \mathbf{q}} E_{\mathbf{k}} \prod_{\substack{\mathbf{k}' \neq \mathbf{k}, \mathbf{k} + \mathbf{q}}} M_{\mathbf{k}'}^{j_{\mathbf{k}'}} a_{-\mathbf{q}, q_z}^\dagger |G\rangle |0_{\text{phot}}\rangle,
 \end{aligned} \tag{4.14}$$

where $j_{\mathbf{k}} = \pm$, and the sums and products over \mathbf{k} , here and in the following, are intended to be for $k < k_F$ unless otherwise specified. In Eq. (4.14) we have neglected border terms, when an electron inside the Fermi sphere is scattered to the outside of it. The latter involve only electrons at a distance q from the border of the Fermi sphere and are thus negligible given that $q/k_F \ll 1$. The r.h.s. of Eq. (4.14) is a sum of terms that we can recognize, from Eq. (4.1), to be the eigenstates of H'_0 . These states,

$$|\psi_f(\mathbf{k}, \mathbf{q}, q_z)\rangle = F_{\mathbf{k}+\mathbf{q}} E_{\mathbf{k}} \prod_{\mathbf{k}' \neq \mathbf{k}, \mathbf{k}+\mathbf{q}} M_{\mathbf{k}'}^{j_{\mathbf{k}'}} a_{\mathbf{q}, q_z}^\dagger |G\rangle |0_{\text{phot}}\rangle, \quad (4.15)$$

with energy

$$\hbar\omega_f(\mathbf{k}, \mathbf{q}, q_z) = \hbar\omega_i + \hbar\omega_{q, q_z} - \frac{\hbar\Omega}{2}[(j_{\mathbf{k}} 1) + (j_{\mathbf{k}+\mathbf{q}} 1)], \quad (4.16)$$

will thus be the available final states for the scattering process leading to THz emission. The term in the squared brackets of Eq. (4.16) is either 2, -2, or 0 since $j_{\mathbf{k}} 1 = \pm 1$. In particular, in order to satisfy energy conservation, from Eq. (4.16), the only final states giving rise to a photonic emission will be those with

$$j_{\mathbf{k}} = j_{\mathbf{k}+\mathbf{q}} = +. \quad (4.17)$$

At this point we can apply Fermi's Golden Rule to calculate the THz emission rate as

$$\gamma^{\text{THz}} = \frac{2\pi}{\hbar^2} \sum_{\mathbf{k}, \mathbf{q}, q_z} \frac{|\Delta\chi_{q, q_z}|^2}{4} \delta(\Omega - \omega_{q, q_z}), \quad (4.18)$$

from which one can check that the only matrix elements giving a non-zero contribution are those that respect Eq. (4.17). As we are assuming that all the electrons are cycling between the two subbands under the effect of the pump laser, on average one quarter of the states will respect such a condition. Given this, and the fact that the terms in the sum of Eq. (4.18) do not depend on \mathbf{k} , we can rewrite Eq. (4.18) as

$$\gamma^{\text{THz}} = \frac{N\pi}{8\hbar^2} \sum_{\mathbf{q}, q_z} |\Delta\chi_{q, q_z}|^2 \delta(\Omega - \omega_{q, q_z}). \quad (4.19)$$

Note that this result depends only on the average number of electrons in the $M_{\mathbf{k}}^\pm$ states, and not on their relative phases. The emission will thus be unaffected by electron dephasing, that would damp the coherence of the collective Rabi oscillations after only a few oscillations [44]. In the following, we use Eq. (4.19) to estimate the quantum efficiency of the THz emission process, both in the case of a free-space emitter and when using a THz cavity to enhance the emission rate.

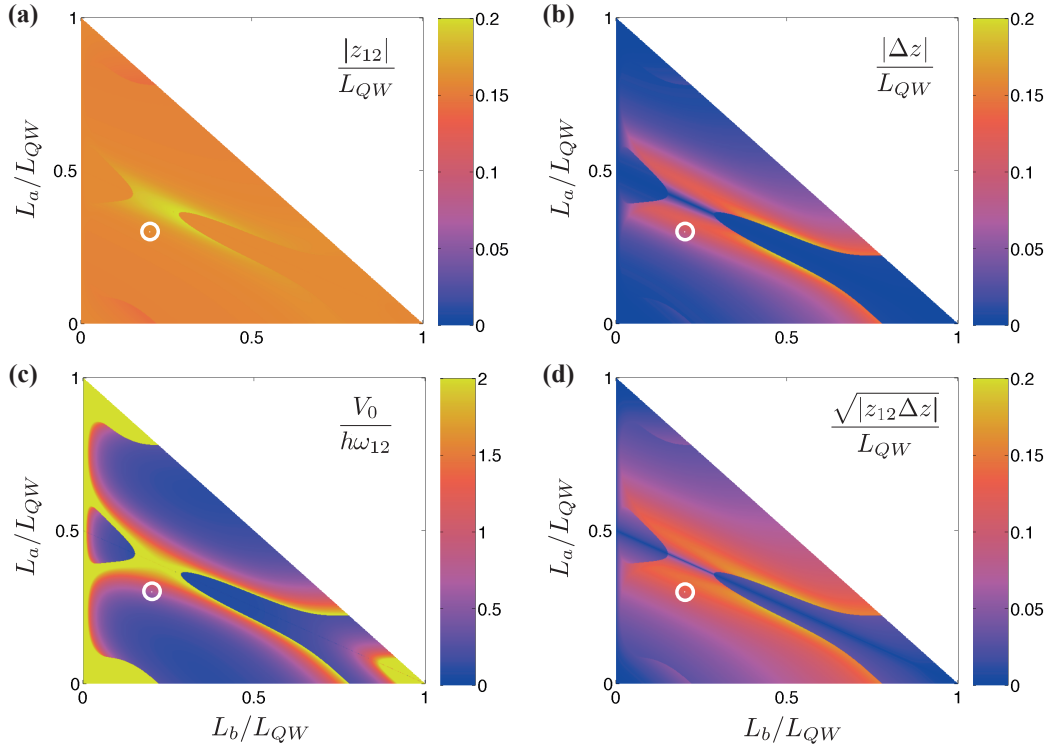


Fig. 4.4 Intersubband (a) and asymmetric (b) dipoles, obtained using the optimization procedure described in the text. In panels (c) and (d) we plot the optimal value of V_0 and of $|z_{12}\Delta z|$, respectively. A circle highlights the point in the parameter space that is used for the numerical estimates given in the main text.

4.3.1 Numerical results

In order to estimate the achievable THz emission rates, and assess the device's technological potentiality, we start here by studying a simple but realistic asymmetric QW structure. The exact degree of asymmetry will have to be chosen carefully; on the one hand, a small degree of asymmetry gives a large z_{12} , but a small Δz , and on the other, excessive asymmetry leads to a large Δz , but a vanishing z_{12} . An efficient THz emitter design must lie between these extremes, with an acceptably large intersubband dipole $e z_{12}$, in order to couple strongly to the pump beam, and a sizeable asymmetric dipole $e \Delta z$, to efficiently emit THz radiation.

A double QW structure, as shown in Figure 4.2(a), comprises a central barrier of height V_0 and width L_b , separating two potential wells of widths L_a and L_c , respectively. The overall QW, of total length L_{QW} , is asymmetric for $L_a \neq L_c$. Full details on the simulation methods are given in Appendix C.2.2.

We explore the parameter space by varying L_a , L_b , and V_0 , in order to maximize the value of $|z_{12}\Delta z|$. This figure of merit allows us to identify structures with sizeable values for both dipoles and, as we will see, the quantum efficiency of the THz emission explicitly depends upon this parameter. The optimization is performed keeping L_{QW} and $\hbar\omega_{12}$ fixed. This procedure thus mimics the search for an optimal structure given a fixed QW's length and pump laser frequency. In particular, we set $\hbar\omega_{12} = 125$ meV and $L_{\text{QW}} = 11.6$ nm, which is the length corresponding to the desired $\hbar\omega_{12}$ when $V_0 = 0$. The height of the central barrier V_0 is allowed to vary up to 250 meV, mindful of the barrier heights obtainable in $\text{Al}_x\text{Ga}_{1-x}\text{As}$ heterostructures. The panels (a) and (b) of Figure 4.4, show dipole values as a function of L_b and L_a , in units of L_{QW} . The corresponding height of the barrier, V_0 , and the value of the maximized figure of merit (normalized to facilitate comparison), are shown in panels (c) and (d). As expected, the asymmetric dipole Δz vanishes on the line $L_a/L_{\text{QW}} = \frac{1}{2}(1 - L_b/L_{\text{QW}})$, corresponding to a symmetric QW case.

For the sake of definiteness, and in order to make numerical estimates, henceforth we set the parameters $L_a = 0.3L_{\text{QW}}$, $L_b = 0.2L_{\text{QW}}$, denoted by the circled point in the parameter space in Figure 4.4, leading to $z_{12} = 0.18L_{\text{QW}}$ and $\Delta z = 0.11L_{\text{QW}}$. While larger values for the dipoles are obtainable in principle, we have chosen these values because they generate results that are stable over a fairly large section of the parameter space, making them robust against device fabrication tolerances. It is important to notice that these dipole values are almost one order of magnitude larger than the values obtainable in quantum dots, for similar emission frequencies, as those estimated in Ref. [182]. This is due to the fact that both the electron density n_{2DEG} and the asymmetric dipole $e\Delta z$ are generally larger in QWs compared to quantum dots.

4.3.2 Free-space emission rate

The free-space THz emission rate γ_0^{THz} of a single QW, per unit surface S , can be estimated directly from Eq. (4.19) with the expressions given by Eqs. (2.50) and (2.51), by transforming the sum over discrete photonic states into an integral,

$$\frac{\gamma_0^{\text{THz}}}{S} = \frac{n_{\text{2DEG}}e^2|\Delta z|^2\sqrt{\epsilon_r}}{12\epsilon_0\pi\hbar c^3}\Omega^3, \quad (4.20)$$

where we considered a QW doped with a uniform surface density $n_{\text{2DEG}} = N/S$. This formula has the same parameter dependency as the emission formula developed in Ref. [182] for emission from quantum dots. From Eq. (4.20), and from the fact that both the asymmetric dipole Δz and the dipole density n_{2DEG} of the structure we are

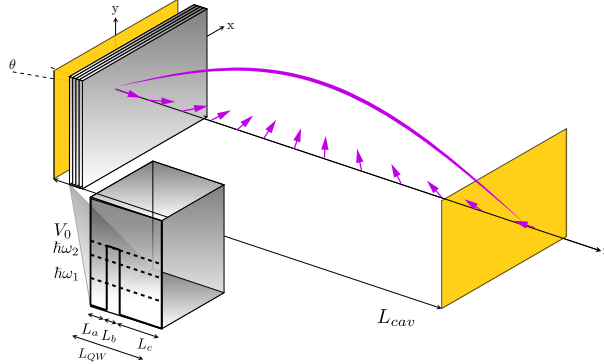


Fig. 4.5 Embedding the quantum well-structure into a sub-wavelength microcavity can be used to enhance the rate of THz emission through the Purcell effect.

considering are one order of magnitude larger than in the quantum dots case, we can expect an emission rate three orders of magnitude larger than in previous quantum dot-based proposals. *A posteriori* this confirms that QWs are an ideal testbed to observe intra-doublet emission.

The free-space quantum efficiency is then given by

$$\eta^0 = \frac{\hbar\omega_{12}N_{\text{QW}}\gamma_0^{\text{THz}}}{\mathcal{I}} = \frac{N_{\text{QW}}n_{\text{2DEG}}e^4|\Delta z|^2z_{12}^2\sqrt{\epsilon_r}\omega_{12}\Omega}{6\epsilon_0^2\pi\hbar^2c^4}, \quad (4.21)$$

where the device is made of N_{QW} identical QWs and $\mathcal{I} = \epsilon_0 c \mathcal{E}^2 / 2$ is the pump power density. The free-space efficiency for $N_{\text{QW}} = 50$ and $n_{\text{2DEG}} = 10^{12} \text{ cm}^{-2}$, and using the QW whose parameters are marked by a white circle in Figure 4.4, is plotted in Figure 4.6 (solid line) as a function of the pump power density, \mathcal{I} (lower horizontal axis), and of the emitted frequency Ω (upper horizontal axis). In particular, considering a pump of strength $\mathcal{I} = 8 \cdot 10^6 \text{ W cm}^{-2}$, from the expression of Ω , Eq. (2.17), one obtains $\Omega/2\pi = 1 \text{ THz}$, which is of the same order of those experimentally observed in Ref. [44]. The free-space quantum efficiency would be then $\eta^0 \simeq 10^{-10}$.

4.3.3 Cavity emission rate

In order to increase the THz emission rate, it is possible to embed the multiple-QW structure into a THz cavity [195]. Since an analysis of the different kinds of THz resonators is out of the scope of the present work, we will limit ourselves to the conceptually simple case of a planar THz cavity. A modification of Eq. (4.20), with a two-dimensional continuum of photonic modes according to Eq. (2.13) and infinitely

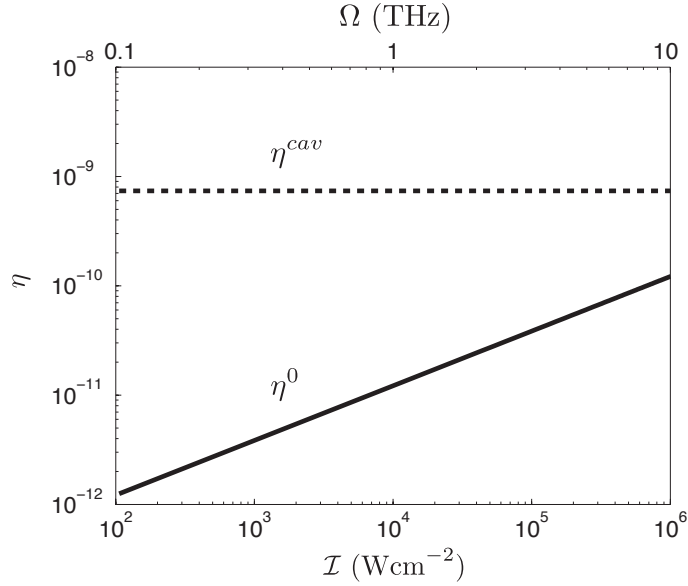


Fig. 4.6 Quantum efficiency for free space η^0 (solid line) and cavity emission η^{cav} (dashed line), as a function of the pump power density \mathcal{I} (lower axis) and of the Rabi frequency Ω (upper axis).

sharp resonance for the cavity then gives [196]

$$\frac{\gamma_{\text{cav}}^{\text{THz}}}{S} = \frac{n_{\text{2DEG}} e^2 |\Delta z|^2}{32 \hbar \epsilon_0 c^2 L_{\text{cav}}} \Omega^2, \quad (4.22)$$

where L_{cav} is the cavity length. The quantum efficiency accordingly becomes

$$\eta^{\text{cav}} = \frac{\hbar \omega_{12} N_{\text{QW}} \gamma_{\text{cav}}^{\text{THz}}}{\mathcal{I}} = \frac{N_{\text{QW}} n_{\text{2DEG}} e^4 |\Delta z|^2 z_{12}^2 \omega_{12}}{16 \epsilon_0^2 \hbar^2 c^3 L_{\text{cav}}}, \quad (4.23)$$

independent of the pump power in the parameter regime we are considering. Note that both η^0 and η^{cav} are proportional to $|z_{12} \Delta z|^2$ (the former only at given emission frequency). This justifies a posteriori our choice of using $|z_{12} \Delta z|$ as our optimisation parameter in Section 4.3.1. The efficiency gain using a two dimensional cavity is thus given by the Purcell factor [6], $F_P = \gamma_{\text{cav}}^{\text{THz}} / \gamma_0^{\text{THz}}$, i.e.

$$F_P = \frac{3\pi c}{8\sqrt{\epsilon_r} L_{\text{cav}} \Omega}. \quad (4.24)$$

To increase the emission efficiency at a fixed pump power it is thus convenient to reduce the cavity length L_{cav} . Present-day THz cavities allow for strong sub-wavelength confinement [197], using plasmonic or localized phonon-plasmon excitations [198, 199].

These cavities have demonstrated a linear confinement $\lambda_{\text{res}}/L_{\text{cav}} \simeq 200$, where λ_{res} is the free-space wavelength of the THz radiation, with quality factors in excess of 100. The cavity efficiency, η^{cav} , is independent on the pump strength, as shown in Figure 4.6 (dashed line); for the parameters chosen in the previous section, and a cavity length $L_{\text{cav}} = 1 \mu\text{m}$, we obtain $\eta^{\text{cav}} \simeq 10^{-9}$, which is competitive with fluorescence efficiency in monolithic THz emitters, with tunable frequencies [182].

4.4 Conclusions

We have shown how asymmetric artificial atoms can be exploited to obtain a resonant fluorescence THz peak from a transition that would normally be dipole-forbidden in centro-symmetric systems. We have developed a many-body theory that allows us to give a reliable estimate of the photon emission achievable in a realistic device, showing that the emission rate can be orders of magnitude larger than in previous quantum dot-based proposals. Numerical results of the attainable efficiency indicate that such an emission channel should be observable in present day experiments, and it could potentially be exploited to realize monolithic THz devices.

Chapter 5

Cooperative light emission in presence of dephasing and nonradiative decay

5.1 Introduction

In Chapter 2, and precisely in §2.1.5, it has been shown that a natural framework to study cooperative light emission is in terms of SU(2) collective spin operators and eigenstates, thanks to the mathematical equivalence of an ensemble of identical two-level systems with spin- $\frac{1}{2}$ particles. The use of Dicke states $|j, m\rangle$ greatly simplifies the description of the dynamics of the quantum system with respect to the light-matter interaction. If the system is initialised with a π -pulse, a $\frac{\pi}{2}$ -pulse, or in any superposition of the symmetrical Dicke states $|\frac{N}{2}, m\rangle$, out of the 2^N states of the total Hilbert space, only the subspace given by the Dicke ladder $j = \frac{N}{2}$ is explored, comprising only $N + 1$ non-degenerate symmetrical Dicke states, because the light-matter coupling preserves the cooperativity j .

Yet in any realistic implementation there are other couplings than a single photonic mode resonant with the transition frequency ω_0 . While the microscopic origin can vary – e.g., atom-atom scattering in an atomic cloud, phonon scattering in solid-state, etc. – the effects can, under appropriate approximations, be described in terms of dephasing and nonradiative decay. Pure dephasing destroys coherence at the rate γ_D and being energy-conserving, it does not change the energy eigenvalue m [200]. Nonradiative decay induces the incoherent de-excitation of a single TLS at a rate γ_{nr} and decreases the energy, $\Delta m < 0$, while also changing j . If we thus consider the simplest case of two

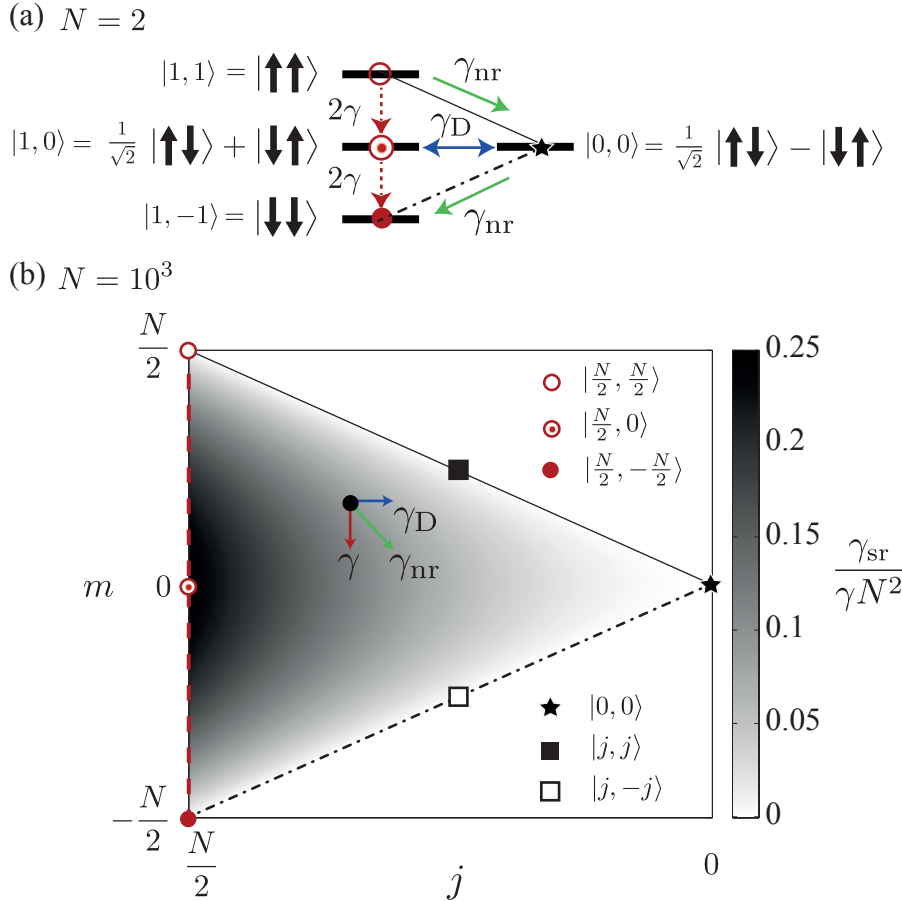


Fig. 5.1 (a): Emission scheme for $N = 2$; the singlet-triplet states $|j, m\rangle$ are connected with spontaneous emission rate γ , dephasing γ_D , and nonradiative emission γ_{nr} . (b): In the phase space of $N = 1000$ TLSs given by the cooperativity j (horizontal axis) and energy m (vertical axis), color plot of the photonic emission rate γ_{sr} in units of γN^2 is shown.

excited TLSs, shown in panel (a) of Figure 5.1, corresponding to the Dicke state $|1, 1\rangle$, nonradiative decay can prompt the two-body system to evolve into the subradiant state $|0, 0\rangle$ and eventually end up in the ground state $|1, -1\rangle$. For $N \gg 1$, this means that the fully inverted state can evolve along multiple trajectories confined in the triangle of Figure 5.1 (b) whose top, right and bottom vertices are given by the states $|\frac{N}{2}, \frac{N}{2}\rangle$, $|0, 0\rangle$, and $|\frac{N}{2}, -\frac{N}{2}\rangle$, respectively. Only in the case of pure superfluorescence the dynamics will be limited to the $N + 1$ states of the longest Dicke ladder, marked by the red dashed line in Figure 5.1 (b). In the opposite limiting condition, that is when the dynamics is dominated by γ_{nr} and γ_D , the system will mostly evolve along the solid and dot-dashed black lines that form the other sides of the triangle in Figure

5.1 (b). More generally though, depending on the relative ratio between $N\gamma$, γ_{nr} and γ_D , the incoherent processes will compete with superradiant light emission and drag the evolution of the system to trace trajectories that explore the area of the triangle. Since the general dynamics can involve any point of the Dicke space, it is worthwhile to reconsider the formula for the light emission rate from a Dicke state $|j, m\rangle$, already introduced in Eq. (2.36),

$$\gamma_{\text{sr}} = (j^2 + j - m^2 + m)\gamma, \quad (5.1)$$

which makes it evident that, while the light emission rate is maximum for the superradiant state $|\frac{N}{2}, 0\rangle$, for which $\gamma_{\text{sr}} \simeq \frac{N^2}{4}$, superradiant light emission can occur for a wide range of states $|j, m\rangle$ contained inside the perimeter of the triangular phase space, provided that $j \gg m$. This fact is highlighted in Figure 5.1 (b) in which a color plot shows the value of Eq. (5.1) for $N = 1000$, in units of γN^2 .

In the following we will thus give a general microscopic quantum treatment of cooperative light emission of N TLSs, with N arbitrarily large, including dephasing and nonradiative decay mechanisms. The choice of describing the evolution of the system in the (j, m) -space allows us to determine and visualise the evolution of the bare energy m and of the cooperativity j , while retaining the intuitive and powerful features of Dicke's formalism. In many of the theoretical research papers on the topic, the underlying microscopic dynamical models assume that j is conserved [2, 49, 59–69, 75, 77, 201]. There have been also works in which the cooperativity j is not assumed to be conserved [58, 202–204], yet their focus is not on studying how the dynamics of the system is affected in different regimes of the parameter space, as we will do in the following. Studies in which dephasing was considered or discussed more in depth dealt with the related phenomenon of optical bistability [70, 71, 78–80], in which a coherent field pumps continuously an ensemble of N TLSs or a dense optical medium, which is contained in a resonant cavity. The radiated field then shows an hysteresis cycle with respect to the driving field. States with $j < \frac{N}{2}$ have been studied for small N [205], for large N employing Monte Carlo methods [87, 96] and as mentioned, mainly in the regime of single-photon excitation, both theoretically [88–92] and experimentally [123, 206, 114]. More generally though, our study considers the full triangular Dicke space (m, j) and so it can be exploited to reassess the role of dark states at low and high excitation number. In condensed matter in general indeed dark states [144, 207, 208] are individuated as those orthogonal to the single bright superradiant transitions that in Dicke's formalism are the symmetrical Dicke states $|\frac{N}{2}, m\rangle$. As the number of excitations becomes greater than one, even in the dilute regime—that is $n \ll N$ and

thus in the lower part of the triangle of Figure 5.1 (b)—as the dark shading shows, only the states in the lower right diagonal side of the perimeter of the triangular spectrum, marked by the dot dashed line in Figure 5.1 (b), are completely subradiant.

In the following Section 5.2 we will provide the master equation to describe the general dynamics of the system. In Section 5.2.1 we will show how different decay rates appear in different points in the phase-space of the triangle in the plane of quantum numbers m and j . We make a second order approximation that allows us to obtain a closed set of equations for the dynamics of the system. In Section 5.3 we will explore the parameter space using these equations and compare our results with the existing results in the literature. On the basis of this data, in Section 5.4 a study of the feasibility of intersubband superfluorescence is performed. Concluding remarks are given in Section 5.5 while more details can be found in Appendix D.

5.2 Main theory

We consider N identical TLSs interacting with light and contained in a sample smaller than the light's wavelength. As we will show in Section 5.4 there are many systems in condensed matter for which this has become a feasible assumption. To describe the quantum dynamics, to the standard superradiant master equation Eq. (2.44) – which has already been introduced in Chapter 2 under the Born and Markov approximations and by tracing over the photonic degrees of freedom – two other sets of Linbladian terms,

$$\dot{\rho} = i\omega_0[\rho, J_z] + \gamma\mathcal{L}_{lm}[\rho] + \gamma_{nr}\mathcal{L}_{nr}[\rho] + \gamma_D\mathcal{L}_D[\rho], \quad (5.2)$$

so that also mechanisms for nonradiative emission and pure dephasing, proportional to γ_{nr} and γ_D , respectively, can be considered in the microscopic description of the dynamics. While the superradiant light emission is given by collective spin operators,

$$\mathcal{L}_{lm}[\rho] = J^- \rho J^+ - \frac{1}{2}(J^+ J^- \rho + \rho J^+ J^-), \quad (5.3)$$

both the nonradiative losses and pure dephasing terms are assumed to be at the single-site level. The nonradiative decay is given by

$$\mathcal{L}_{nr}[\rho] = \sum_i J_i^- \rho J_i^+ - \frac{1}{2}(J_i^+ J_i^- \rho + \rho J_i^+ J_i^-). \quad (5.4)$$

The last term in Eq. (5.2) accounts for pure dephasing, which we assume it too to occur at the single-site level,

$$\mathcal{L}_D[\rho] = \sum_i J_{z_i} \rho J_{z_i} - \frac{1}{2}(J_{z_i}^2 \rho - \rho J_{z_i}^2). \quad (5.5)$$

Eq. (5.2) will be the starting point of all of the following analysis and approximations, as it can be quite flexibly applied to different experimental implementations. For example ω_0 can include the Lamb shift [10] in case of an atomic system. The rate γ can refer to the free-space spontaneous emission or, in case the system is weakly coupled to an optical cavity, it can already include Purcell enhancement. Moreover, besides strictly nonradiative relaxation mechanisms, Eq. (5.4) can refer to light emission in modes other than the superradiant one.

We stress that in Eq. (5.2), among the superoperators, only the term $\mathcal{L}_{lm}[\rho]$ has collective operators, while $\mathcal{L}_{nr}[\rho]$ and $\mathcal{L}_D[\rho]$ have single TLS operators. While in Eq. (5.4) and in Eq. (5.5) the two terms $\sum_i^N J_{+i} J_{-i} = J_z + \frac{N}{2}$ and $J_{z_i}^2 = \frac{1}{4}$ can be expressed using collective spin operators, the first terms on the r.h.s. of the same equations cannot. This introduces a considerable challenge in the proposition of studying the dynamics in terms of Dicke states, because then it is not evident what the action of a TLS Pauli's operator means e.g., $J_{+i} |j, m\rangle$ requires the calculation of the full Hilbert space, and the advantages of Dicke's formalism seem to vanish. We will find different ways to tackle this problem. The first one is to calculate in each point of the triangular phase space of Figure 5.1 what are the rates of change of the cooperativity and bare energy of the collective system.

5.2.1 Emission rates

We can use Eq. (5.2) to project onto a pure Dicke state $\frac{d}{dt}m(t) = \langle j, m | \dot{\rho} J_z | j, m \rangle$ and do similarly for \mathbf{J}^2 . We obtain the exact equations

$$\frac{d}{dt}m(t) = -\gamma(j(t) + m(t))(j(t) - m(t) + 1) - \gamma_{nr}(\frac{N}{2} + m(t)) \quad (5.6a)$$

$$\begin{aligned} \frac{d}{dt}[j(t)(j(t) + 1)] &= -\gamma_D[j(t)(j(t) + 1) - \frac{N}{2} - m(t)^2] \\ &\quad - \gamma_{nr}[(N - 1)m(t) + m(t)^2 + j(t)(j(t) + 1) - N]. \end{aligned} \quad (5.6b)$$

Let us discuss some properties of Eq. (5.6). Since the dynamics of the system is dissipative, the total bare energy is bound to decrease with time and thus $\frac{d}{dt}m(t) \leq 0$ at any time, as one can see in Eq. (5.6a). The sign of Eq. (5.6b) instead is a function of j

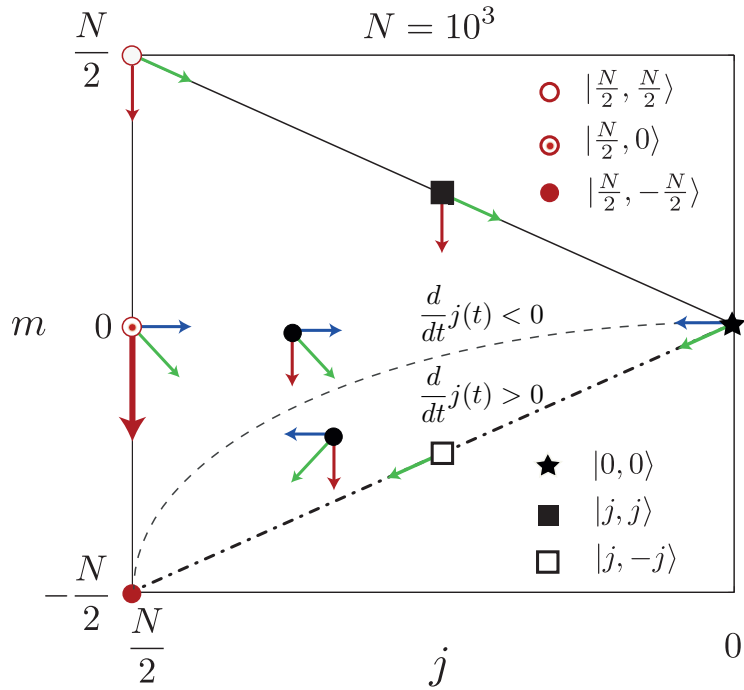


Fig. 5.2 Two different sections of the phase space are delimited by a grey dashed line: In the upper part, $\frac{d}{dt}j(t) < 0$, in the lower part $\frac{d}{dt}j(t) > 0$. Relative strengths of the light emission (red vertical arrow), pure dephasing (blue horizontal arrow) and nonradiative decay (green oblique arrow) are depicted for different Dicke states.

and m , and can be positive or negative depending on the point of the triangular space phase considered and the value of $\frac{\gamma_D}{\gamma_{nr}}$. In Figure 5.2 the boundary between the two areas for which $\frac{d}{dt}j(t) < 0$ and $\frac{d}{dt}j(t) > 0$ is shown for $N = 1000$ and $\frac{\gamma_{nr}}{\gamma_D} = 100$, as the greater this ratio, the greater the portion of the phase space for which $\frac{d}{dt}j(t) > 0$. In Figure 5.3 the two different portions of phase space are coloured in white for $\frac{d}{dt}j(t) < 0$ and in different shades of grey for $\frac{d}{dt}j(t) > 0$, whether $\frac{\gamma_{nr}}{\gamma_D} = 0.1$ (dark grey), $\frac{\gamma_{nr}}{\gamma_D} = 1$ (grey), $\frac{\gamma_{nr}}{\gamma_D} = 10$ (light grey), showing the effect on the dynamics of the system dependent on the relative strength of the couplings. We do not assume any hierarchy among γ_D , γ_{nr} , γ , and in Figure 5.2 report the contribution of each mechanism to the dynamics with a different colour code. Since we are interested in the limit $N \gg 1$, e.g. $N = 10^6$, we only assume that terms $\mathcal{O}(N^n)$ dominate over terms $\mathcal{O}(N^{n-1})$, with $n > 1$. For the

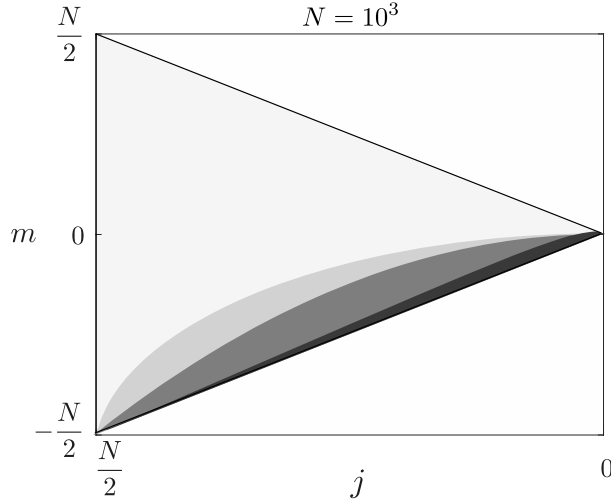


Fig. 5.3 For $N = 1000$ and $\gamma = 1$, $\gamma_{\text{nr}} = 10$, we highlight how the two different areas $\frac{d}{dt}j(t) < 0$ (white) and $\frac{d}{dt}j(t) > 0$ (different shades of grey) change with the ratio $\frac{\gamma_{\text{nr}}}{\gamma_D}$: $\frac{\gamma_{\text{nr}}}{\gamma_D} = 0.1$ (dark grey), $\frac{\gamma_{\text{nr}}}{\gamma_D} = 1$ (grey), $\frac{\gamma_{\text{nr}}}{\gamma_D} = 10$ (light grey).

state $|\frac{N}{2}, \frac{N}{2}\rangle$ (superfluorescence),

$$\begin{aligned} \frac{d}{dt}m(t) &\simeq -(\gamma + \gamma_{\text{nr}})N \\ \frac{d}{dt}j(t) &\simeq -\gamma_{\text{nr}}N. \end{aligned} \quad (5.7)$$

The rates in Eq. (5.7) apply also to $|\frac{N}{4}, \frac{N}{4}\rangle$ and other states on the upper diagonal. For the state $|\frac{N}{2}, 0\rangle$ (superradiance),

$$\begin{aligned} \frac{d}{dt}m(t) &\simeq -\gamma N^2 \\ \frac{d}{dt}j(t) &\simeq -(\gamma_D + \gamma_{\text{nr}})N, \end{aligned} \quad (5.8)$$

which shows the superradiant decay downwards but also the tendency to explore the inner area of the triangle phase space. For dark states, the dynamics is controlled by incoherent processes only. For the state $|0, 0\rangle$

$$\begin{aligned} \frac{d}{dt}m(t) &\simeq -\gamma_{\text{nr}}N \\ \frac{d}{dt}j(t) &\simeq (\gamma_D + \gamma_{\text{nr}})N \end{aligned} \quad (5.9)$$

while for the state $|\frac{N}{4}, -\frac{N}{4}\rangle$ and other states on the lower diagonal

$$\begin{aligned} \frac{d}{dt}m(t) &\simeq -\gamma_{\text{nr}}N \\ \frac{d}{dt}j(t) &\simeq \gamma_{\text{nr}}N. \end{aligned} \quad (5.10)$$

Both Eq. (5.9) and Eq. (5.10) show that subradiant states eventually decay into the ground state $|\frac{N}{2}, -\frac{N}{2}\rangle$.

5.2.2 Closed system dynamics

Another way to study the dynamics given by Eq. (5.2) is to calculate the average value of collective operators. In the most general way with regard to the collective spin algebra, we can define $X = J_+^p J_z^r J_-^q$, where $n, p, q \in \mathbb{N} + \{0\}$, and then calculate

$$\langle \dot{X} \rangle = \text{Tr}[\dot{\rho}X] \quad (5.11)$$

using Eq. (5.2) explicitly in terms of other normally-ordered collective operators $X' = J_+^{p'} J_z^{r'} J_-^{q'}$ [here and in the following we might use $\langle X \rangle$ short notation for $\langle X(t) \rangle$]. In order to obtain this result, we exploit some relations between sums of TLSs' spin operators and collective spin operators, reported in Appendix D.2.1. We are interested in the very basic properties of the system, conveyed already by $\langle J_z(t) \rangle$, the total average inversion, and $\langle \mathbf{J}^2(t) \rangle$, the average cooperativity, whose dynamics can be also be calculated using the identity

$$\mathbf{J}^2 = J_z^2 - J_z + J^+ J^-. \quad (5.12)$$

Yet even these simple operators couple to higher order momenta of the kind of X , in an infinite set of coupled equations. Now, although the coupling is to infinite order, the nonlinearity of the TLS actually helps us reducing the complexity of the problem. Indeed the real set of coupled equations is only of order N^2 [10], because the system saturates after N excitations and thus the action of terms containing J_\pm^p with $p > N$ gives zero, allowing us to close the system. Although this is a major difference with respect to sets of bosonic operators, this still remains a very complex system, especially for large N , which is a regime we wish to investigate. The only solution to further simplify the study of the dynamics given by Eq. (5.2) is to truncate the set of coupled equations by approximating the value of higher order momenta with products of lower momenta. This is indeed routinely done in many systems and is a path followed also in the semiclassical treatment of the standard superradiant master equation, Eq. (2.44),

for which the first-order approximation $\langle J_z^2 \rangle = \langle J_z \rangle^2$, allows to solve for $J_z(t)$ [this solution is reported in Appendix D.2.1.1.] By considering Eq. (5.11) for \mathbf{J}^2, J_z, J_z^2 and making a second order approximation for $\langle J_z^3 \rangle = \langle J_z \rangle \langle J_z^2 \rangle$ and $\langle J_z \mathbf{J}^2 \rangle = \langle J_z \rangle \langle \mathbf{J}^2 \rangle$, we obtain

$$\langle \dot{J}_z \rangle = -\gamma \langle J^+ J^- \rangle - \gamma_{\text{nr}} \left(\frac{N}{2} + \langle J_z \rangle \right) \quad (5.13a)$$

$$\begin{aligned} \langle \dot{J}_z^2 \rangle &= \gamma \left(\langle \mathbf{J}^2 \rangle - 2 \langle J_z \rangle \langle \mathbf{J}^2 \rangle + 2 \langle J_z \rangle \langle J_z^2 \rangle - 3 \langle J_z^2 \rangle + \langle J_z \rangle \right) \\ &\quad + \gamma_{\text{nr}} \left(\frac{N}{2} - (N-1) \langle J_z \rangle - 2 \langle J_z^2 \rangle \right) \end{aligned} \quad (5.13b)$$

$$\langle \dot{\mathbf{J}}^2 \rangle = \gamma_D \left(\frac{N}{2} + \langle J_z^2 \rangle - \langle \mathbf{J}^2 \rangle \right) + \gamma_{\text{nr}} (N - (N-1) \langle J_z \rangle - \langle J_z^2 \rangle - \langle \mathbf{J}^2 \rangle), \quad (5.13c)$$

which, plugging Eq. (5.12) into the first term on the r.h.s. of Eq. (5.13a), gives a closed system of only *three* first-order nonlinear differential equations in three variables.

Before proceeding with exploring the physics of the system using this result, we assess the robustness of the approximation by comparing approximate time evolutions obtained from Eq. (5.13) with the exact dynamics of Eq. (5.2). This can be done only for small N , since it requires the calculation in the TLS basis of the full density matrix, which is composed of $2^N \times 2^N$ elements. In Figure 5.4, $\langle J_z(t) \rangle$ and $\langle \mathbf{J}^2(t) \rangle$ are calculated for $N = 7$ with the exact linear equations (solid blue line) and compared to the approximated nonlinear quantities (dashed green line) derived by solving Eq. (5.13) numerically as a function of time. We plot them, for $\gamma = 1$, $\gamma_{\text{nr}} = 0.1$ and increasing dephasing rates $\gamma_D = 0.1$ (thinnest line), 1, 10, 100 (thickest line). As visible, there is very good agreement between the exact and approximated solutions. We point out that this second order approximation is effectively a mean-field approximation that is expected to improve with increasing N .

Moreover we assess if the second order approximation we make is better than a semiclassical first-order approximation. To do so we calculate $\langle J_z(t) \rangle$ and $\langle \mathbf{J}^2(t) \rangle$ using both methods and then compare the approximated quantities to the exact ones using a measure to compare two functions $f(t), g(t)$, such that $d(f, h) = \frac{\max_t |f(t) - g(t)|}{\max_{h=f,g} |h(t)|}$. In the two panels of Figure 5.5 there is a comparison between the (semiclassical) first order approximation $\langle X \rangle_I$ and the second order approximation we make in Eq. (5.13) $\langle X \rangle_{II}$. We plot $\epsilon(J_z) = d(\langle J_z \rangle, \langle J_z \rangle_I) - d(\langle J_z \rangle, \langle J_z \rangle_{II})$ and $\epsilon(\mathbf{J}^2) = d(\langle \mathbf{J}^2 \rangle, \langle \mathbf{J}^2 \rangle_I) - d(\langle \mathbf{J}^2 \rangle, \langle \mathbf{J}^2 \rangle_{II})$ for $N = 7$, $\gamma = 1$ in the phase space of γ_D and γ_{nr} . For both quantities, in all of the parameter space the second order approximation is better than the semiclassical first order approximation.

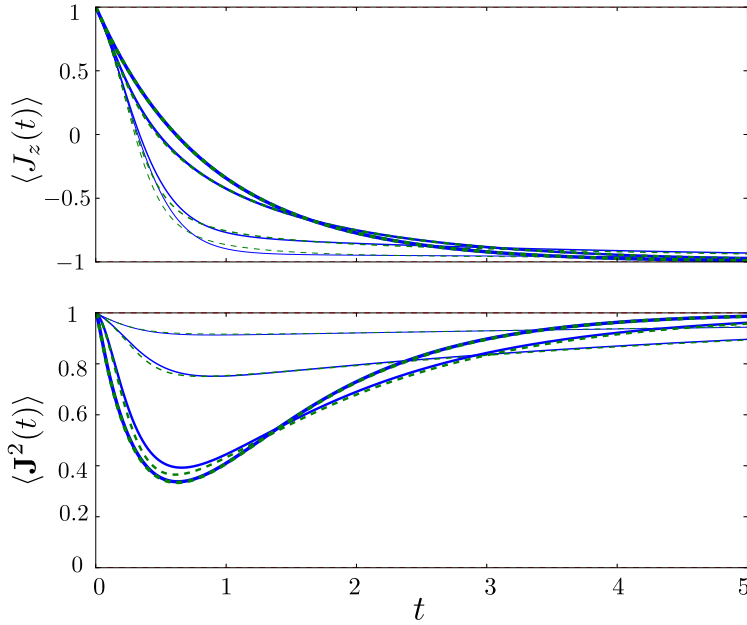


Fig. 5.4 $\langle J_z(t) \rangle$ in units of $\frac{N}{2}$ (top panel) and $\langle \mathbf{J}^2(t) \rangle$ in units of $\frac{N}{2}(\frac{N}{2} + 1)$ (bottom panel) as functions of t for $N = 7$. The plots of the exact quantities (blue solid line) and of the approximated quantities from the nonlinear equations (dashed green line) agree well. Here $\gamma_D = 0.1$ (thinnest), 1, 10, 100 (thickest), $\gamma_{nr} = 0.1$, $\gamma = 1$. Here $t_D = \log(7)/7 \simeq 0.12$.

5.3 Numerical study of superfluorescence

Thanks to Eq. (5.13), we are now in a position to study numerically the dynamics given by Eq. (5.2). We can vary the number of emitters N and the coupling strengths, γ , γ_D , and γ_{nr} . We focus on one initial condition in particular, when the system is initially in the fully excited state $|\frac{N}{2}, \frac{N}{2}\rangle$, to assess the feasibility of superfluorescence in regimes of strong dephasing and nonradiative decay. Since in general in solid state dephasing is faster than nonradiative emission, we will investigate the regime $\gamma_D \gg \gamma_{nr}, \gamma$.

We select two different quantities to characterise the cooperative nature of the light-emission dynamics. The first one is the delay time at which the peak of superradiant pulse appears, t_D . For the numerical simulations, we define operatively the delay time as the time at which $\langle J_z(t) \rangle = 0$, which also corresponds to the peak in light-emission if this is not at all prevented by the competing mechanisms. One can clearly see that this is analytically the case in the semiclassical limit, Eq. (D.25) of Appendix D.2.1.1. A color plot in the parameter space given by N and $\frac{N\gamma}{\gamma_D}$ is given in Figure 5.6 (a) normalised over t_0 which is the delay time when nonradiative effects dominate the

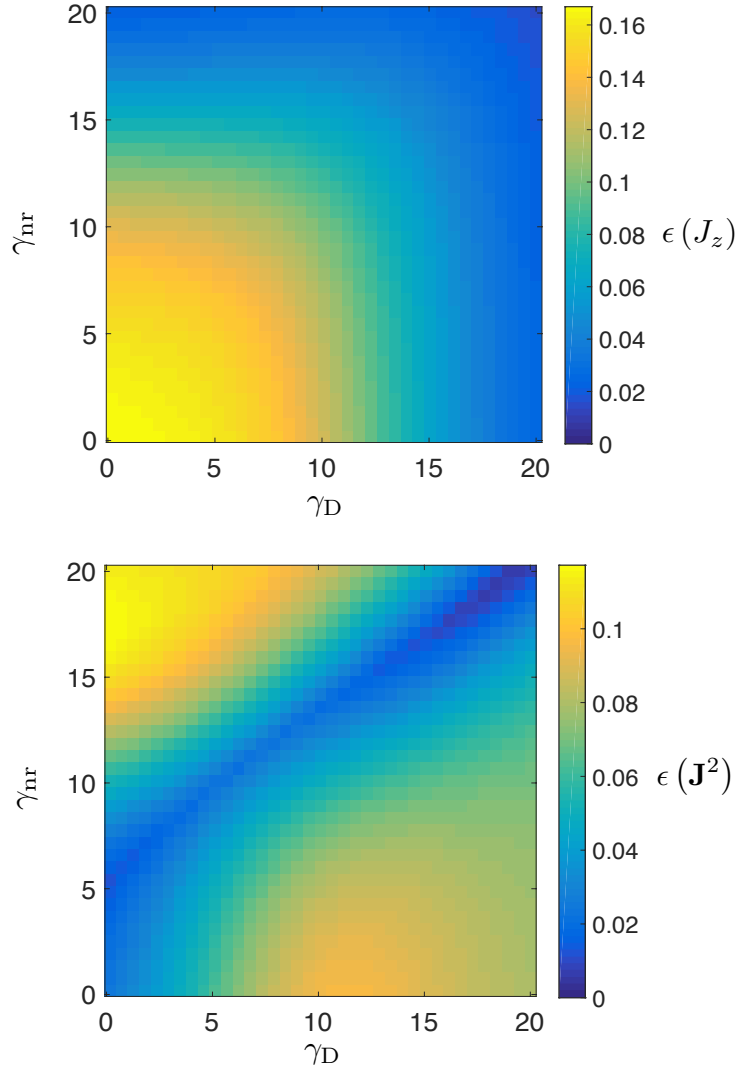


Fig. 5.5 Colour plots of $\epsilon(J_z)$ (top panel) and $\epsilon(\mathbf{J}^2)$ (bottom panel) for $N = 7$, in the phase space of γ_{nr} and γ_{D} , for $\gamma = 1$.

dynamics, $\langle J_z(t) \rangle \approx N \left(e^{-(\gamma_{\text{nr}} + \gamma_{\text{D}})t} - \frac{1}{2} \right)$, and $\langle J_z(t_0) \rangle = 0$, i.e. $t_0 = \log(2) (\gamma + \gamma_{\text{nr}})^{-1}$. The second figure of merit is the ratio r between the energy that is converted into light and the one that is lost nonradiatively, and that we can calculate by (numerically) integrating in time the first and the second terms on the r.h.s. of Eq. (5.13a), respectively. A colorplot of the intensity of r is shown in Figure 5.6 (b) in the same parameter space. Let us explain the choice of the grouping of the variables, that is why N on the vertical axis is compared to $\gamma N / \gamma_{\text{D}}$ on the horizontal one. In models in which dephasing is included, a condition [99–101] for the appearance of superfluorescence is

$T_2 \gg (t_D t_{sr})^{\frac{1}{2}}$, where t_{sr} is the time of the superradiance pulse, i.e. it can be quantified also by the FWHM of the pulse peak. In the large sample regime, for which $L \gg \lambda_0$, and which was accessed experimentally in Ref. [100], the delay time can be estimated as $t_D^{LS} = t_{sr}^{LS} \left(\frac{1}{4} \log(2\pi N) \right)^2$ and $t_{sr}^{LS} = \frac{8\pi S}{3\lambda_0^2} \frac{1}{\gamma N}$.

Assuming $A \simeq \lambda_0^2$ (small sample regime) as our formalism implies, we find

$$T_2 = (t_D^{LS} t_{sr}^{LS})^{\frac{1}{2}} \approx \frac{2 \log(2\pi N)}{\gamma N} \quad (5.14)$$

and using $T_2 = \gamma_D^{-1}$ we find the critical condition $N_c(x) = \frac{1}{2\pi} e^{x/2}$ with $x = \frac{N\gamma}{\gamma_D}$ for the occurrence of superfluorescence. We plot this as a dashed line and see that qualitatively this matches the onset of the superradiant emission regime.

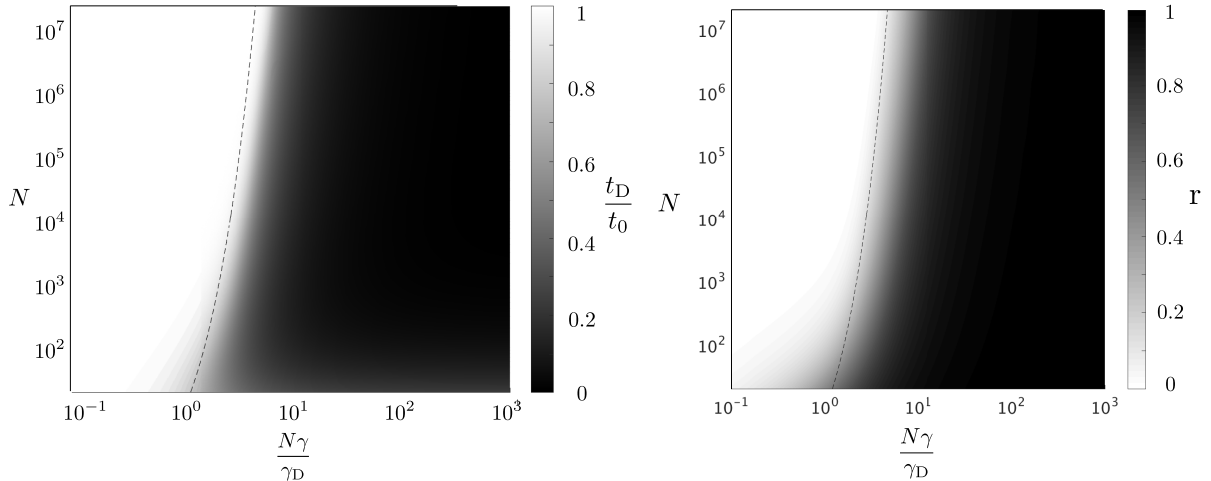


Fig. 5.6 Calculated (a) delay time t_D and (b) photonic ratio r in the parameter space given by $\frac{N\gamma}{\gamma_D}$ (horizontal axis) and N (vertical axis) for an initially fully inverted ensemble. A dashed line marks approximated analytical expression for t_D^{LS} .

5.4 Intersubband superfluorescence

The theory developed in the precedent section applies in general terms to a collection of N TLSs. More specifically, it can find applications in the case of electronic transitions in the solid state, in particular with reference to quantum dots. A large, but not extremely large, collection of quantum dots can be contained in a portion of space smaller than the resonance wavelength, the essential condition for the observation of cooperative light emission.

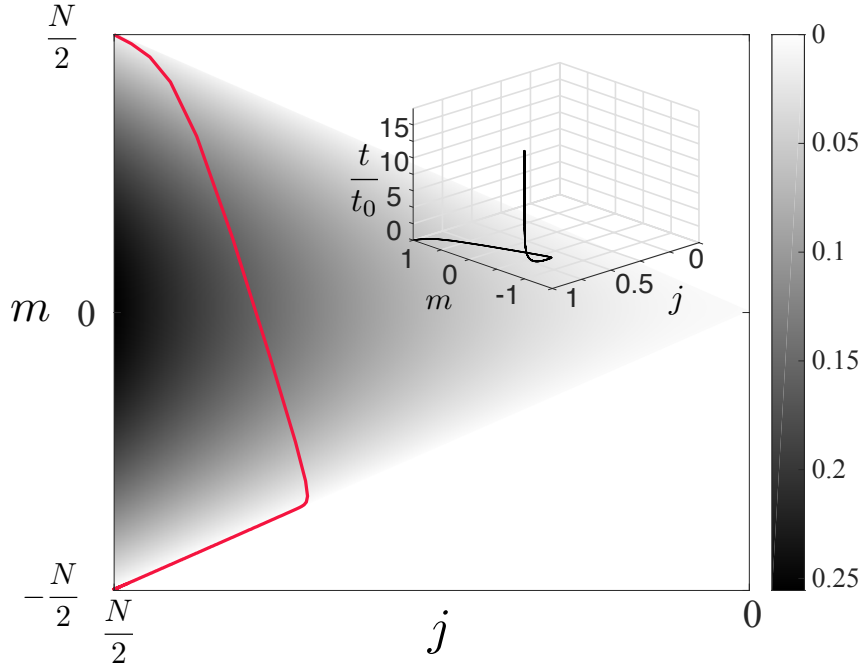


Fig. 5.7 Plot of the trajectory traced by a state experiencing suboptimal superfluorescence, in the phase space (j, m) with $N = 1000$, $\gamma = 1$, $\gamma_D = 100$, $\gamma_{nr} = 10$. The shading and the colorbar report the value of $\gamma_{sr}/(\gamma N^2)$. Inset: Time evolution of $\langle J_z(t) \rangle$, notice that $t_D/t_0 \approx 0.1$, with the axes of m and j normalised by $\frac{N}{2}$.

Not only excitonic interband transitions can be used to implement the TLSs in practice, but interestingly also intersublevel transitions of doped semiconductor quantum dots, with the appealing property that in this second case the wavelengths are longer and possibly fall in the THz regime [209]. Of course a major problem to overcome in this case would be the effective source that initialises the system in the highly excited superfluorescent state. As mentioned in Chapter 2 there is a substantial lack of such coherent THz sources in the first place, so that full inversion by electrical means could also be explored.

Another option available for the exploration of cooperative light emission in quantum dots (actually at the interface of quantum wells that represent effective zero-dimensional traps) is that of a large quantum dots in which multiple excitons are confined in each one[114].

Superradiant effects have been observed in undoped and doped QWs [57, 123], as discussed in the literature review of §2.1.5.6. Indeed we assess the feasibility of obtaining cooperative light emission from the ISBTs of a doped QW. While the formalism developed in this Chapter is certainly more apt to describe a collection of

excitonic TLSs, the crucial idea that here we bring forward is that the light-emission of ISBTs, studied in momentum space, can be compared to a collection of TLSs in real space. With a π -pulse of a laser it is then possible to coherently populate the second conduction subband. The electrons eventually thermalize through various mechanisms, which have been reviewed in Section 2.2.1. The TLS approximation is valid for ISBTs only when the in-plane momentum of the emitted photon, q , has an upper bound smaller than the resolution of the in-plane momentum of any two electrons in the 2DEG, Δk [163],

$$\frac{q}{\Delta k} < 1, \quad (5.15)$$

which is the opposite regime to the one necessary to observe, in case of continuous pumping, interference effects in the central peak of the Mollow triplet, Eq. (3.17). We determine the experimental conditions for which the l.h.s. of Eq. (5.15) is minimised. Since $q \leq q_{\text{tot}}$ and we can control $q_{\text{tot}} = \frac{\sqrt{\epsilon_r} \omega_{12}}{c}$, both ϵ_r and ω_{12} should be minimised. For the semiconductor materials used in the fabrication of QWs, typically $\sqrt{\epsilon_r} \simeq 3 - 4$ does not change consistently. Since $\omega_{12} \propto \frac{1}{L_{\text{QW}}^2}$, long QWs emitting in the far-infrared are preferable to short structures. The other variable that can be changed in Eq. (5.15) is Δk , which we assume to be estimated from the momentum-position uncertainty relation in high-quality samples. The finite size of the laser spot exciting the 2DEG localizes an area that gives an upper bound on the uncertainty of their position in the plane of growth of the QW. In the TLS regime, we can then define

$$J_{\mathbf{k}}^+ = c_{2,\mathbf{k}}^\dagger c_{1,\mathbf{k}} \quad (5.16)$$

$$J_{z_{\mathbf{k}}} = \frac{1}{2}(c_{2,\mathbf{k}}^\dagger c_{2,\mathbf{k}} - c_{1,\mathbf{k}}^\dagger c_{1,\mathbf{k}}) \quad (5.17)$$

and then $J^+ = \sum_{|\mathbf{k}| < k_F} J_{\mathbf{k}}^+$ and $J_z = \sum_{|\mathbf{k}| < k_F} J_{z_{\mathbf{k}}}$, so that we can map the ISBTs operators into the algebra of the collective spin operators and the theoretical treatment of the previous sections in terms of spin operators applies here. There are two crucial advantages of this system with respect to other solid-state systems such as quantum dots, a system that has already been thoroughly used to investigate cooperative light emission. The first one is that all quantum dots have different characteristics as they cannot be in principle identical TLSs—the 2DEG instead is characterized by the fact that all electrons can be considered undistinguishable and limitations depend mostly on the purity of the sample. The second key factor is that each ISBT representing a TLS excitation is formed of only a single electron: This allows much higher concentrations of TLSs per unit area in a QW than other nanostructures. In doped QWs the 2DEG

surface densities can be further increased with doping, $n_{\text{2DEG}} = 10^{11} - 10^{12} \text{ cm}^{-2}$, while the intersubband resonance frequency is lower than for interband transitions. This means that the concentration of emitters can be further increased to obtain many TLSs within a resonant wavelength, λ_{12} , ensuring the fact that the condition of the small sample regime of superradiance is fulfilled [2, 47]. While spontaneous photon emission typically occurs on picosecond to nanosecond timescale, incoherent intrasubband dynamics, i.e. dephasing, occurs on a shorter timescale (femtoseconds to picoseconds) and is characterized by Coulomb scattering, interface roughness scattering, and phonon scattering, as discussed in Section 2.2.1. If we consider a typical dephasing time of $\gamma_D^{-1} = 100 \text{ fs} = 10^{-13} \text{ s}$ and a spontaneous emission time of $\gamma^{-1} = 1 \text{ ns} = 10^{-9} \text{ s}$, then $\frac{\gamma}{\gamma_D} = 10^{-3}$, yet in a QW with $n_{\text{2DEG}} = 10^{12} \text{ cm}^{-2}$ in which the 2DEG is optically excited with a laser of waist $w \sim 10 \mu\text{m}$, this leads to $N \approx 10^6$ together with $\frac{N\gamma}{\gamma_D} = 10^3$: As visible in Figure 5.6, both figures of merit show that superfluorescence would occur. In Figure 5.7 we highlight how superfluorescent light emission can occur even in suboptimal conditions. We consider $N = 1000$, for $\gamma = 1$, $\gamma_D = 100$, $\gamma_{\text{nr}} = 10$ and thus $\frac{\gamma N}{\gamma_D} = 10$, just above the threshold for the onset of the cooperative behaviour. Indeed the system decays rapidly, with a time of the order of t_D into a subradiant state from which, in a second stage, the remaining excitation is released nonradiatively. In the inset of Figure 5.7 a plot in the Dicke phase space and time helps to appreciate the two timescales.

5.5 Conclusions

We have performed a study of cooperative light emission of a collection of N TLSs in the case in which, together with the superradiant emission channel, other incoherent mechanisms are significant. Pure dephasing and nonradiative decay have been introduced in a master equation that models the dynamics of the many-body quantum system. A second-order approximation leads to a closed system of only three equations, allowing us to study the dynamics for large ensembles. The numerical study focused on the feasibility of observing superfluorescence. Characteristic parameters of ISBTs point to the fact that superfluorescence could be observed. Our treatment of the cooperative dynamics can also apply to other solid-state systems, such as intersublevel transitions in quantum dots. An additional application would be that of superradiant THz emission, taking advantage of the fact that artificial atoms, and especially ISBTs in asymmetric quantum wells open up otherwise forbidden emission channels.

Further investigations instead could ascertain the role of Coulomb scattering on the superfluorescent dynamics.

Chapter 6

Conclusions

We have investigated characteristics of resonance fluorescence and cooperative light emission of intersubband transitions. Regarding resonance fluorescence, intersubband transitions map onto a collection of two-level systems quite naturally as long as they are driven and coherent phenomena determine the evolution of the many-body system. Yet as the spontaneous coupling to the free electromagnetic field is included, this simplified picture can break down. We have calculated the matrix elements relative to the photon scattering of this many-body system, showing that while the three-peaked structure of the Mollow triplet is conserved, the intensity of the central peak of the Mollow triplet varies, depending on the average coherence in the quasi-two-dimensional electron gas. This feature of the variable integrated fluorescence could indeed be used itself as a measure of the coherence of the quasi two-dimensional electron gas by optical means [163]. The fact that quantum wells can be designed with nanometric precision allows to explore with greater freedom the light-matter interaction, as asymmetric structures can be obtained that do not find a parallel in atomic systems or artificial atoms that can be described as symmetrical two-level systems. As we have shown, this opens up not only a fundamental paradigm in the study of light-matter interaction, but it can be used for interesting optoelectronic applications in the search for compact and tunable terahertz emitters [162].

Moreover, we have shown that even in the regime in which intersubband transitions map onto a collection of two-level systems, this is a physical system with very interesting properties with regard to cooperative light emission. Indeed the much sought after limit of Dicke's superradiance, in which a large number of two-level emitters are contained within a wavelength of the resonant light, finds here a new paradigm. We have explored the possibility to obtain the cooperative light-emission mechanism that is most challenging to observe—superfluorescence—and at the same time the most

intriguing one. From a purely fundamental perspective, the onset of superfluorescence is a beautiful example of the emergence of quantum coherence from spontaneous symmetry breaking [74]. Moreover on the applicative side, it is the easiest phenomenon to initialise, as it requires a system that is excited at saturation, something achievable with a π -pulse. Yet the delay time with which this phenomenon occurs, which can be longer than competing coherence-breaking mechanisms, hinders its observations. We have performed a comprehensive theoretical study to include such effects for a collection of two-level systems and verified numerically that superfluorescence can be observed in the parameter range given by intersubband transitions. The high electron densities that can be obtained in the limited area set by a wavelength of the resonant light make intersubband transitions a compelling platform for the verification of superfluorescence and superradiant effects. We hope that the investigations performed in this thesis will prompt experimental research aiming at verifying the effects.

Appendix A

Second quantization for intersubband transitions

A.1 Intersubband commutation relations

Second quantization is a useful quantum mechanics formalism for many-body systems [210], such as the 2DEG. The effect of applying a creation (destruction) operator to the state of the system is that of creating (destroying) a particle relative to that quantum number. Differently from first quantization, many-particle states of fermions (bosons) do not need to be antisymmetrized (symmetrized) by calculating *a posteriori* the Slater-determinant (permanent) of the total system. In second quantization such normalization is already natively taken into account by the formalism. The canonical anticommutation (commutation) relations between the creation and destruction operators take care of the fermionic (bosonic) nature of the particles. For the fermionic creation and destruction operators

$$\{c_{i,\mathbf{k}}, c_{j,\mathbf{k}'}^\dagger\} = \delta_{ij} \delta(\mathbf{k} - \mathbf{k}') , \quad (\text{A.1})$$

where i, j label a subband and \mathbf{k} the in-plane electronic momentum of a given electron. For the bosonic operators

$$[a_{\mathbf{q},q_z}, a_{\mathbf{q}',q'_z}^\dagger] = \delta(\mathbf{q} - \mathbf{q}') \delta(q_z - q'_z) , \quad (\text{A.2})$$

where \mathbf{q} and q_z are the in-plane and out-of-plane components of the photonic momentum.

With reference to the calculation techniques, mathematical expressions are simplified using the fact that the action of a fermionic creation operator on an occupied state

(and that of a fermionic destruction operator on an empty state) gives zero. In general, to simplify an expression in this way, the matrix element requires some reordering of the operators. This task involves performing commutation of pairs of operators, iterating it until the desired order e.g., normal order, is obtained. For this reason, instead of Eq. (A.1), it is often more useful the correspondent fermionic commutation relation,

$$[c_{i,\mathbf{k}}, c_{j,\mathbf{k}'}^\dagger] = 2c_{i,\mathbf{k}}c_{j,\mathbf{k}'}^\dagger - \delta_{ij}\delta(\mathbf{k} - \mathbf{k}') . \quad (\text{A.3})$$

A.2 Intersubband light-matter coupling

Incoherent photon emission can scatter electrons between states belonging to different Rabi doublets, as shown in Fig.(5.4) (b) by the dashed arrows. Under strong pumping, this effect gives rise to the Mollow triplet in the frequency fluorescence spectrum. The effect can be described considering a two-level system, $|\varphi\rangle = \{|\varphi_1\rangle, |\varphi_2\rangle\}$, interacting with the vacuum electric field \mathcal{E}_0 according to

$$V = -\mathbf{d} \cdot \mathcal{E}_0, \quad (\text{A.4})$$

where \mathbf{d} is the intersubband dipole moment. In symmetrical systems, only the off-diagonal terms $V_{ij} = \langle \varphi_i | V | \varphi_j \rangle$ with $i \neq j$, are non-zero. Recently however, it has been pointed out that the development in controlling the design of quantum emitters can be used to engineer asymmetric systems, where the parity of the eigenfunction is not well defined[182]. Then the optical transitions between the upper and lower state of each doublet are no more forbidden $\langle \varphi_i | V | \varphi_i \rangle \neq 0$, as shown in Figure 4.1. The dipole operator $\mathbf{d} = e\mathbf{r}$, where e is the electron charge, and $\mathbf{r} = (\mathbf{x}, z)$, can be written in second quantisation by projecting it on the electron states in the two subbands

$$\mathbf{r} = \sum_{\substack{\mathbf{k}, \mathbf{k}' \\ j, j' = \{1, 2\}}} \mathbf{r}_{j, \mathbf{k}}^{j', \mathbf{k}'} c_{j, \mathbf{k}}^\dagger c_{j', \mathbf{k}'} . \quad (\text{A.5})$$

The dipole matrix elements are determined by the in-plane symmetry of the system. The spatial wavefunction of an electron in the j -th subband is $\varphi_j(\mathbf{r}) = e^{i\mathbf{k} \cdot \mathbf{x}} \psi_j(z)$ and thus

$$\mathbf{x}_{j, \mathbf{k}}^{j', \mathbf{k}'} = \mathbf{x}_{\mathbf{k}}^{\mathbf{k}'} \delta_{j, j'} \quad z_{j, \mathbf{k}}^{j', \mathbf{k}'} = z_{jj'} \delta(\mathbf{k} - \mathbf{k}') \quad (\text{A.6})$$

with

$$\mathbf{x}_{\mathbf{k}'}^{\mathbf{k}'} = \int e^{i(\mathbf{k}-\mathbf{k}') \cdot \mathbf{x}} d\mathbf{x} \quad z_{ij} = \int \psi_i^*(z) z \psi_j(z) dz. \quad (\text{A.7})$$

From Eq. (A.6) we can see that only the z component of the field can see the asymmetry, and as such, as usual for ISBTs, we can consider just a transverse magnetic (TM) polarised field, whose z component is given by

$$\mathcal{E}_{0z} = \sum_{\mathbf{q}, q_z} \mathcal{E}_0(q, q_z) e^{i\mathbf{q} \cdot \mathbf{r}} (a_{q_z, -\mathbf{q}}^\dagger + a_{q_z, \mathbf{q}}) \sin \theta \mathbf{e}_z, \quad (\text{A.8})$$

where \mathbf{e}_z is a unit vector, θ is the angle with the z -axis, $\mathcal{E}_0(q, q_z) = (\hbar \omega_{q, q_z} / 2\epsilon_0 \epsilon_r \mathcal{V})^{1/2}$ is the field amplitude, $\omega_{q, q_z} = c \sqrt{q^2 + q_z^2} / \sqrt{\epsilon_r}$, where c is the speed of light, \mathcal{V} is the quantisation volume, and ϵ_0 and ϵ_r are the absolute and relative permittivity.

Appendix B

Intersubband resonance fluorescence

In this Appendix we give the step-by-step calculations of the Rabi oscillations visibility, in Section B.1, and of the resonance fluorescence photon emission rate, in Section B.2, used in Chapter 3.

B.1 Visibility of the collective Rabi oscillations

The fraction of electrons in the second subband can be calculated from the evolved electronic state in Eq. (3.8) as

$$n_2(t) = \frac{1}{N} \langle \psi_{\text{el}}(t) | \sum_{\mathbf{k}} c_{2,\mathbf{k}}^\dagger c_{2,\mathbf{k}} | \psi_{\text{el}}(t) \rangle = \frac{1}{N} \sum_{\mathbf{k}} \sin^2 \left(\frac{\phi_{\mathbf{k}} - \Omega t}{2} \right) \stackrel{\text{IID}}{=} \langle \sin^2 \left(\frac{\phi - \Omega t}{2} \right) \rangle, \quad (\text{B.1})$$

where N is the total number of electrons. In the last passage of Eq. (B.1) we assumed that the phases $\phi_{\mathbf{k}}$ are independent identically distributed (IID) random variables, so that $\frac{1}{N} \sum_{\mathbf{k}} g(\phi_{\mathbf{k}}) = \langle g(\phi) \rangle$ for any function $g(\phi)$.

Assuming that Rabi oscillations are faster than dephasing, their visibility can be operationally quantified as the difference between the maximum and the average of the population oscillations, that is

$$C = 2 \left(\max_t n_2(t) - \frac{1}{2} \right), \quad (\text{B.2})$$

where we chose the normalisation factor in order to have $0 \leq C \leq 1$. Inserting Eq. (B.1) in Eq. (B.2) and developing the sine we obtain

$$\begin{aligned} C &= 2 \max_t [\langle \sin^2 \left(\frac{\phi - \Omega t}{2} \right) \rangle] - 1 \\ &= 2 \max_t [-(\langle \cos^2 \frac{\phi}{2} \rangle \cos^2 \frac{\Omega t}{2} + \langle \sin^2 \frac{\phi}{2} \rangle \sin^2 \frac{\Omega t}{2} + \frac{1}{2} \langle \sin \phi \rangle \sin \Omega t)] + 1. \end{aligned} \quad (\text{B.3})$$

The maximum over time can be found by taking the time derivative of the expression between the square brackets in Eq. (B.3) and by imposing it equal to zero, that is

$$\langle \sin \phi \rangle \cos \Omega t + \left(\langle \sin^2 \frac{\phi}{2} \rangle - \langle \cos^2 \frac{\phi}{2} \rangle \right) \sin \Omega t = 0, \quad (\text{B.4})$$

which is satisfied for

$$\Omega t = \arctan \left(\frac{\langle \sin \phi \rangle}{\langle \cos^2 \frac{\phi}{2} \rangle - \langle \sin^2 \frac{\phi}{2} \rangle} \right). \quad (\text{B.5})$$

After some straightforward algebra Eq. (B.3) can thus be rewritten in its final form as

$$C = \sqrt{\langle \cos \phi \rangle^2 + \langle \sin \phi \rangle^2}. \quad (\text{B.6})$$

Let us discuss qualitatively how the electron coherence of the system changes over time in a typical experiment of continuous pumping. At $t = 0$ all electrons lie in the first subband and we can assume that all $\phi_{\mathbf{k}} = 0$, as shown graphically in Fig. 3.2(a). As the pump is switched on, the electrons start oscillating and for $t \ll \tau_{\text{coh}}$ relative phases will not have diffused much, as shown in Fig. 3.2(b). Their distribution will thus be strongly peaked around a well defined value $\bar{\phi}$, and the average values in Eq. (B.6) will effectively reduce to evaluate the functions at $\bar{\phi}$: $C = \sqrt{\cos^2 \bar{\phi} + \sin^2 \bar{\phi}} = 1$, for any value of $\bar{\phi}$. At times comparable to the coherence time, $t \approx \tau_{\text{coh}}$, with the pump still illuminating the system, more electrons will have been involved in incoherent scattering processes, as visible in Fig. 3.2(c), decreasing the visibility of the Rabi oscillations. Finally, for times much longer than the coherence time, $t \gg \tau_{\text{coh}}$, the phases of the different electrons will be completely randomized, as schematized by Fig. 3.2(d). In this case the phase averages in Eq. (B.6) will be over an uniform distribution, $\langle \cos \phi \rangle = \langle \sin \phi \rangle = 0$, leading to $C = 0$.

B.2 Photon emission rate

In order to describe the fluorescence we use the Hamiltonian of the free electromagnetic field, Eq. (2.2), The coupling between the electromagnetic field and the ISBT is given

in the rotating wave approximation by the interaction term

$$V = \sum_{\mathbf{k}, \mathbf{q}, q_z} \chi_{q, q_z} (c_{2, \mathbf{k}+\mathbf{q}}^\dagger c_{1, \mathbf{k}} a_{\mathbf{q}, q_z} + c_{1, \mathbf{k}}^\dagger c_{2, \mathbf{k}+\mathbf{q}} a_{\mathbf{q}, q_z}^\dagger), \quad (\text{B.7})$$

that in the rotating frame, and in interaction representation with respect to $H_{\text{phot}} + H'$, becomes

$$V(t) = \sum_{\mathbf{k}, \mathbf{q}, q_z} \chi_{q, q_z} e^{i(\omega_{12} - \omega_{q, q_z})t} e^{iH't/\hbar} c_{2, \mathbf{k}+\mathbf{q}}^\dagger c_{1, \mathbf{k}} a_{\mathbf{q}, q_z} e^{-iH't/\hbar} + \text{H.c.} \quad (\text{B.8})$$

The rate of emitted photons from the system, γ_{Mol} , can be calculated by dividing the total number of emitted photons by the interaction time

$$\gamma_{\text{Mol}} = \frac{N_{\text{phot}}(t)}{t} = \frac{1}{t} \langle \psi(t) | \sum_{\mathbf{q}, q_z} a_{\mathbf{q}, q_z}^\dagger a_{\mathbf{q}, q_z} | \psi(t) \rangle, \quad (\text{B.9})$$

where $|\psi(t)\rangle$, the total system wave vector in interaction representation, can be obtained by calculating to first order in V the evolution of the electronic state in Eq. (3.7) and of the photonic vacuum, $|0_{\text{phot}}\rangle$

$$|\psi(t)\rangle = |\psi_{\text{el}}(0)\rangle \otimes |0_{\text{phot}}\rangle - \frac{i}{\hbar} \int_{-t/2}^{t/2} V(\tau) |\psi_{\text{el}}(0)\rangle \otimes |0_{\text{phot}}\rangle d\tau. \quad (\text{B.10})$$

Using Eq. (B.8) and Eq. (B.10), the photon population can be calculated as

$$N_{\text{phot}}(t) = \frac{1}{\hbar^2} \iint_{-t/2}^{t/2} d\tau d\tau' \langle \psi(0) | V(\tau) \sum_{\mathbf{q}, q_z} a_{\mathbf{q}, q_z}^\dagger a_{\mathbf{q}, q_z} V(\tau') | \psi(0) \rangle, \quad (\text{B.11})$$

and after some straightforward algebra Eq. (B.9) can be rewritten explicitly as

$$\gamma_{\text{Mol}} = \frac{1}{4\hbar^2 t} \sum_{\mathbf{k}, \mathbf{q}, q_z} |\chi_{q, q_z}|^2 \left| \int_{-t/2}^{t/2} e^{i(\omega_{12} - \omega_{q, q_z})\tau} f_{\mathbf{k}, \mathbf{q}}(\tau) d\tau \right|^2, \quad (\text{B.12})$$

with $f_{\mathbf{k}, \mathbf{q}}(\tau) = \cos\left(\frac{\phi_{\mathbf{k}} + \phi_{\mathbf{k}+\mathbf{q}}}{2} - \Omega\tau\right) - \cos\left(\frac{\phi_{\mathbf{k}} - \phi_{\mathbf{k}+\mathbf{q}}}{2}\right)$. The integrand in Eq. (B.12) contains only phase factors linear in τ and as such, for long enough times, Eq. (B.12) will be given by a sum of squared Dirac delta-like functions. Using the usual trick of formally transforming $\delta(\omega)^2 = \delta(0)\delta(\omega) = \frac{t\delta(\omega)}{2\pi}$, we obtain

$$\begin{aligned} \gamma_{\text{Mol}} = & \frac{\pi}{8\hbar^2} \sum_{\mathbf{k}, \mathbf{q}, q_z} |\chi_{q, q_z}|^2 [4 \cos^2\left(\frac{\phi_{\mathbf{k}} - \phi_{\mathbf{k}+\mathbf{q}}}{2}\right) \delta(\omega_{q, q_z} - \omega_{12}) \\ & + \delta(\omega_{q, q_z} - (\omega_{12} + \Omega)) + \delta(\omega_{q, q_z} - (\omega_{12} - \Omega))]. \end{aligned} \quad (\text{B.13})$$

We assume that the phases are IID random variables. The sum over \mathbf{k} of the only term depending on \mathbf{k} in Eq. (B.13) thus becomes

$$\begin{aligned} \frac{1}{N} \sum_{\mathbf{k}} 4 \cos^2\left(\frac{\phi_{\mathbf{k}} - \phi_{\mathbf{k}+\mathbf{q}}}{2}\right) &= \frac{1}{N} \sum_{\mathbf{k}} 2(1 + \cos \phi_{\mathbf{k}} \cos \phi_{\mathbf{k}+\mathbf{q}} + \sin \phi_{\mathbf{k}} \sin \phi_{\mathbf{k}+\mathbf{q}}) \\ &\stackrel{IID}{=} 2(1 + \langle \cos \phi \rangle^2 + \langle \sin \phi \rangle^2). \end{aligned} \quad (\text{B.14})$$

Finally, inserting Eq. (B.14) into Eq. (B.13), and exploiting Eq. (B.6), we obtain

$$\gamma_{\text{Mol}} = \frac{1}{8}(1 + C^2)\gamma_0(\omega_{12}) + \frac{1}{16}\gamma_0(\omega_{12} + \Omega) + \frac{1}{16}\gamma_0(\omega_{12} - \Omega), \quad (\text{B.15})$$

with $\gamma_0(\omega)$ being the spontaneous emission rate of N two-level systems with bare frequency ω , given in Eq. (2.12). Notice that, for long times $t \gg \tau_{\text{coh}}$, $C = 0$ and we recover $\gamma_{\text{Mol}} \simeq \frac{\gamma_0(\omega_{12})}{4}$ where, as discussed in Ref. [162], the factor $\frac{1}{4}$ comes from the fact that both the initial and the final state have average and uncorrelated filling factors $\frac{1}{2}$.

Appendix C

Light-matter coupling in asymmetric systems

In this Appendix we give more details on light-matter coupling when asymmetric electronic potentials are used to break the symmetry of the emitter and open up new light-emission mechanisms. We start by reviewing in Section C.1 the physics of polarization in atomic systems, with a comparison between the static, §C.1.1, and the dynamical (or ac) Stark effect. In Section C.2 some calculations and methods used in Chapter 4 are reported. In §C.2.1, the general eigenstates used for the calculation of light-emission transition rates are calculated. In §C.2.2 the calculation of the electronic eigenfunctions in an asymmetric QW structure as the one used in the simulations of Chapter 4.

C.1 Polarizability in atomic systems

C.1.1 The static Stark effect

Atoms were historically the first system in which quantum optics experiments have been performed [24]. Although atomic systems are centro-symmetric, their symmetry can be broken, for example by applying a static electric field. Indeed, the point-like nucleus and the electronic cloud rearrange their spatial dislocation in order to eliminate the force induced by the field. A similar and simpler setting can be described classically, when a charged sphere is placed in an external electric field. The electric field induces a dipole moment into the system, as the single charges rearrange in order to minimize the potential energy. Of course this problem on an atomic level needs to be treated in the context of quantum theory.

The coupling of the atom with an external, static electric field is described by the interaction Hamiltonian

$$V = - \mathbf{d} \cdot \boldsymbol{\mathcal{E}}_{\text{stat}}, \quad (\text{C.1})$$

where \mathbf{d} is the dipole induced by the field. The problem can be treated perturbatively with regard to the atomic Hamiltonian, H_0 , since the energy correction is several orders of magnitude smaller than the eigenfrequencies, $\hbar\omega_n$, which form a discrete energy spectrum. Up to first order in perturbation, the interaction will transform the unperturbed orbital, $|n^{(0)}\rangle$, into

$$|n\rangle = |n^{(0)}\rangle + \sum_{k \neq n} \frac{\langle k^{(0)} | \mathbf{d} | n^{(0)} \rangle \cdot \boldsymbol{\mathcal{E}}_{\text{stat}} | k^{(0)} \rangle}{\hbar\omega_{nk}}, \quad (\text{C.2})$$

where $\hbar\omega_{nm} = \hbar\omega_n - \hbar\omega_m$ gives the difference in energy between the unperturbed orbitals $|n^{(0)}\rangle$ and $|m^{(0)}\rangle$. There is no first-order energy correction due to the static Stark effect, and the splitting, also known in the literature as Stark shift [211], is given by the second order correction, being it quadratic in the field strength,

$$E_n^{(2)} = -\frac{1}{2}\alpha_n \boldsymbol{\mathcal{E}}_{\text{stat}}^2, \quad (\text{C.3})$$

where we introduced the electric polarizability for a state $|n\rangle$,

$$\alpha_n = \sum_{k \neq n} \frac{2|\langle k^{(0)} | \mathbf{d} | n^{(0)} \rangle|^2}{\hbar\omega_{kn}}. \quad (\text{C.4})$$

Assuming that the dipole is parallel to the field, up to first order, its matrix elements are given by

$$\begin{aligned} \langle n | d | m \rangle &= \langle n^{(0)} | d | m^{(0)} \rangle + \sum_{k \neq n} \frac{\langle n^{(0)} | d | k^{(0)} \rangle \boldsymbol{\mathcal{E}}_{\text{stat}} \langle k^{(0)} | d | m^{(0)} \rangle}{\hbar\omega_{nk}} \\ &\quad + \sum_{k' \neq m} \frac{\langle k'^{(0)} | d | m^{(0)} \rangle \boldsymbol{\mathcal{E}}_{\text{stat}} \langle n^{(0)} | d | k'^{(0)} \rangle}{\hbar\omega_{mk'}}. \end{aligned} \quad (\text{C.5})$$

C.1.1.1 TLS approximation

In most cases, Eq. (C.5) can be simplified by assuming that the atom is a TLS, so that the dipole matrix elements for the transition dipole between the two different states,

$m \neq n$, are given only by

$$\begin{aligned}\langle n | d | m \rangle &\simeq \langle n^{(0)} | d | m^{(0)} \rangle + \frac{\langle n^{(0)} | d | m^{(0)} \rangle \mathcal{E}_{\text{stat}}}{\hbar \omega_{nm}} (\langle m^{(0)} | d | m^{(0)} \rangle - \langle n^{(0)} | d | n^{(0)} \rangle) \\ &= \langle n^{(0)} | d | m^{(0)} \rangle,\end{aligned}\quad (\text{C.6})$$

since we assumed that the unperturbed basis' states have well-defined parity, leading to

$$\langle k^{(0)} | d | k^{(0)} \rangle = 0, \quad \forall k. \quad (\text{C.7})$$

Thus, in the case of a TLS, Eq. (C.4) reduces to

$$\alpha_n = \frac{2|d_{nm}^{(0)}|^2}{\hbar \omega_{mn}}, \quad (\text{C.8})$$

where we introduced the notation $d_{nm}^{(0)} = \langle n^0 | d | m^{(0)} \rangle$.

C.1.1.2 General dipole term

The result for a TLS given in Eq. (C.6) can be used to account explicitly for two given states, $|n^{(0)}\rangle$ and $|m^{(0)}\rangle$, in the general case where transitions to other energy levels shall be included. Eq. (C.5) can be rearranged as

$$\langle n | d | m \rangle = \langle n^{(0)} | d | m^{(0)} \rangle + \sum_{k \neq n, m} \langle n^{(0)} | d | k^{(0)} \rangle \langle k^{(0)} | d | m^{(0)} \rangle \mathcal{E}_{\text{stat}} \left(\frac{1}{\hbar \omega_{mk}} + \frac{1}{\hbar \omega_{nk}} \right). \quad (\text{C.9})$$

In Eq. (C.9) we notice that the matrix elements can be rewritten, using resolutions of the identity, as

$$\sum_{k \neq n, m} \langle n^{(0)} | d | k^{(0)} \rangle \langle k^{(0)} | d | m^{(0)} \rangle = \langle n^{(0)} | dd | m^{(0)} \rangle = e^2 \int_{-\infty}^{\infty} \psi_n^{*(0)}(z) z^2 \psi_m^{(0)}(z) dz, \quad (\text{C.10})$$

which is equal to zero if $\psi_m^{(0)}(z)$, $\psi_n^{(0)}(z)$, the unperturbed eigenfunctions, have the same parity, while

$$\langle n | d | m \rangle = \langle n^{(0)} | d | m^{(0)} \rangle \text{ if } n, m \text{ have different parity,} \quad (\text{C.11})$$

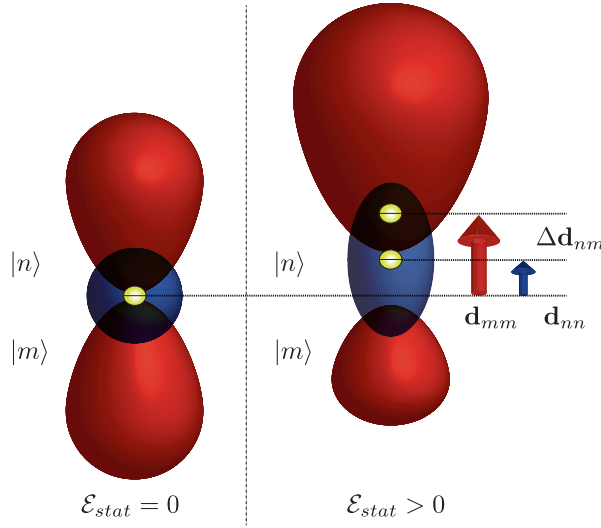


Fig. C.1 In an atom, the symmetry of the electronic orbitals can be broken by applying an external static electric field, $\mathcal{E}_{\text{stat}}$. The asymmetric dipole moment, $\Delta\mathbf{d}_{nm} = \langle n | \mathbf{d} | n \rangle - \langle m | \mathbf{d} | m \rangle$, is limited to grow differentially, as all orbitals are deformed, as shown by the appearance of the two induced dipoles, \mathbf{d}_{nn} and \mathbf{d}_{mm} respectively.

and

$$\langle n | d | m \rangle = \sum_{k \neq n, m} \langle k^{(0)} | d | m^{(0)} \rangle \mathcal{E}_{\text{stat}} \langle n^{(0)} | d | k^{(0)} \rangle \left(\frac{1}{\hbar\omega_{nk} + \hbar\omega_{mn}} + \frac{1}{\hbar\omega_{nk}} \right) \quad (\text{C.12})$$

if n, m have same parity. A particular case of Eq. (C.12) is given by $n = m$, so that the diagonal matrix elements of the induced dipole operator are given by

$$\langle n | d | n \rangle = \sum_{k \neq n} \frac{2 | \langle k^{(0)} | d | n^{(0)} \rangle |^2}{\hbar\omega_{nk}} \mathcal{E}_{\text{stat}} = \alpha_n \mathcal{E}_{\text{stat}} \quad (\text{C.13})$$

where in the last passage of the equation above we used Eq. (C.4).

C.1.1.3 Asymmetric dipole and magic wavelengths

Eq. (C.13) shows that the applied field causes a static polarization, generally shifting two orbitals with different intensity and giving rise to an asymmetric dipole

$$\Delta\mathbf{d}_{nm} = \langle n | \mathbf{d} | n \rangle - \langle m | \mathbf{d} | m \rangle. \quad (\text{C.14})$$

By plugging Eq. (C.2) into Eq. (C.14), up to first order, we can rewrite it in terms of polarizabilities,

$$\Delta \mathbf{d}_{\text{nm}} = (\alpha_n - \alpha_m) \boldsymbol{\mathcal{E}}_{\text{stat}}, \quad (\text{C.15})$$

From Eq. (C.15) it is clear that maximizing $\Delta \mathbf{d}_{\text{nm}}$ is equivalent to maximizing the difference in the polarizability of the two states. One should notice that, as shown by Eq. (C.3), the Stark shift of the two energy levels is then different, something to take care of in the following discussion on the spontaneous emission. In the TLS approximation, we can plug Eq. (C.8) into Eq. (C.15) so that

$$\Delta \mathbf{d}_{\text{nm}} \simeq 4 \frac{|d_{nm}^{(0)}|^2}{\hbar \omega_{mn}} \boldsymbol{\mathcal{E}}_{\text{stat}}, \quad (\text{C.16})$$

Moreover, we observe that maximizing the difference in the two states polarizabilities thus is basically the opposite of finding a “magic wavelength” [212, 213] for which the *dynamical* (i.e. frequency-dependent) polarizabilities of the two states cancel each other, a task needed in many application involving high precision measurement (from atomic clock measurements to quantum simulation in optical lattices) where one wants the transition frequencies to change not [214]. Indeed, the dynamical polarizability can be defined as

$$\alpha_n(\omega) = \alpha_n \frac{\omega_{kn}^2}{\omega_{kn}^2 - \omega^2}, \quad (\text{C.17})$$

that is,

$$\alpha_n(\omega) = \sum_{k \neq n} \frac{2}{\hbar} \frac{|\langle k^{(0)} | \mathbf{d} | n^{(0)} \rangle|^2 \omega_{kn}}{\omega_{kn}^2 - \omega^2}, \quad (\text{C.18})$$

from which it is clear that this definition is consistent for far-detuned frequencies only. It might happen that for a given magic wavelength, $\omega_{\text{magic}} = 2\pi c/\lambda_{\text{magic}}$, $\alpha_n(\omega_{\text{magic}}) = \alpha_m(\omega_{\text{magic}})$, and the Stark shift experienced by the two states is the same. In this case even an optical field is treated in the perturbation formalism used for the common static electric fields, correcting the polarizability expression with the dynamical polarizability.

C.1.1.4 Static and ac Stark shift: A comparison

We can now compare the two energy shifts for the case of a TLS, due to either a static or a dynamic electric field. Using this result in Eq. (C.3), and the expression of the Rabi frequency Ω , Eq. (2.17), and using the factor A to quantify the proportionality

between the amplitudes of the two fields, $\mathcal{E}_{\text{stat}} = A\mathcal{E}$, the ratio between the ac and static Stark shift for a TLS, up to second order in perturbation, is given by

$$\frac{|\Delta\mathcal{E}^{\text{stat}}|}{|\Delta\mathcal{E}^{\text{ac}}|} = \frac{\frac{1}{2}\alpha_1 A^2 \mathcal{E}^2}{\hbar\Omega} = \frac{\Omega}{\omega_{12}} A^2, \quad (\text{C.19})$$

which shows how, for static and dynamic fields of comparable strength, the ac interaction is several orders of magnitude stronger than the static one, as the ratio $\Omega/\omega_{21} \ll 1$, even for strong driving, as shown in Table 2.1.

C.2 Asymmetric artificial atom in a quantum well

C.2.1 General eigenstates

In Sec. 4.3, we calculated the THz emission, limiting ourselves to the case in which no electrons are locked into double-occupancy states ($N_F = 0$). However, under the effect of the pump beam, electrons will be actually scattered into such states, as shown in Fig. 4.3(c). Other scattering mechanisms, both radiative and nonradiative, will subsequently scatter away those blocked electrons. In this Appendix we develop a more detailed theory taking into account these processes, considering the emission for a general state in the form of Eq. (4.1).

Applying V_{THz} to such a state we obtain, using Eqs. (4.6), (4.10) and (4.11)

$$\begin{aligned} V_{\text{THz}} |\psi_i\rangle &= \frac{1}{\sqrt{2}} \sum_{\substack{\mathbf{k}, \mathbf{q}, q_z \\ \mathbf{k} \in S_+}} \Delta\chi_{q, q_z} F_{\mathbf{k} + \mathbf{q}} E_{\mathbf{k}} \prod_{\mathbf{k}' \in S_+ + S_- - \{\mathbf{k}\}} M_{\mathbf{k}'}^{j_{\mathbf{k}'}} \prod_{\mathbf{k}' \in S_F} F_{\mathbf{k}'} \prod_{\mathbf{k}' \in S_E} E_{\mathbf{k}'} a_{-\mathbf{q}, q_z}^\dagger |G\rangle |0_{\text{phot}}\rangle \\ &+ \sum_{\substack{\mathbf{k}, \mathbf{q}, q_z \\ \mathbf{k} \in S_F}} \Delta\chi_{q, q_z} F_{\mathbf{k} + \mathbf{q}} \prod_{\mathbf{k}' \in S_+} M_{\mathbf{k}'}^+ \prod_{\mathbf{k}' \in S_-} M_{\mathbf{k}'}^- \prod_{\mathbf{k}' \in S_F - \{\mathbf{k}\}} F_{\mathbf{k}'} \prod_{\mathbf{k}' \in S_E} E_{\mathbf{k}'} a_{-\mathbf{q}, q_z}^\dagger |G\rangle |0_{\text{phot}}\rangle. \end{aligned} \quad (\text{C.20})$$

The two lines of Eq. (C.20) give rise to 4 different terms each, depending on which set $\mathbf{k} + \mathbf{q}$ belongs to, each of these terms describing a different scattering channel. At the same time, only 4 of these 8 terms, those for which the difference between the numbers of $M_{\mathbf{k}}^+$ and $M_{\mathbf{k}}^-$ operators is strictly smaller than $N_+ - N_-$, will give rise to resonant emission processes. Moreover, we make the assumption, to be confirmed a posteriori, that most of the electrons are coupled to the laser pump, and only few are locked in double-occupancy $F_{\mathbf{k}}$ states. We can thus limit ourselves to terms of the lowest order in $\frac{N_F}{N}$.

In the first line of Eq. (C.20), if both \mathbf{k} and $\mathbf{k} + \mathbf{q}$ are in S_+ , we obtain a result analogous to that of the previous section, describing a scattering from two single-occupancy states to a full and an empty state, the only difference being the normalization of the sum over electronic and photonic wave vectors in Eq. (4.18). The total contribution to the emission of the scattering process from states such that $\mathbf{k}, \mathbf{k} + \mathbf{q} \in S_+$, sketched in Fig. 4.3(a), can be estimated by using Eq. (4.3), assuming that $N_+ = N_-$, so that after straightforward manipulation, $\frac{N_+^2}{N} \simeq (\frac{N}{4} - N_F)$, where the term of order N_F^2/N has been neglected. We thus obtain

$$\gamma_{\text{THz}}^{++ \rightarrow EF} = (1 - 4 \frac{N_F}{N}) \gamma_{\text{THz}}. \quad (\text{C.21})$$

If instead $\mathbf{k} + \mathbf{q}$ belongs to S_E , we obtain

$$\begin{aligned} & \frac{1}{\sqrt{2}} \sum_{\mathbf{k}, \mathbf{q}, q_z} \Delta \chi_{q, q_z} F_{\mathbf{k} + \mathbf{q}} E_{\mathbf{k}} \prod_{\mathbf{k}' \in S_{\mathbf{k}}} M_{\mathbf{k}'}^{j_{\mathbf{k}'}} \prod_{\mathbf{k}' \in S_F} F_{\mathbf{k}'} \prod_{\mathbf{k}' \in S_E} E_{\mathbf{k}'} a_{-\mathbf{q}, q_z}^\dagger |G\rangle |0_{\text{phot}}\rangle = \\ & \frac{1}{2} \sum_{\mathbf{k}, \mathbf{q}, q_z} \Delta \chi_{q, q_z} (M_{\mathbf{k} + \mathbf{q}}^+ + M_{\mathbf{k} + \mathbf{q}}^-) E_{\mathbf{k}} \prod_{\mathbf{k}' \in S_{\mathbf{k}}} M_{\mathbf{k}'}^{j_{\mathbf{k}'}} \prod_{\mathbf{k}' \in S_F} F_{\mathbf{k}'} \prod_{\mathbf{k}' \in S_E - \{\mathbf{k} + \mathbf{q}\}} E_{\mathbf{k}'} a_{-\mathbf{q}, q_z}^\dagger |G\rangle |0_{\text{phot}}\rangle, \end{aligned} \quad (\text{C.22})$$

where in both lines of the equation above the sums in \mathbf{k} and $\mathbf{k} + \mathbf{q}$ are limited to $\mathbf{k} \in S_+, \mathbf{k} + \mathbf{q} \in S_E$ and $S_{\mathbf{k}} = S_+ + S_- - \{\mathbf{k}\}$. This describes a process, sketched in Fig. 4.3(b), in which an electron with energy $\hbar\Omega$ scatters into an empty \mathbf{k} -subspace, giving rise to a state of energy $-\hbar\Omega$, an empty one, and a photon. The emission rate of this process can be calculated analogously to what has been done in Eq. (4.19), but with the normalization $\frac{N_+ N_F}{N}$

$$\gamma_{\text{THz}}^{+E \rightarrow E-} = \frac{2N_F}{N} \gamma_{\text{THz}}. \quad (\text{C.23})$$

Finally, the second line of Eq. (C.20) gives a non-negligible contribution only for $\mathbf{k} + \mathbf{q} \in S_+$, describing a process, sketched in Fig. 4.3(c), in which one of the two electrons of a full state, and an electron in a state with energy $\hbar\Omega$, scatter into a full state and a state with energy $-\hbar\Omega$, and we obtain

$$\begin{aligned} & \sum_{\mathbf{k}, \mathbf{q}, q_z} F_{\mathbf{k} + \mathbf{q}} \prod_{\mathbf{k}' \in S_+} M_{\mathbf{k}'}^+ \prod_{\mathbf{k}' \in S_-} M_{\mathbf{k}'}^- \prod_{\mathbf{k}' \in S_F - \{\mathbf{k}\}} F_{\mathbf{k}'} \prod_{\mathbf{k}' \in S_E} E_{\mathbf{k}'} a_{-\mathbf{q}, q_z}^\dagger |G\rangle |0_{\text{phot}}\rangle \\ & = \frac{1}{\sqrt{2}} \sum_{\mathbf{k}, \mathbf{q}, q_z} \Delta \chi_{q, q_z} F_{\mathbf{k} + \mathbf{q}} \prod_{\mathbf{k}' \in S_+ - \{\mathbf{k} + \mathbf{q}\}} M_{\mathbf{k}'}^+ \prod_{\mathbf{k}' \in S_-} M_{\mathbf{k}'}^- \prod_{\mathbf{k}' \in S_F - \{\mathbf{k}\}} F_{\mathbf{k}'} \prod_{\mathbf{k}' \in S_E} E_{\mathbf{k}'} a_{-\mathbf{q}, q_z}^\dagger |G\rangle |0_{\text{phot}}\rangle, \end{aligned}$$

where in both lines of the equation above the sums in \mathbf{k} and $\mathbf{k} + \mathbf{q}$ are limited to $\mathbf{k} \in S_F, \mathbf{k} + \mathbf{q} \in S_+$. Also in this case the relevant normalization for the sum over the wave vectors is $\frac{N_+ N_F}{N}$, giving an emission rate

$$\gamma_{\text{THz}}^{F+ \rightarrow -F} = \frac{2N_F}{N} \gamma_{\text{THz}}. \quad (\text{C.24})$$

The remaining emission process, $FE \rightarrow --$, sketched in Fig. 4.3(d), can be ignored, as the scattering occurs from two initial uncoupled states, $F_{\mathbf{k}}$ and $E_{\mathbf{k}+\mathbf{q}}$, and it is thus of second order in N_F .

We thus obtain the important result that, to the first order in N_F , the emission rate does not depend on N_F , as

$$\gamma_{\text{THz}}^{++ \rightarrow EF} + \gamma_{\text{THz}}^{+E \rightarrow E-} + \gamma_{\text{THz}}^{F+ \rightarrow -F} = \gamma_{\text{THz}}. \quad (\text{C.25})$$

In order to ascertain if the first order approximation is adequate, we need to estimate the number of electrons that are locked in double occupancy states. In fact, the semiconductor also allows many nonradiative energy relaxation channels that cool the electron gas, so we can write, always to the first order in N_F/N , a rate equation for the total number of electrons that are coupled to the pump laser $N_e = N_+ + N_-$,

$$\frac{dN_e}{dt} = -2\gamma_{\text{THz}}^{++ \rightarrow EF} + 2\gamma_{\text{nr}} N_F, \quad (\text{C.26})$$

where γ_{nr} is the rate of nonradiative relaxation. At equilibrium we have

$$\frac{N_F}{N} = \frac{1}{4 + \frac{N\gamma_{\text{nr}}}{\gamma_{\text{THz}}}}. \quad (\text{C.27})$$

Given the extremely fast nonradiative phonon-assisted intersubband recombination, N_F/N in Eq. (C.27) can be safely taken to be vanishing, thus a posteriori confirming our initial approximation.

C.2.2 Numerical model of asymmetric quantum well

The electronic charge distribution in z is found by solving the 1D Schrödinger equation for a single particle,

$$H\psi(z) = \left[-\frac{\hbar^2}{2m^*} \frac{d^2}{dz^2} + V_{\text{QW}}(z) \right] \psi(z) \quad (\text{C.28})$$

where for example the potential $V_{\text{QW}}(z)$ is a well of infinite walls at $z = 0$ and $z = L_{\text{QW}}$, with an internal barrier of height V_0 and length L_b ,

$$V_{\text{QW}}(z) = \begin{cases} \infty & z = 0 \\ 0 & 0 < z < a \\ V_0 & L_a < z < L_a + L_b \\ 0 & L_a + L_b < z < L_a + L_b + L_c \\ \infty & z = L_a + L_b + L_c \end{cases} \quad (\text{C.29})$$

where $L_{\text{QW}} = L_a + L_b + L_c$. In terms of operators acting on an eigenvector, the Schrödinger equation is written as

$$[T + V_{\text{QW}}] |\psi\rangle = E |\psi\rangle \quad (\text{C.30})$$

where T is the kinetic energy and V_{QW} the potential energy. The equation can be solved in k -space by Fourier transform. First, the eigenstate can be rewritten in terms of eigenstates of k_z (that in the following we simply denote as k), $|\psi\rangle = \sum_k |k\rangle \langle k| \psi\rangle = \sum_k \psi_k |k\rangle$, where we assumed that due to the fact that the potential $V_{\text{QW}}(z)$ confines the wavefunction in $0 < z < L_{\text{QW}}$, only discrete wavevectors are needed in the decomposition of the eigenfunction. Eq. (C.30) can then be rewritten as

$$\sum_k \left[\left(\frac{\hbar^2 k^2}{2m^*} - E \right) \delta_{k,k'} + \langle k' | V | k \rangle \right] \psi_k = 0 \quad (\text{C.31})$$

In Eq. (C.31), we can work out the term regarding the potential,

$$\begin{aligned} \sum_k \langle k' | V | k \rangle &= \sum_k \frac{1}{2\pi} \int dz e^{i(k-k')z} V_{\text{QW}}(z) = \sum_k \frac{1}{2\pi} (1 + e^{i(k-k')L_{\text{QW}}} + \delta_{k,k'} V_0 b) \\ &\quad + \sum_{k,k' \neq k} \frac{1}{2\pi} \frac{i}{(k' - k)} V_0 e^{i(k-k')L_a} (e^{i(k-k')L_a} - 1) \end{aligned} \quad (\text{C.32})$$

where we used $\psi(z) = \langle z | \psi \rangle = \frac{1}{\sqrt{2\pi}} \sum_k e^{ikz} \psi_k$ and in the last line we used Eq. (C.29). One can find the eigenvalues E and eigenfunctions ψ_k by diagonalizing the Hamiltonian of Eq. (C.31), which has potential terms on all matrix elements, k, k' , including on the main diagonal, plus the kinetic terms only on the main diagonal. One can diagonalize the equation by fixing a maximum value $k_{\max} = k$ on which one projects the Hamiltonian. Upon diagonalization, using the eigenvectors ψ_k it is then possible to calculate the eigenfunctions $\psi(z_i) = \frac{1}{\sqrt{2\pi}} \sum_k e^{ikz_i} \psi_k$.

Appendix D

N two-level systems: Further properties and dynamics

D.1 Dicke states and collective spin operators

D.1.1 Collective spin operators' algebra

Here we define the collective spin operators used for the study of N identical TLSs, and report some useful relations. The Pauli matrices of each i th TLS are

$$\sigma_{x_i} = \begin{pmatrix} 0 & 1 \\ 1 & 0 \end{pmatrix}_i, \quad \sigma_{y_i} = \begin{pmatrix} 0 & -i \\ i & 0 \end{pmatrix}_i, \quad \sigma_{z_i} = \begin{pmatrix} 1 & 0 \\ 0 & -1 \end{pmatrix}_i, \quad (\text{D.1})$$

for which $[\sigma_{\alpha_i}, \sigma_{\beta_j}] = \delta_{i,j} 2i\epsilon_{\alpha\beta\gamma}\sigma_{\gamma_i}$ hold, with $\alpha, \beta, \gamma = \{x, y, z\}$. The raising operators are defined as $\sigma_i^\pm = \frac{1}{2}(\sigma_{x_i} \pm i\sigma_{y_i})$. The collective spin operators are defined as $J_{z_i} = \frac{1}{2}\sigma_{z_i}$. In general $J_z = \sum_i^N J_{z_i}$ and their algebra is $[J_\alpha, J_\beta] = i\epsilon_{\alpha\beta\gamma}J_\gamma$. Since the light-matter interaction is characterized by the raising and lowering operators, $J_\pm = \sum_i^N J_{\pm_i}$ (notice that $J_{\pm_i} = \sigma_i^\pm$) it will be useful to use the following commutation relations

$$[J_z, J_\pm] = \pm J_\pm \quad (\text{D.2})$$

$$[J_+, J_-] = 2J_z. \quad (\text{D.3})$$

Using this last commutation relation and $J_\pm = J_x \pm iJ_y$ we can write each J_z in terms of J_+ and J_- only. In this way we obtain, for

$$\mathbf{J}^2 := J_x^2 + J_y^2 + J_z^2, \quad (\text{D.4})$$

these identities

$$\mathbf{J}^2 = J_z^2 + \frac{1}{2}(J_+J_- + J_-J_+) = J_z^2 \pm J_z + J_\mp J_\pm. \quad (\text{D.5})$$

We also report the following relations, which will prove useful in the study of the superradiant dynamics,

$$[J_{z_i}, (J_\pm)^n] = \pm n J_{\pm i} (J_\pm)^{n-1} \quad (\text{D.6})$$

and

$$J_z^r J_{\pm i} = J_{\pm i} (J_z \pm 1)^r \text{ and then } J_z^r J_\pm = J_\pm (J_z \pm 1)^r \quad (\text{D.7})$$

$$[J_+, J_-^q] = 2 \sum_{k=0}^q (q-k) J_-^{q-1} \quad (\text{D.8})$$

$$[J_z, J_\pm^n] = \pm n J_\pm^n \quad (\text{D.9})$$

It is also possible to rewrite Eq. (D.8) as

$$[J_+, J_-^q] = q (2J_z + (q-1)) J_-^{(q-1)}. \quad (\text{D.10})$$

We also point out that multiplications of TLS operators give collective operators and identities, $\sum_i J_{\pm i} J_{\mp i} = \frac{N}{2} \pm J_z$ and $\sum_i J_{z_i} J_{\pm i} = \pm \frac{1}{2} J_\pm$ and that it is always $J_{z_i}^2 = \frac{1}{4}$.

D.1.2 Degeneracy of Dicke states

Here we determine $D_{|j,m\rangle}$, the degeneracy of a given Dicke state $|j, m\rangle$ [48]. We could also refer to $D_{|j,m\rangle}$ as the dimension of the subspace of eigenstates degenerate with respect to the quantum numbers j, m . Consider the state $|j, j\rangle$, which is the maximally excited state of that multiplet, being $m = j$. By applying multiple times the lowering operator, we hop down all states with $|m| \leq j$, according to

$$(J_-)^{j-m} |j, j\rangle = \prod_{k=0}^{j-m-1} \alpha_{j,j-k}^- |j, m\rangle \quad (\text{D.11})$$

where $\alpha_{j,m}^-$ is determined by Eq. (2.35). For fixed j thus, all states have the same degeneracy, $D_{|j,m\rangle} = D_j$. Now consider the state $|j-1, j-1\rangle$, with j greater than 0. Since $|m| \leq j$, all states with $m = j-1$ will be $|j-1, j-1\rangle, |j, j-1\rangle, \dots, |\frac{N}{2}, j-1\rangle$. These are all the states with $m = j-1$ and thus the sum of their degeneracies is given by Eq. (2.30), and we can find the relation $d_{j-1} = D_{j-1} + D_j + \dots + D_{\frac{N}{2}}$. We consider analogously $d_j = D_j + \dots + D_{\frac{N}{2}}$ and see that $D_{j-1} = d_{j-1} - d_j$, which is thus

determined solely by Eq. (2.30). After straightforward algebra we can write

$$D_j = \frac{N!(2j+1)}{(\frac{N}{2} + j + 1)!(\frac{N}{2} - j)!} \quad (\text{D.12})$$

from which we notice in particular that $D_{\frac{N}{2}} = D_{|\frac{N}{2}, m\rangle} = 1, \forall m$. The degeneracy of the Dicke state $|j, m\rangle$ tells us that it is necessary to find some other quantum number to univocally individuate a given eigenstate and map it to the TLS basis. A Dicke state $|j, m\rangle$ is thus always univocally individuated in terms of TLSs if an additional symmetry quantum number a is introduced, and the Dicke state can be written as $|j, m, a\rangle$ [2, 48]. Notice that the light-matter interaction expressed by the action of the ladder operators J_+ and J_- cannot change the symmetry quantum number a . The density matrix of the system can be written by determining the probabilities $p_{j,m,a}$ univocally in the form

$$\rho = \sum_{\substack{jma \\ j'm'a'}} \sqrt{p_{jma} p_{j'm'a'}} |j, m, a\rangle \langle j', m', a'| \quad (\text{D.13})$$

where $\text{Tr}[\rho] = \sum_{j,m,a} p_{jma} = 1$. In Eq. (D.13), the sums over j, m, a , it is explicit the complexity of mapping the Dicke states' basis into the one of TLSs and also to calculate what is the action of a TLS operator as J_{+i} on a Dicke state $|j, m, a\rangle$. It is possible nevertheless to map the Dicke states $|j, m, a\rangle$ into TLS states with the following procedure. The states $|\frac{N}{2}, m\rangle$ are non-degenerate. Since $J^- |\frac{N}{2}, \frac{N}{2}\rangle = \alpha_{\frac{N}{2}, \frac{N}{2}}^- |\frac{N}{2}, \frac{N}{2} - 1\rangle$ and, as visible in Figure 2.3, only one other Dicke state has $\frac{N}{2} - 1$ excitations, i.e. $|\frac{N}{2} - 1, \frac{N}{2} - 1\rangle$, which can be found by orthogonalisation, and so can all the states $|\frac{N}{2} - 1, \frac{N}{2} - 1, a\rangle$ with different symmetry quantum numbers a . Applying the ladder operator J_- allows us to find all the other states in the same Dicke ladder, $|\frac{N}{2} - 1, m, a\rangle$. By iteration of the procedure one can find all of the Dicke states of the Hilbert space. Using Eq. (D.12) it is possible to count the number of states using the Dicke basis and verify that

$$n_{\text{states}} = \sum_{|j,m\rangle} D_{|j,m\rangle} = \sum_j D_j (2j+1) = N! \sum_{j=j_{\min}}^{N/2} \frac{(2j+1)^2}{(\frac{N}{2} + j + 1)!(\frac{N}{2} - j)!} = 2^N. \quad (\text{D.14})$$

We point out that the dimension of the Hilbert space can be counted also in the TLS basis

$$n_{\text{states}} = \sum_{m=-N/2}^{N/2} d_m = \sum_{m=-N/2}^{N/2} \binom{N}{\frac{N}{2} + m} = \sum_{k=0}^N \binom{N}{k} = 2^N. \quad (\text{D.15})$$

If instead one would like to count how many Dicke states $|j, m\rangle$ are there in the (j, m) plane disregarding the symmetry degeneracy, one has to divide the calculation for N even or odd. For N even, $j_{\min} = 0$ and

$$n_{j,m}^{\text{Neven}} = \sum_{j=0}^{N/2} (2j+1) = \left(\frac{N}{2} + 1\right)^2, \quad (\text{D.16})$$

where the last line is obtained using $\sum_{j=1}^n j = \frac{n}{2}(n+1)$. For N odd instead, $j_{\min} = 1/2$,

$$n_{j,m}^{\text{Nodd}} = \sum_{j=1/2}^{N/2} (2j+1) = \sum_{k=0}^{(N-1)/2} (2k+1) + (N+1)/2 = \left(\frac{N}{2} + 1\right)^2 - \frac{1}{4} \quad (\text{D.17})$$

and we used $\sum_{j=1/2}^{N/2} j = \frac{1}{2} \sum_{k=0}^{(N-1)/2} (2k+1) = \frac{1}{2} + \frac{3}{2} + \dots + \frac{N}{2}$. In both cases thus the number of Dicke states in the (j, m) plane is $\simeq \frac{N^2}{4}$. There vast majority of states $\sim 2^N - \frac{N^2}{4}$ are hidden in the degeneracy lifted by the symmetry quantum number a .

D.2 Cooperative dynamics

D.2.1 General superradiant master equation

We consider the master equation of Eq. (5.2), that we report here for clarity,

$$\begin{aligned} \dot{\rho} = & -i\omega_0[J_z, \rho] + \gamma \left(J_- \rho J_+ - \frac{1}{2} J_+ J_- \rho - \frac{1}{2} \rho J_+ J_- \right) \\ & + \gamma_D \sum_i \left(J_{z_i} \rho J_{z_i} - \frac{N}{4} \rho \right) + \gamma_{\text{nr}} \sum_i \left(J_{-i} \rho J_{+i} - \frac{1}{2} J_{+i} J_{-i} \rho - \frac{1}{2} \rho J_{+i} J_{-i} \right) \end{aligned} \quad (\text{D.18})$$

and calculate any operator of the collective spin algebra. We choose normal ordering to calculate, for any operator $X = J_+^p J_z^r J_-^q$, what is the dynamics of its average value,

$$\begin{aligned} \frac{d}{dt}\langle X \rangle &= -i\omega_0(q-p)\langle X \rangle \\ &\quad + \gamma_D \left(-\frac{1}{2}(p+q)\langle X \rangle + pq\langle J_+^{p-1}(J_z-1)^r(\frac{N}{2}+J_z)J_-^{q-1} \rangle \right) \\ &\quad + \gamma(\langle J_+^{p+1}J_z^rJ_-^{q+1} \rangle - \langle J_+^{p+1}(J_z+1)^rJ_-^{q+1} \rangle + (p+q)\langle J_+^pJ_z^{r+1}J_-^q \rangle \\ &\quad + \frac{1}{2}[p(p-1)+q(q-1)]\langle X \rangle) \\ &\quad + \gamma_{nr} \left(\langle J_+^p(J_z-1)^r(J_z+\frac{N}{2})J_-^q \rangle - \frac{1}{2}(p+q+N)\langle X \rangle - \langle J_+^pJ_z^{r+1}J_-^q \rangle \right), \end{aligned} \quad (D.19)$$

which, noting that $(J_z \pm 1)^r = \sum_{k=0}^r C(r, k)(\pm 1)^{r-k}J_z^k$ can be rewritten as

$$\begin{aligned} \frac{d}{dt}\langle X \rangle &= -i\omega_0(q-p)\langle X \rangle \\ &\quad + \gamma_D[-\frac{1}{2}(p+q)\langle X \rangle + pq \sum_{k=0}^r C(r, k)(-1)^{r-k}\langle J_+^{p-1}J_z^k(\frac{N}{2}+J_z)J_-^{q-1} \rangle] \\ &\quad + \gamma[-\sum_{k=0}^{r-1} C(r, k)\langle J_+^{p+1}J_z^k J_-^{q+1} \rangle + (p+q)\langle J_+^pJ_z^{r+1}J_-^q \rangle + \frac{1}{2}(p^2+q^2-p-q)\langle X \rangle] \\ &\quad + \gamma_{nr}[\sum_{k=0}^{r-1} C(r, k)(-1)^{r-k}\langle J_+^pJ_z^k(J_z+\frac{N}{2})J_-^q \rangle - \frac{1}{2}(p+q)\langle X \rangle], \end{aligned} \quad (D.20)$$

where $C(r, k)$ is the binomial coefficient of r in k . We point out that in the third and fourth line of Eq. (D.20) we reduced the sums to $r-1$ to make the expression more compact. Using Eq. (D.5), the dynamics of $\langle \dot{J}_z \rangle, \langle \dot{J}_z^2 \rangle, \langle \dot{\mathbf{J}}^2 \rangle$ are given by

$$\begin{aligned} \langle \dot{J}_z \rangle &= \gamma (\langle J_z^2 \rangle - \langle J_z \rangle - \langle \mathbf{J}^2 \rangle) - \gamma_{nr} \left(\frac{N}{2} + \langle J_z \rangle \right) \\ \langle \dot{J}_z^2 \rangle &= \gamma (\langle \mathbf{J}^2 \rangle - 2\langle J_z \mathbf{J}^2 \rangle + 2\langle J_z^3 \rangle - 3\langle J_z^2 \rangle + \langle J_z \rangle) + \gamma_{nr} \left(\frac{N}{2} - (N-1)\langle J_z \rangle - 2\langle J_z^2 \rangle \right) \\ \langle \dot{\mathbf{J}}^2 \rangle &= \gamma_D \left(\frac{N}{2} + \langle J_z^2 \rangle - \langle \mathbf{J}^2 \rangle \right) + \gamma_{nr} (N - (N-1)\langle J_z \rangle - \langle J_z^2 \rangle - \langle \mathbf{J}^2 \rangle). \end{aligned} \quad (D.21)$$

D.2.1.1 Semiclassical limit

Let us review first the condition that is usually found in the literature [47], for which there is no dephasing and nonradiative emission, $\gamma_D, \gamma_{nr} = 0$. In this case the dynamics reduces to that given by Eq. (2.44) and $\langle \mathbf{J}^2 \rangle$ is conserved. If we also assume that $\langle J_z^2 \rangle \sim \langle J_z \rangle^2$ (semiclassical approximation) we find that the dynamics is given only by

$$\langle \dot{J}_z \rangle = \gamma (\langle J_z \rangle^2 - \langle J_z \rangle - \langle \mathbf{J}^2 \rangle) \quad (D.22)$$

which, setting $x = \langle J_z \rangle$, $a = \langle \mathbf{J}^2 \rangle$ can be written as

$$\dot{x} = \gamma(-a - x + x^2). \quad (\text{D.23})$$

This is a Riccati equation that is solved by

$$x(t) = \frac{1}{2} - \frac{1}{2}(4a+1)^{\frac{1}{2}} \tanh\left(\frac{1}{2}(4a+1)^{\frac{1}{2}}\gamma(t-t_D)\right) \quad (\text{D.24})$$

where we fixed the free constant c_1 to be $c_1 = -\gamma t_D$. Assuming that $j = \frac{N}{2}$, for $N \gg 1$ it gives

$$\langle J_z(t) \rangle = -\frac{N}{2} \tanh\left(\frac{N}{2}\gamma(t-t_D)\right), \quad (\text{D.25})$$

and since in Eq. (2.44) the time derivative of Eq. (D.25), the lost energy, is completely converted in radiated energy, the intensity of the emitted light is exactly proportional to $\propto \frac{N^2}{4} \operatorname{sech}^2\left(\frac{N}{2}\gamma(t-t_D)\right)$, which gives a bell-like peak centred on $t = t_D$.

D.2.2 Collective dephasing term

It is possible to consider, in addition to the dynamics of Eq. (D.18), a collective dephasing term

$$\gamma_{\text{CD}} \mathcal{L}[\rho] = \gamma_{\text{CD}} \left(J_z \rho J_z - \frac{1}{2} \rho J_z^2 - \frac{1}{2} J_z^2 \rho \right), \quad (\text{D.26})$$

and show, using the iterated commutation relation $[J_z, J_{\pm}^n] = \pm n J_z^{\pm n}$, that for a general operator in the form $X = J_+^p J_z^r J_-^q$, when $\dot{\rho} = \gamma_{\text{CD}} \mathcal{L} \rho$, then

$$\langle \dot{X} \rangle = -\frac{1}{2}(p+q)^2 \gamma_{\text{CD}} \langle X \rangle \quad (\text{D.27})$$

$$\langle X(t) \rangle = \langle X(0) \rangle e^{-\frac{1}{2}(p+q)^2 \gamma_{\text{CD}} t}. \quad (\text{D.28})$$

This also correctly predicts that $\langle \dot{J}_z^r \rangle = 0$ and tells us that Eq. (D.26) is an energy preserving mechanism ($H_0 = \hbar\omega_{12} J_z$). Using $\mathbf{J}^2 = J_z^2 - J_z + J^+ J^-$ we find that $\frac{d}{dt} \langle \mathbf{J}^2(t) \rangle = \frac{d}{dt} \langle J^+ J^-(t) \rangle$ under the action of Eq. (D.26), and thus, with relevance to the three equations we have studied in the main text,

$$\langle \dot{J}_z \rangle = 0, \quad \langle J_z(t) \rangle = \langle J_z(0) \rangle \quad (\text{D.29})$$

$$\langle \dot{J}_z^2 \rangle = 0, \quad \langle J_z^2(t) \rangle = \langle J_z^2(0) \rangle \quad (\text{D.30})$$

$$\langle \dot{\mathbf{J}}^2 \rangle = -\frac{1}{2}(p+q)^2 \gamma_{\text{CD}} \mathbf{J}^2, \quad \langle \mathbf{J}^2(t) \rangle = \langle \mathbf{J}^2(0) \rangle e^{-\frac{1}{2}(p+q)^2 \gamma_{\text{CD}} t}. \quad (\text{D.31})$$

D.2.3 Maxwell-Bloch Equations

The Maxwell-Bloch equations are a closed system of equations relating macroscopic quantities of the system: the total polarization, \mathcal{P} , the electrical field of the emitted radiation, \mathcal{E}_{rad} , and the population inversion of the emitters, n [or generally of the optical medium]. They can be derived in different ways. The easiest one is probably to consider the light-atom coupling Hamiltonian and derive from it equations for \mathcal{P} , \mathcal{E}_{rad} , n . One then consider Maxwell's equation for the envelope of the electric field, slowly varying in space and time and has three coupled equations if one makes the appropriate identities.

Another approach is to derive them from the quantum dynamics of an *open* system, that is from the master equation for a light-atom density matrix. This allows to include already from the quantum model dissipative effects as the loss of coherence. This is what has been done by Bonifacio and Lugiato [67, 70] in the case of superfluorescence and optical bistability. We follow this path and consider the master equation

$$\dot{\rho} = -i[\omega_{\text{cav}}a^\dagger a + \omega_0 J_z + \Omega(J_+ a + J_- a^\dagger), \rho] + \gamma_D \mathcal{L}_D[\rho] + \kappa \mathcal{L}_{\text{cav}}[\rho] \quad (\text{D.32})$$

in which κ is the constant giving the rate of photonic losses out of the cavity, ω_{cav} the resonance frequency of the cavity $\mathcal{L}_D[\rho] = J_{z_i}\rho J_{z_i} - \frac{1}{2}\{J_{z_i}^2, \rho\}$ and $\mathcal{L}_{\text{cav}}[\rho] = a\rho a^\dagger - \frac{1}{2}\{a^\dagger a, \rho\}$, from which we obtain

$$\langle \dot{J}_z \rangle = -i\Omega(\langle J_+ a \rangle - \langle J_- a^\dagger \rangle) \quad (\text{D.33})$$

$$\langle \dot{J}_- \rangle = -i\omega_0 \langle J_- \rangle - i2\Omega \langle J_z a \rangle - \frac{1}{2}\gamma_D \langle J_- \rangle + \gamma \langle J_z J_- \rangle \quad (\text{D.34})$$

$$\langle \dot{a} \rangle = -i\omega_{\text{cav}} \langle a \rangle - i\Omega \langle J_- \rangle - \frac{1}{2}\kappa \langle a \rangle. \quad (\text{D.35})$$

From Eq. (D.34) $\langle \dot{J}_+ \rangle$ can be derived and from Eq. (D.35) $\langle \dot{a}^\dagger \rangle$ can be derived. We can make the factorization $\langle O_F O_A \rangle = \langle O_F \rangle \langle O_A \rangle$ where O_F, O_A is any field, atom operator, respectively. Then by renaming

$$n \leftrightarrow 2\langle J_z \rangle \quad (\text{D.36a})$$

$$\mathcal{P} \leftrightarrow \langle J_- \rangle \quad (\text{D.36b})$$

$$\mathcal{E}_{\text{rad}} \leftrightarrow i\langle a \rangle \quad (\text{D.36c})$$

and setting $T_2 = \gamma_D^{-1}$ we obtain

$$\partial_t n = -2\Omega (\mathcal{P}^* \mathcal{E}_{\text{rad}} + \mathcal{P} \mathcal{E}_{\text{rad}}^*) \quad (\text{D.37a})$$

$$(\partial_t + i\omega_0) \mathcal{P} = -\frac{1}{2T_2} \mathcal{P} - \Omega n \mathcal{E}_{\text{rad}} \quad (\text{D.37b})$$

$$(\partial_t + i\omega_{\text{cav}}) \mathcal{E}_{\text{rad}} = \Omega \mathcal{P} - \frac{1}{2} \kappa \mathcal{E}_{\text{rad}}, \quad (\text{D.37c})$$

which are an equivalent formulation of Maxwell-Bloch's equations.

D.2.4 Characteristic function

It is possible to define a characteristic function in the usual sense of (classical) statistical mechanics: By deriving the characteristic function in terms of auxiliary conjugate variables, all moments of the system's operators can be calculated. This is provided that one fixes a given order of operators when defining the momenta. This is indeed a generalization of the Wigner function that is used to formalize in terms of coherent states a bosonic dynamics. The Wigner function uses Weyl's symmetry to order operators. Here we rely instead on a normally ordered characteristic function such that we define

$$\chi_N(z, w, z^*) = \text{Tr} [e^{izJ_+} e^{iwJ_z} e^{iz^*J_-} \rho], \quad (\text{D.38})$$

where the c -numbers w, z, z^* have been introduced. All operators' momenta can be calculated as

$$\frac{\partial^{p+r+q} \chi_N(z, w, z^*)}{\partial (iz)^p \partial (iw)^r \partial (iz^*)^q} |_{z=z^*=w=0} = \text{Tr} [J_+^p J_z^r J_-^q \rho] \quad (\text{D.39})$$

In particular one can notice that the dynamics of the system can be expressed in terms of the characteristic function as in the Schrödinger representation, $\dot{\chi}_N(z, w, z^*) = \text{Tr} [e^{izJ_+} e^{iwJ_z} e^{iz^*J_-} \dot{\rho}]$ and thus

$$\frac{d}{dt} \frac{\partial^{p+r+q} \chi_N(z, w, z^*)}{\partial (iz)^p \partial (iw)^r \partial (iz^*)^q} |_{z=z^*=w=0} = \frac{d}{dt} \langle J_+^p J_z^r J_-^q \rangle. \quad (\text{D.40})$$

We can plug Eq. (D.20) into Eq. (D.40) and obtain an explicit expression for χ_N ,

$$\begin{aligned} \dot{\chi}_N(z, w, z^*) &= [\omega_0(z^* \partial_{iz^*} - z \partial_{iz}) \\ &\quad + \gamma_D \left(-\frac{i}{2} z \partial_{iz} - \frac{i}{2} z^* \partial_{iz^*} - zz^* e^{-iw} \left(\frac{N}{2} + \partial_{iw} \right) \right) \\ &\quad + \gamma \left(\partial_{iz} \partial_{iz^*} - e^{iw} \partial_{iz} \partial_{iz^*} + iz^* \partial_{iw} \partial_{iz^*} + iz \partial_{iz} \partial_{iw} - \frac{1}{2} z^{*2} \partial_{iz^*}^2 - \frac{1}{2} z^2 \partial_{iz}^2 \right) \\ &\quad + \gamma_{nr} \left(-\frac{i}{2} z \partial_{iz} - \frac{i}{2} z^* \partial_{iz^*} - \partial_{iw} + e^{iw} \left(\frac{N}{2} + \partial_{iw} \right) - \frac{N}{2} \right)] \chi_N(z, w, z^*). \end{aligned} \quad (\text{D.41})$$

(D.42)

For the derivation of Eq. (D.42) the Baker-Campbell-Hausdorff formula has been used,

$$e^{iB} A e^{-iB} = A + i[B, A] + \frac{i^2}{2!} [B, [B, A]] + \dots \quad (\text{D.43})$$

to write the time derivative of the general momenta of the spin operators in normal order,

$$e^{iz^* J_-} J_z e^{-iz^* J_-} = J_z + iz^* J_- \quad (\text{D.44})$$

$$e^{iz^* J_-} J_+ e^{-iz^* J_-} = J_+ - i2z^* J_z + z^{*2} J_- \quad (\text{D.45})$$

$$e^{iw J_z} J_{-i} e^{-iw J_z} = J_{-i} e^{-iw} \quad (\text{D.46})$$

$$e^{iz J_+} J_{zi} e^{-iz J_+} = J_{zi} - iz J_{+i}, \quad (\text{D.47})$$

from which one can derive all the others by conjugation, exchange of the imaginary identity $i \rightarrow -i$, or sum of terms \sum_i . In simpler systems, the Fourier transform of the time derivative of the characteristic function leads to Fokker-Planck equations for quasi-probability distributions.

References

- [1] B. R. Mollow, *Power spectrum of light scattered by two-level systems*, Phys. Rev. **188**, 1969 (1969).
- [2] R. H. Dicke, *Coherence in spontaneous radiation processes*, Phys. Rev. **93**, 99 (1954).
- [3] D. F. Walls and G. J. Milburn, *Quantum optics* (Springer, 2007).
- [4] H. J. Kimble, *The quantum internet*, Nature (London) **453**, 1023 (2008).
- [5] S. De Liberato, *Cavity quantum electrodynamics and intersubband polaritonics of a two dimensional electron gas*, Ph.D. thesis, Université Paris-Diderot - Paris VII (2009).
- [6] E. M. Purcell, *Spontaneous emission probabilities at radio frequencies*, Phys. Rev. **69**, 681 (1946).
- [7] R. J. Glauber, *The quantum theory of optical coherence*, Phys. Rev. **130**, 2529 (1963).
- [8] S. H. Autler and C. H. Townes, *Stark effect in rapidly varying fields*, Phys. Rev. **100**, 703 (1955).
- [9] M. Lax, *Formal theory of quantum fluctuations from a driven state*, Phys. Rev. **129**, 2342 (1963).
- [10] H. J. Carmichael, *Statistical Methods in Quantum Optics 1: Master Equations and Fokker-Planck Equations* (Springer, 1999).
- [11] H. J. Carmichael and D. F. Walls, *A quantum-mechanical master equation treatment of the dynamical Stark effect*, J. Phys. B **9**, 1199 (1976).
- [12] Z. Ficek and T. Rudolph, *Quantum interference in a driven two-level atom*, Phys. Rev. A **60**, R4245 (1999).
- [13] E. del Valle and F. P. Laussy, *Mollow triplet under incoherent pumping*, Phys. Rev. Lett. **105**, 233601 (2010).
- [14] D. P. S. McCutcheon and A. Nazir, *Model of the optical emission of a driven semiconductor quantum dot: Phonon-enhanced coherent scattering and off-resonant sideband narrowing*, Phys. Rev. Lett. **110**, 217401 (2013).

- [15] H. J. Kimble and L. Mandel, *Theory of resonance fluorescence*, Phys. Rev. A **13**, 2123 (1976).
- [16] G. Lindblad, *On the generators of quantum dynamical semigroups*, Comm. Math. Phys. **48**, 119 (1976).
- [17] H. J. Carmichael, A. S. Lane, and D. F. Walls, *Resonance fluorescence from an atom in a squeezed vacuum*, Phys. Rev. Lett. **58**, 2539 (1987).
- [18] P. Zhou and S. Swain, *Quantum interference in resonance fluorescence for a driven V atom*, Phys. Rev. A **56**, 3011 (1997).
- [19] E. del Valle, F. P. Laussy, and C. Tejedor, *Luminescence spectra of quantum dots in microcavities. ii. fermions*, Phys. Rev. B **79**, 235326 (2009).
- [20] A. Ridolfo, O. D. Stefano, S. Portolan, S. Savasta, and R. Girlanda, *Photoluminescence of single quantum dots in microcavities*, J. Phys.: Conf. Ser. **210**, 012025 (2010).
- [21] F. Schuda, C. R. S. Jr, and M. Hercher, *Observation of the resonant Stark effect at optical frequencies*, J. Phys. B **7**, L198 (1974).
- [22] F. Y. Wu, R. E. Grove, and S. Ezekiel, *Investigation of the spectrum of resonance fluorescence induced by a monochromatic field*, Phys. Rev. Lett. **35**, 1426 (1975).
- [23] R. E. Grove, F. Y. Wu, and S. Ezekiel, *Measurement of the spectrum of resonance fluorescence from a two-level atom in an intense monochromatic field*, Phys. Rev. A **15**, 227 (1977).
- [24] S. Haroche and J. M. Raimond, *Exploring the quantum* (Oxford University Press, Oxford, 2006).
- [25] X. Xu, B. Sun, P. R. Berman, D. G. Steel, A. S. Bracker, D. Gammon, and L. J. Sham, *Coherent optical spectroscopy of a strongly driven quantum dot*, Science **317**, 929 (2007).
- [26] A. Muller, E. B. Flagg, P. Bianucci, X. Y. Wang, D. G. Deppe, W. Ma, J. Zhang, G. J. Salamo, M. Xiao, and C. K. Shih, *Resonance fluorescence from a coherently driven semiconductor quantum dot in a cavity*, Phys. Rev. Lett. **99**, 187402 (2007).
- [27] N. A. Vamivakas, Y. Zhao, C.-Y. Lu, and M. Atatüre, *Spin-resolved quantum-dot resonance fluorescence*, Nature Phys. **5**, 198 (2009).
- [28] E. B. Flagg, A. Muller, J. W. Robertson, S. Founta, D. G. Deppe, M. Xiao, W. Ma, G. J. Salamo, and C. K. Shih, *Resonantly driven coherent oscillations in a solid-state quantum emitter*, Nature Phys. **5**, 203 (2009).
- [29] S. Ates, S. M. Ulrich, S. Reitzenstein, A. Löffler, A. Forchel, and P. Michler, *Post-selected indistinguishable photons from the resonance fluorescence of a single quantum dot in a microcavity*, Phys. Rev. Lett. **103**, 167402 (2009).

- [30] S. M. Ulrich, S. Ates, S. Reitzenstein, A. Löffler, A. Forchel, and P. Michler, *Dephasing of triplet-sideband optical emission of a resonantly driven InAs/GaAs quantum dot inside a microcavity*, Phys. Rev. Lett. **106**, 247402 (2011).
- [31] A. Ulhaq, S. Weiler, S. M. Ulrich, R. Roszbach, M. Jetter, and P. Michler, *Cascaded single-photon emission from the Mollow triplet sidebands of a quantum dot*, Nature Photon. **6**, 238 (2012).
- [32] S. Weiler, D. Stojanovic, S. M. Ulrich, M. Jetter, and P. Michler, *Postselected indistinguishable single-photon emission from the Mollow triplet sidebands of a resonantly excited quantum dot*, Phys. Rev. B **87**, 241302 (2013).
- [33] R.-C. Ge, S. Weiler, A. Ulhaq, S. M. Ulrich, M. Jetter, P. Michler, and S. Hughes, *Mollow quintuplets from coherently excited quantum dots*, Opt. Lett. **38**, 1691 (2013).
- [34] A. Ulhaq, S. Weiler, C. Roy, S. M. Ulrich, M. Jetter, S. Hughes, and P. Michler, *Detuning-dependent Mollow triplet of a coherently-driven single quantum dot*, Opt. Express **21**, 4382 (2013).
- [35] Y.-M. He, Y. He, Y.-J. Wei, D. Wu, M. Atatüre, C. Schneider, S. Höfling, M. Kamp, C.-Y. Lu, and J.-W. Pan, *On-demand semiconductor single-photon source with near-unity indistinguishability*, Nature Nanot. **8**, 213 (2013).
- [36] Y.-J. Wei, Y. He, Y.-M. He, C.-Y. Lu, J.-W. Pan, C. Schneider, M. Kamp, S. Höfling, D. P. S. McCutcheon, and A. Nazir, *Temperature-dependent Mollow triplet spectra from a single quantum dot: Rabi frequency renormalization and sideband linewidth insensitivity*, Phys. Rev. Lett. **113**, 097401 (2014).
- [37] G. Wrigge, I. Gerhardt, J. Hwang, G. Zumofen, and V. Sandoghdar, *Efficient coupling of photons to a single molecule and the observation of its resonance fluorescence*, Nature Phys. **4**, 60 (2008).
- [38] M. Baur, S. Philipp, R. Bianchetti, J. M. Fink, M. Göppl, L. Steffen, P. J. Leek, A. Blais, and A. Wallraff, *Measurement of Autler-Townes and Mollow transitions in a strongly driven superconducting qubit*, Phys. Rev. Lett. **102**, 243602 (2009).
- [39] O. Astafiev, A. M. Zagoskin, A. A. Abdumalikov, Y. A. Pashkin, T. Yamamoto, K. Inomata, Y. Nakamura, and J. S. Tsai, *Resonance fluorescence of a single artificial atom*, Science **327**, 840 (2010).
- [40] K. Koshino, H. Terai, K. Inomata, T. Yamamoto, W. Qiu, Z. Wang, and Y. Nakamura, *Observation of the three-state dressed states in circuit quantum electrodynamics*, Phys. Rev. Lett. **110**, 263601 (2013).
- [41] M. Saba, F. Quochi, C. Ciuti, D. Martin, J.-L. Staehli, B. Deveaud, A. Mura, and G. Bongiovanni, *Direct observation of the excitonic ac Stark splitting in a quantum well*, Phys. Rev. B **62**, R16322 (2000).
- [42] F. Quochi, G. Bongiovanni, A. Mura, J. L. Staehli, B. Deveaud, R. P. Stanley, U. Oesterle, and R. Houdré, *Strongly driven semiconductor microcavities: From the polariton doublet to an ac Stark triplet*, Phys. Rev. Lett. **80**, 4733 (1998).

- [43] A. Hayat, C. Lange, L. A. Rozema, A. Darabi, H. M. van Driel, A. M. Steinberg, B. Nelsen, D. W. Snoke, L. N. Pfeiffer, and K. W. West, *Dynamic Stark effect in strongly coupled microcavity exciton polaritons*, Phys. Rev. Lett. **109**, 033605 (2012).
- [44] J. F. Dynes, M. D. Frogley, M. Beck, J. Faist, and C. C. Phillips, *ac Stark splitting and quantum interference with intersubband transitions in quantum wells*, Phys. Rev. Lett. **94**, 157403 (2005).
- [45] M. D. Frogley, J. F. Dynes, M. Beck, J. Faist, and C. C. Phillips, *Gain without inversion in semiconductor nanostructures*, Nature Mater. **5**, 175 (2006).
- [46] B. M. Garraway, *The Dicke model in quantum optics: Dicke model revisited*, Philosophical Transactions of the Royal Society of London A: Mathematical, Physical and Engineering Sciences **369**, 1137 (2011), <http://rsta.royalsocietypublishing.org/content/369/1939/1137.full.pdf>.
- [47] M. Gross and S. Haroche, *Superradiance: An essay on the theory of collective spontaneous emission*, Phys. Rep. **93**, 301 (1982).
- [48] L. Mandel and E. Wolf, *Optical coherence and quantum optics* (Cambridge University Press, Cambridge, 1995).
- [49] R. Bonifacio, P. Schwendimann, and F. Haake, *Quantum statistical theory of superradiance. I*, Phys. Rev. A **4**, 302 (1971).
- [50] M. O. Scully and M. S. Zubairy, *Quantum optics* (Cambridge University Press, Cambridge, 1997).
- [51] M. Fox, *Quantum Optics: An Introduction* (Oxford University Press, Oxford, 2006).
- [52] H. J. Carmichael, *Statistical Methods in Quantum Optics 2: Non-Classical Fields* (Springer-Verlag, Berlin, Heidelberg, 2008).
- [53] R. Bonifacio (Ed.), *Dissipative systems in quantum optics: Resonance fluorescence, optical bistability, superfluorescence*, Vol. 1 (Springer-Verlag, 1982).
- [54] M. Leonid I, *Superradiance and related phenomena*, Phys. Usp. **42**, 107 (1999).
- [55] T. Brandes, *Coherent and collective quantum optical effects in mesoscopic systems*, Phys. Rep. **408**, 315 (2005).
- [56] G. D. Lin and S. F. Yelin, *Superradiance: An Integrated Approach to Cooperative Effects in Various Systems - Advances in Atomic Molecular and Optical Physics* (Academic Press, 2012).
- [57] K. Cong, Q. Zhang, Y. Wang, G. T. Noe II, A. Belyanin, and J. Kono, *Dicke superradiance in solids*, J. Opt. Soc. Am. B **33**, C80 (2016).
- [58] R. H. Lehmberg, *Radiation from an N-atom system. I. General formalism*, Phys. Rev. A **2**, 883 (1970).

- [59] F. T. Arecchi and E. Courtens, *Cooperative phenomena in resonant electromagnetic propagation*, Phys. Rev. A **2**, 1730 (1970).
- [60] R. Bonifacio, P. Schwendimann, and F. Haake, *Quantum statistical theory of superradiance. II*, Phys. Rev. A **4**, 854 (1971).
- [61] N. E. Rehler and J. H. Eberly, *Superradiance*, Phys. Rev. A **3**, 1735 (1971).
- [62] G. S. Agarwal, *Master-equation approach to spontaneous emission. III. Many-body aspects of emission from two-level atoms and the effect of inhomogeneous broadening*, Phys. Rev. A **4**, 1791 (1971).
- [63] V. Degiorgio and F. Ghielmetti, *Approximate solution to the superradiance master equation*, Phys. Rev. A **4**, 2415 (1971).
- [64] C. R. Stroud, J. H. Eberly, W. L. Lama, and L. Mandel, *Superradiant effects in systems of two-level atoms*, Phys. Rev. A **5**, 1094 (1972).
- [65] F. Haake and R. J. Glauber, *Quantum statistics of superradiant pulses*, Phys. Rev. A **5**, 1457 (1972).
- [66] L. M. Narducci, C. A. Coulter, and C. M. Bowden, *Exact diffusion equation for a model for superradiant emission*, Phys. Rev. A **9**, 829 (1974).
- [67] R. Bonifacio and L. A. Lugiato, *Cooperative radiation processes in two-level systems: Superfluorescence*, Phys. Rev. A **11**, 1507 (1975).
- [68] R. J. Glauber and F. Haake, *Superradiant pulses and directed angular momentum states*, Phys. Rev. A **13**, 357 (1976).
- [69] P. Drummond and H. Carmichael, *Volterra cycles and the cooperative fluorescence critical point*, Opt. Comm. **27**, 160 (1978).
- [70] R. Bonifacio and L. A. Lugiato, *Optical bistability and cooperative effects in resonance fluorescence*, Phys. Rev. A **18**, 1129 (1978).
- [71] M. Gronchi and L. A. Lugiato, *Erratum to: Fokker-Planck equation for optical bistability*, Lett. Nuovo Cimento **23**, 593 (1978).
- [72] D. Polder, M. F. H. Schuurmans, and Q. H. F. Vrehen, *Superfluorescence: Quantum-mechanical derivation of Maxwell-Bloch description with fluctuating field source*, Phys. Rev. A **19**, 1192 (1979).
- [73] M. Schuurmans and D. Polder, *Superfluorescence and amplified spontaneous emission: A unified theory*, Phys. Lett. A **72**, 306 (1979).
- [74] Q. H. F. Vrehen, M. F. H. Schuurmans, and D. Polder, *Superfluorescence: Macroscopic quantum fluctuations in the time domain*, Nature (London) **285**, 70 (1980).
- [75] F. Haake, J. Haus, H. King, G. Schröder, and R. Glauber, *Delay-time statistics and inhomogeneous line broadening in superfluorescence*, Phys. Rev. Lett. **45**, 558 (1980).

- [76] F. Haake, J. W. Haus, H. King, G. Schröder, and R. Glauber, *Delay-time statistics of superfluorescent pulses*, Phys. Rev. A **23**, 1322 (1981).
- [77] P. D. Drummond, *Observables and moments of cooperative resonance fluorescence*, Phys. Rev. A **22**, 1179 (1980).
- [78] H. J. Carmichael, J. S. Satchell, and S. Sarkar, *Nonlinear analysis of quantum fluctuations in absorptive optical bistability*, Phys. Rev. A **34**, 3166 (1986).
- [79] S. Sarkar and J. S. Satchell, *Solution of master equations for small bistable systems*, J. Phys. A **20**, 2147 (1987).
- [80] S. Sarkar and J. S. Satchell, *Optical bistability with small numbers of atoms*, Europhys. Lett. **3**, 797 (1987).
- [81] N. Kiesel, C. Schmid, G. Tóth, E. Solano, and H. Weinfurter, *Experimental observation of four-photon entangled Dicke state with high fidelity*, Phys. Rev. Lett. **98**, 063604 (2007).
- [82] C. Thiel, J. von Zanthier, T. Bastin, E. Solano, and G. S. Agarwal, *Generation of symmetric Dicke states of remote qubits with linear optics*, Phys. Rev. Lett. **99**, 193602 (2007).
- [83] S. Campbell, M. S. Tame, and M. Paternostro, *Characterizing multipartite symmetric Dicke states under the effects of noise*, New J. Phys. **11**, 073039 (2009).
- [84] W. Wieczorek, R. Krischek, N. Kiesel, P. Michelberger, G. Tóth, and H. Weinfurter, *Experimental entanglement of a six-photon symmetric Dicke state*, Phys. Rev. Lett. **103**, 020504 (2009).
- [85] B. Lücke, J. Peise, G. Vitagliano, J. Arlt, L. Santos, G. Tóth, and C. Klempt, *Detecting multiparticle entanglement of Dicke states*, Phys. Rev. Lett. **112**, 155304 (2014).
- [86] L. Aolita, F. de Melo, and L. Davidovich, *Open-system dynamics of entanglement: A key issues review*, Rep. Prog. Phys. **78**, 042001 (2015).
- [87] J. P. Clemens and H. J. Carmichael, *Stochastic initiation of superradiance in a cavity: An approximation scheme within quantum trajectory theory*, Phys. Rev. A **65**, 023815 (2002).
- [88] M. O. Scully, *Collective Lamb shift in single photon Dicke superradiance*, Phys. Rev. Lett. **102**, 143601 (2009).
- [89] M. O. Scully and A. A. Svidzinsky, *The super of superradiance*, Science **325**, 1510 (2009).
- [90] M. O. Scully, *Single photon subradiance: Quantum control of spontaneous emission and ultrafast readout*, Phys. Rev. Lett. **115**, 243602 (2015).

- [91] P. A. Vetter, L. Wang, D.-W. Wang, and M. O. Scully, *Single photon subradiance and superradiance revisited: A group theoretic analysis of subradiant states*, Phys. Scripta **91**, 023007 (2016).
- [92] P. Longo, C. H. Keitel, and J. Evers, *Tailoring superradiance to design artificial quantum systems*, Sci. Rep. **6**, 23628 (2016).
- [93] G. L. Celardo, P. Poli, L. Lussardi, and F. Borgonovi, *Cooperative robustness to dephasing: Single-exciton superradiance in a nanoscale ring to model natural light-harvesting systems*, Phys. Rev. B **90**, 085142 (2014).
- [94] K. D. B. Higgins, S. C. Benjamin, T. M. Stace, G. J. Milburn, B. W. Lovett, and E. M. Gauger, *Superabsorption of light via quantum engineering*, Nature Commun. **5** (2014).
- [95] V. V. Temnov and U. Woggon, *Superradiance and subradiance in an inhomogeneously broadened ensemble of two-level systems coupled to a low-Q cavity*, Phys. Rev. Lett. **95**, 243602 (2005).
- [96] V. V. Temnov and U. Woggon, *Photon statistics in the cooperative spontaneous emission*, Opt. Express **17**, 5774 (2009).
- [97] V. I. Yukalov and E. P. Yukalova, *Dynamics of quantum dot superradiance*, Phys. Rev. B **81**, 075308 (2010).
- [98] P. Grünwald, G. K. G. Burau, H. Stoltz, and W. Vogel, *Superfluorescence spectra of excitons in quantum wells*, Phys. Rev. B **88**, 195308 (2013).
- [99] M. S. Malcuit, J. J. Maki, D. J. Simkin, and R. W. Boyd, *Transition from superfluorescence to amplified spontaneous emission*, Phys. Rev. Lett. **59**, 1189 (1987).
- [100] J. J. Maki, M. S. Malcuit, M. G. Raymer, R. W. Boyd, and P. D. Drummond, *Influence of collisional dephasing processes on superfluorescence*, Phys. Rev. A **40**, 5135 (1989).
- [101] P. D. Drummond and M. G. Raymer, *Quantum theory of propagation of nonclassical radiation in a near-resonant medium*, Phys. Rev. A **44**, 2072 (1991).
- [102] C. M. Bowden and G. P. Agrawal, *Maxwell-Bloch formulation for semiconductors: Effects of coherent Coulomb exchange*, Phys. Rev. A **51**, 4132 (1995).
- [103] P. P. Vasil'ev, *Role of a high gain of the medium in superradiance generation and in observation of coherent effects in semiconductor lasers*, Quant. Elect. **29**, 842 (1999).
- [104] J. R. Ott, M. Wubs, P. Lodahl, N. A. Mortensen, and R. Kaiser, *Cooperative fluorescence from a strongly driven dilute cloud of atoms*, Phys. Rev. A **87**, 061801 (2013).
- [105] J.-H. Li, *Controllable optical bistability in a four-subband semiconductor quantum well system*, Phys. Rev. B **75**, 155329 (2007).

- [106] O. Kyriienko, A. V. Kavokin, and I. A. Shelykh, *Superradiant terahertz emission by dipolaritons*, Phys. Rev. Lett. **111**, 176401 (2013).
- [107] O. Kyriienko, E. A. Ostrovskaya, O. A. Egorov, I. A. Shelykh, and T. C. H. Liew, *Bistability in microcavities with incoherent optical or electrical excitation*, Phys. Rev. B **90**, 125407 (2014).
- [108] M. Amthor, T. C. H. Liew, C. Metzger, S. Brodbeck, L. Worschech, M. Kamp, I. A. Shelykh, A. V. Kavokin, C. Schneider, and S. Höfling, *Optical bistability in electrically driven polariton condensates*, Phys. Rev. B **91**, 081404 (2015).
- [109] N. Skribanowitz, I. P. Herman, J. C. MacGillivray, and M. S. Feld, *Observation of Dicke superradiance in optically pumped HF gas*, Phys. Rev. Lett. **30**, 309 (1973).
- [110] R. Florian, L. O. Schwan, and D. Schmid, *Time-resolving experiments on Dicke superfluorescence of O₂⁻ centers in KCl. Two-color superfluorescence*, Phys. Rev. A **29**, 2709 (1984).
- [111] A. F. van Loo, A. Fedorov, K. Lalumière, B. C. Sanders, A. Blais, and A. Wallraff, *Photon-mediated interactions between distant artificial atoms*, Science **342**, 1494 (2013).
- [112] J. A. Mlynek, A. A. Abdumalikov, C. Eichler, and A. Wallraff, *Observation of Dicke superradiance for two artificial atoms in a cavity with high decay rate*, Nature Commun. **5** (2014).
- [113] M. Scheibner, T. Schmidt, L. Worschech, A. Forchel, G. Bacher, T. Passow, and D. Hommel, *Superradiance of quantum dots*, Nature Phys. **3**, 106 (2007).
- [114] P. Tighineanu, R. S. Daveau, T. B. Lehmann, H. E. Beere, D. A. Ritchie, P. Lodahl, and S. Stobbe, *Single-photon superradiance from a quantum dot*, Phys. Rev. Lett. **116**, 163604 (2016).
- [115] V. V. Zheleznyakov, V. V. Kocharovski, and V. V. Kocharovski, *Polarization waves and super-radiance in active media*, Sov. Phys. Usp. **32**, 835 (1989).
- [116] A. A. Belyanin, V. V. Kocharovsky, and V. V. Kocharovsky, *Collective QED processes of electron - hole recombination and electron - positron annihilation in a strong magnetic field*, J. Eur. Opt. Soc. B **9**, 1 (1997).
- [117] A. A. Belyanin, V. V. Kocharovsky, and V. V. Kocharovsky, *Superradiant generation of femtosecond pulses in quantum-well heterostructures*, J. Eur. Opt. Soc. B **10**, L13 (1998).
- [118] Y. D. Jho, X. Wang, J. Kono, D. H. Reitze, X. Wei, A. A. Belyanin, V. V. Kocharovsky, V. V. Kocharovsky, and G. S. Solomon, *Cooperative recombination of a quantized high-density electron-hole plasma in semiconductor quantum wells*, Phys. Rev. Lett. **96**, 237401 (2006).

- [119] G. T. Noe II, J.-H. Kim, J. Lee, Y. Wang, A. K. Wojcik, S. A. McGill, D. H. Reitze, A. A. Belyanin, and J. Kono, *Giant superfluorescent bursts from a semiconductor magneto-plasma*, Nature Phys. **8**, 219 (2012).
- [120] J.-H. Kim, G. T. Noe II, S. A. McGill, Y. Wang, A. K. Wójcik, A. A. Belyanin, and J. Kono, *Fermi-edge superfluorescence from a quantum-degenerate electron-hole gas*, Sci. Rep. **3**, 3283 (2013).
- [121] J.-H. Kim, J. Lee, G. T. Noe II, Y. Wang, A. K. Wójcik, S. A. McGill, D. H. Reitze, A. A. Belyanin, and J. Kono, *Renormalized energies of superfluorescent bursts from an electron-hole magnetoplasma with high gain in $In_xGa_{1-x}As$ quantum wells*, Phys. Rev. B **87**, 045304 (2013).
- [122] Q. Zhang, T. Arikawa, E. Kato, J. L. Reno, W. Pan, J. D. Watson, M. J. Manfra, M. A. Zudov, M. Tokman, M. Erukhimova, A. Belyanin, and J. Kono, *Superradiant decay of cyclotron resonance of two-dimensional electron gases*, Phys. Rev. Lett. **113**, 047601 (2014).
- [123] T. Laurent, Y. Todorov, A. Vasanelli, A. Delteil, C. Sirtori, I. Sagnes, and G. Beaudoin, *Superradiant emission from a collective excitation in a semiconductor*, Phys. Rev. Lett. **115**, 187402 (2015).
- [124] I. Shtrichman, C. Metzner, E. Ehrenfreund, D. Gershoni, K. D. Maranowski, and A. C. Gossard, *Depolarization shift of the intersubband resonance in a quantum well with an electron-hole plasma*, Phys. Rev. B **65**, 035310 (2001).
- [125] A. A. Anappara, A. Tredicucci, F. Beltram, G. Biasiol, L. Sorba, S. De Liberato, and C. Ciuti, *Cavity polaritons from excited-subband transitions*, Appl. Phys. Lett. **91**, 231118 (2007).
- [126] G. Gunter, A. A. Anappara, J. Hees, A. Sell, G. Biasiol, L. Sorba, S. De Liberato, C. Ciuti, A. Tredicucci, A. Leitenstorfer, and R. Huber, *Sub-cycle switch-on of ultrastrong light-matter interaction*, Nature (London) **458**, 178 (2009).
- [127] F. Capasso, C. Liu, E. R. Weber, and R. K. Willardson, *Intersubband Transitions in Quantum Wells: Physics and Device Applications* (Academic Press, 1999).
- [128] D. E. Nikonov, A. Imamoglu, L. V. Butov, and H. Schmidt, *Collective intersubband excitations in quantum wells: Coulomb interaction versus subband dispersion*, Phys. Rev. Lett. **79**, 4633 (1997).
- [129] A. A. Batista and D. S. Citrin, *Rabi flopping in a two-level system with a time-dependent energy renormalization: Intersubband transitions in quantum wells*, Phys. Rev. Lett. **92**, 127404 (2004).
- [130] H. Sakaki, T. Noda, K. Hirakawa, M. Tanaka, and T. Matsusue, *Interface roughness scattering in GaAs/AlAs quantum wells*, Appl. Phys. Lett. **51**, 1934 (1987).
- [131] S. Nicolay, *Physics and applications of intersubband transitions in nitride based heterostructures*, Ph.D. thesis, IPEQ, Lausanne (2008).

- [132] T. Unuma, M. Yoshita, T. Noda, H. Sakaki, and H. Akiyama, *Intersubband absorption linewidth in GaAs quantum wells due to scattering by interface roughness, phonons, alloy disorder, and impurities*, J. Appl. Phys. **93**, 1586 (2003).
- [133] J. Faist, F. Capasso, C. Sirtori, D. L. Sivco, A. L. Hutchinson, S. N. G. Chu, and A. Y. Cho, *Measurement of the intersubband scattering rate in semiconductor quantum wells by excited state differential absorption spectroscopy*, Appl. Phys. Lett. **63**, 1354 (1993).
- [134] J. Faist, C. Sirtori, F. Capasso, L. Pfeiffer, and K. W. West, *Phonon limited intersubband lifetimes and linewidths in a two dimensional electron gas*, Appl. Phys. Lett. **64**, 872 (1994).
- [135] J. N. Heyman, K. Unterrainer, K. Craig, B. Galdrikian, M. S. Sherwin, K. Campman, P. F. Hopkins, and A. C. Gossard, *Temperature and intensity dependence of intersubband relaxation rates from photovoltage and absorption*, Phys. Rev. Lett. **74**, 2682 (1995).
- [136] K. Craig, B. Galdrikian, J. N. Heyman, A. G. Markelz, J. B. Williams, M. S. Sherwin, K. Campman, P. F. Hopkins, and A. C. Gossard, *Undressing a collective intersubband excitation in a quantum well*, Phys. Rev. Lett. **76**, 2382 (1996).
- [137] K. L. Vodopyanov, V. Chazapis, C. C. Phillips, B. Sung, and J. S. Harris, *Intersubband absorption saturation study of narrow III-V multiple quantum wells in the $\lambda=2.8\text{-}9\ \mu\text{m}$ spectral range*, Semicond. Sci. Tech. **12**, 708 (1997).
- [138] R. A. Kaindl, K. Reimann, M. Woerner, T. Elsaesser, R. Hey, and K. H. Ploog, *Homogeneous broadening and excitation-induced dephasing of intersubband transitions in a quasi-two-dimensional electron gas*, Phys. Rev. B **63**, 161308 (2001).
- [139] J. B. Williams, M. S. Sherwin, K. D. Maranowski, and A. C. Gossard, *Dissipation of intersubband plasmons in wide quantum wells*, Phys. Rev. Lett. **87**, 037401 (2001).
- [140] T. Ando, A. B. Fowler, and F. Stern, *Electronic properties of two-dimensional systems*, Rev. Mod. Phys. **54**, 437 (1982).
- [141] M. Virgilio, D. Sabbagh, M. Ortolani, L. Di Gaspare, G. Capellini, and M. De Seta, *Physical mechanisms of intersubband-absorption linewidth broadening in s-Ge/SiGe quantum wells*, Phys. Rev. B **90**, 155420 (2014).
- [142] R. Ferreira and G. Bastard, *Evaluation of some scattering times for electrons in unbiased and biased single- and multiple-quantum-well structures*, Phys. Rev. B **40**, 1074 (1989).
- [143] C. A. Ullrich and G. Vignale, *Collective intersubband transitions in quantum wells: A comparative density-functional study*, Phys. Rev. B **58**, 15756 (1998).
- [144] S. De Liberato and C. Ciuti, *Quantum theory of electron tunneling into intersubband cavity polariton states*, Phys. Rev. B **79**, 075317 (2009).

- [145] S. De Liberato and C. Ciuti, *Stimulated scattering and lasing of intersubband cavity polaritons*, Phys. Rev. Lett. **102**, 136403 (2009).
- [146] S. De Liberato and C. Ciuti, *Quantum theory of intersubband polarons*, Phys. Rev. B **85**, 125302 (2012).
- [147] S. De Liberato and C. Ciuti, *Quantum phases of a multimode bosonic field coupled to flat electronic bands*, Phys. Rev. Lett. **110**, 133603 (2013).
- [148] K. Zhao, G. Chen, B.-S. Li, and A. Shen, *Mid-infrared intersubband absorptions in ZnO/ZnMgO multiple quantum wells*, Appl. Phys. Lett. **104**, 212104 (2014), <http://dx.doi.org/10.1063/1.4880816>.
- [149] M. Virgilio, M. Ortolani, M. Teich, S. Winnerl, M. Helm, D. Sabbagh, G. Capellini, and M. De Seta, *Combined effect of electron and lattice temperatures on the long intersubband relaxation times of Ge/Si_xGe_{1-x} quantum wells*, Phys. Rev. B **89**, 045311 (2014).
- [150] M. Tonouchi, *Cutting-edge terahertz technology*, Nature Photon. **1**, 97 (2007).
- [151] L. Vicarelli, M. S. Vitiello, D. Coquillat, A. Lombardo, A. C. Ferrari, W. Knap, M. Polini, V. Pellegrini, and A. Tredicucci, *Graphene field-effect transistors as room-temperature terahertz detectors*, Nature Mater. **11**, 865 (2012).
- [152] T. Nagatsuma, G. Ducournau, and C. C. Renaud, *Advances in terahertz communications accelerated by photonics*, Nat. Photon. **10**, 371 (2016).
- [153] J. Faist, F. Capasso, D. L. Sivco, C. Sirtori, A. L. Hutchinson, and A. Y. Cho, *Quantum cascade laser*, Science **264**, 553 (1994).
- [154] R. Kohler, A. Tredicucci, F. Beltram, H. E. Beere, E. H. Linfield, A. G. Davies, D. A. Ritchie, R. C. Iotti, and F. Rossi, *Terahertz semiconductor-heterostructure laser*, Nature (London) **417**, 156 (2002).
- [155] K. V. Kavokin, M. A. Kaliteevski, R. A. Abram, A. V. Kavokin, S. Sharkova, and I. A. Shelykh, *Stimulated emission of terahertz radiation by exciton-polariton lasers*, Appl. Phys. Lett. **97** (2010).
- [156] S. De Liberato, C. Ciuti, and C. C. Phillips, *Terahertz lasing from intersubband polariton-polariton scattering in asymmetric quantum wells*, Phys. Rev. B **87**, 241304 (2013).
- [157] S. Huppert, O. Lafont, E. Baudin, J. Tignon, and R. Ferreira, *Terahertz emission from multiple-microcavity exciton-polariton lasers*, Phys. Rev. B **90**, 241302 (2014).
- [158] G. Christmann, A. Askopoulos, G. Deligeorgis, Z. Hatzopoulos, S. I. Tsintzos, P. G. Savvidis, and J. J. Baumberg, *Oriented polaritons in strongly-coupled asymmetric double quantum well microcavities*, Appl. Phys. Lett. **98**, 081111 (2011).

- [159] I. G. Savenko, I. A. Shelykh, and M. A. Kaliteevski, *Nonlinear terahertz emission in semiconductor microcavities*, Phys. Rev. Lett. **107**, 027401 (2011).
- [160] E. del Valle and A. Kavokin, *Terahertz lasing in a polariton system: Quantum theory*, Phys. Rev. B **83**, 193303 (2011).
- [161] A. V. Kavokin, I. A. Shelykh, T. Taylor, and M. M. Glazov, *Vertical cavity surface emitting terahertz laser*, Phys. Rev. Lett. **108**, 197401 (2012).
- [162] N. Shammah, C. C. Phillips, and S. De Liberato, *Terahertz emission from ac Stark-split asymmetric intersubband transitions*, Phys. Rev. B **89**, 235309 (2014).
- [163] N. Shammah and S. De Liberato, *Theory of intersubband resonance fluorescence*, Phys. Rev. B **92**, 201402 (2015).
- [164] N. Shammah, C. C. Phillips, and S. De Liberato, *Terahertz emission from asymmetric, doped quantum wells under resonant pumping*, J. Phys.: Conf. Ser. **619**, 012021 (2015).
- [165] M. Lewenstein, T. W. Mossberg, and R. J. Glauber, *Dynamical suppression of spontaneous emission*, Phys. Rev. Lett. **59**, 775 (1987).
- [166] R. Binder, S. W. Koch, M. Lindberg, N. Peyghambarian, and W. Schäfer, *Ultrafast adiabatic following in semiconductors*, Phys. Rev. Lett. **65**, 899 (1990).
- [167] A. Schülzgen, R. Binder, M. E. Donovan, M. Lindberg, K. Wundke, H. M. Gibbs, G. Khitrova, and N. Peyghambarian, *Direct observation of excitonic Rabi oscillations in semiconductors*, Phys. Rev. Lett. **82**, 2346 (1999).
- [168] A. Zrenner, E. Beham, S. Stufler, F. Findeis, M. Bichler, and G. Abstreiter, *Coherent properties of a two-level system based on a quantum-dot photodiode*, Nature (London) **418**, 612 (2002).
- [169] R. A. Kaindl, S. Lutgen, M. Woerner, T. Elsaesser, B. Nottelmann, V. M. Axt, T. Kuhn, A. Hase, and H. Künzel, *Ultrafast dephasing of coherent intersubband polarizations in a quasi-two-dimensional electron plasma*, Phys. Rev. Lett. **80**, 3575 (1998).
- [170] B. N. Murdin, W. Heiss, C. J. G. M. Langerak, S.-C. Lee, I. Galbraith, G. Strasser, E. Gornik, M. Helm, and C. R. Pidgeon, *Direct observation of the LO phonon bottleneck in wide GaAs/Al_xGa_{1-x}As quantum wells*, Phys. Rev. B **55**, 5171 (1997).
- [171] K. L. Campman, H. Schmidt, A. Imamoglu, and A. C. Gossard, *Interface roughness and alloy disorder scattering contributions to intersubband transition linewidths*, Appl. Phys. Lett. **69**, 2554 (1996).
- [172] F. J. Murphy, A. O. Bak, M. Matthews, E. Dupont, H. Amrania, and C. C. Phillips, *Linewidth-narrowing phenomena with intersubband cavity polaritons*, Phys. Rev. B **89**, 205319 (2014).

- [173] M. Geiser, F. Castellano, G. Scalari, M. Beck, L. Nevou, and J. Faist, *Ultrastrong coupling regime and plasmon polaritons in parabolic semiconductor quantum wells*, Phys. Rev. Lett. **108**, 106402 (2012).
- [174] W. Kohn, *Cyclotron resonance and de Haas-van Alphen oscillations of an interacting electron gas*, Phys. Rev. **123**, 1242 (1961).
- [175] Y. Todorov, A. M. Andrews, R. Colombelli, S. De Liberato, C. Ciuti, P. Klang, G. Strasser, and C. Sirtori, *Ultrastrong light-matter coupling regime with polariton dots*, Phys. Rev. Lett. **105**, 196402 (2010).
- [176] A. Delteil, A. Vasanelli, Y. Todorov, C. Feuillet Palma, M. Renaudat St-Jean, G. Beaudoin, I. Sagnes, and C. Sirtori, *Charge-induced coherence between intersubband plasmons in a quantum structure*, Phys. Rev. Lett. **109**, 246808 (2012).
- [177] O. Kyriienko and I. A. Shelykh, *Intersubband polaritonics revisited*, J. Nanophot. **6**, 061804 (2012).
- [178] L. Nguyen-thê, S. De Liberato, M. Bamba, and C. Ciuti, *Effective polariton-polariton interactions of cavity-embedded two-dimensional electron gases*, Phys. Rev. B **87**, 235322 (2013).
- [179] C. W. Luo, K. Reimann, M. Woerner, T. Elsaesser, R. Hey, and K. H. Ploog, *Phase-resolved nonlinear response of a two-dimensional electron gas under femtosecond intersubband excitation*, Phys. Rev. Lett. **92**, 047402 (2004).
- [180] Y. Busby, M. De Seta, G. Capellini, F. Evangelisti, M. Ortolani, M. Virgilio, G. Grossi, G. Pizzi, P. Calvani, S. Lupi, M. Nardone, G. Nicotra, and C. Spinella, *Near- and far-infrared absorption and electronic structure of Ge-SiGe multiple quantum wells*, Phys. Rev. B **82**, 205317 (2010).
- [181] S. Graf, H. Sigg, K. Köhler, and W. Bächtold, *Direct observation of depolarization shift of the intersubband resonance*, Phys. Rev. Lett. **84**, 2686 (2000).
- [182] O. V. Kibis, G. Y. Slepyan, S. A. Maksimenko, and A. Hoffmann, *Matter coupling to strong electromagnetic fields in two-level quantum systems with broken inversion symmetry*, Phys. Rev. Lett. **102**, 023601 (2009).
- [183] I. G. Savenko, O. V. Kibis, and I. A. Shelykh, *Asymmetric quantum dot in a microcavity as a nonlinear optical element*, Phys. Rev. A **85**, 053818 (2012).
- [184] D. Dini, R. Köhler, A. Tredicucci, G. Biasiol, and L. Sorba, *Microcavity polariton splitting of intersubband transitions*, Phys. Rev. Lett. **90**, 116401 (2003).
- [185] C. Ciuti, G. Bastard, and I. Carusotto, *Quantum vacuum properties of the intersubband cavity polariton field*, Phys. Rev. B **72**, 115303 (2005).
- [186] M. F. Pereira, *Intersubband antipolaritons: Microscopic approach*, Phys. Rev. B **75**, 195301 (2007).

- [187] A. A. Anappara, S. De Liberato, A. Tredicucci, C. Ciuti, G. Biasiol, L. Sorba, and F. Beltram, *Signatures of the ultrastrong light-matter coupling regime*, Phys. Rev. B **79**, 201303 (2009).
- [188] A. A. Anappara, A. Tredicucci, G. Biasiol, and L. Sorba, *Electrical control of polariton coupling in intersubband microcavities*, Appl. Phys. Lett. **87** (2005).
- [189] A. Ridolfo, M. Leib, S. Savasta, and M. J. Hartmann, *Photon blockade in the ultrastrong coupling regime*, Phys. Rev. Lett. **109**, 193602 (2012).
- [190] P. Tighineanu, M. L. Andersen, A. S. Sørensen, S. Stobbe, and P. Lodahl, *Probing electric and magnetic vacuum fluctuations with quantum dots*, Phys. Rev. Lett. **113**, 043601 (2014).
- [191] C. S. Wood, S. C. Bennett, D. Cho, B. P. Masterson, J. L. Roberts, C. E. Tanner, and C. E. Wieman, *Measurement of parity nonconservation and an anapole moment in Cesium*, Science **275**, 1759 (1997).
- [192] J. Mitroy, M. S. Safronova, and C. W. Clark, *Theory and applications of atomic and ionic polarizabilities*, J. Phys. B **43**, 202001 (2010).
- [193] L. Windholz and M. Musso, *Stark-effect investigations of the Sodium D2 line*, Phys. Rev. A **39**, 2472 (1989).
- [194] J. F. Dynes, M. D. Frogley, J. Rodger, and C. C. Phillips, *Optically mediated coherent population trapping in asymmetric semiconductor quantum wells*, Phys. Rev. B **72**, 085323 (2005).
- [195] A. Kavokin, J. J. Baumberg, G. Malpuech, and F. P. Laussy, *Microcavities* (Oxford University Press, Oxford, 2007).
- [196] K. Kakazu and Y. S. Kim, *Quantization of electromagnetic fields in cavities and spontaneous emission*, Phys. Rev. A **50**, 1830 (1994).
- [197] Y. Todorov, I. Sagnes, I. Abram, and C. Minot, *Purcell enhancement of spontaneous emission from quantum cascades inside mirror-grating metal cavities at THz frequencies*, Phys. Rev. Lett. **99**, 223603 (2007).
- [198] C. Feuillet-Palma, Y. Todorov, R. Steed, A. Vasanelli, G. Biasiol, L. Sorba, and C. Sirtori, *Extremely sub-wavelength THz metal-dielectric wire microcavities*, Opt. Express **20**, 29121 (2012).
- [199] J. D. Caldwell, O. J. Glembocki, Y. Francescato, N. Sharac, V. Giannini, F. J. Bezares, J. P. Long, J. C. Owrusky, I. Vurgaftman, J. G. Tischler, V. D. Wheeler, N. D. Bassim, L. M. Shirey, R. Kasica, and S. A. Maier, *Low-loss, extreme subdiffraction photon confinement via Silicon Carbide localized surface phonon polariton resonators*, Nano Lett. **13**, 3690 (2013).
- [200] M. B. Plenio and S. F. Huelga, *Dephasing-assisted transport: Quantum networks and biomolecules*, New J. Phys. **10**, 113019 (2008).

- [201] M. Delanty, S. Rebić, and J. Twamley, *Superradiance and phase multistability in circuit quantum electrodynamics*, New J. Phys. **13**, 053032 (2011).
- [202] R. Friedberg, S. Hartmann, and J. Manassah, *Limited superradiant damping of small samples*, Phys. Lett. A **40**, 365 (1972).
- [203] R. Friedberg and S. R. Hartmann, *Temporal evolution of superradiance in a small sphere*, Phys. Rev. A **10**, 1728 (1974).
- [204] C. T. Lee, *Transition from incoherence to coherence in the spontaneous emission of extended systems*, Phys. Rev. A **13**, 1657 (1976).
- [205] H. Nha and H. J. Carmichael, *Stochastic initiation of superradiance in a cavity: Decoherence through pseudospin exchange*, Phys. Rev. A **66**, 053806 (2002).
- [206] W. Guerin, M. O. Araújo, and R. Kaiser, *Subradiance in a large cloud of cold atoms*, Phys. Rev. Lett. **116**, 083601 (2016).
- [207] G. Milburn and P. Alsing, Directions in quantum optics: A collection of papers dedicated to the memory of Dan Walls, (Springer, Berlin, Heidelberg, 2001) Chap. Quantum Phase Transitions in a Linear Ion Trap, pp. 303–312.
- [208] C. Emery, *Dark-states in multi-mode multi-atom Jaynes–Cummings systems*, J. Phys. B **46**, 224008 (2013).
- [209] E. A. Zibik, T. Grange, B. A. Carpenter, N. E. Porter, R. Ferreira, G. Bastard, D. Stehr, S. Winnerl, M. Helm, H. Y. Liu, M. S. Skolnick, and L. R. Wilson, *Long lifetimes of quantum-dot intersublevel transitions in the terahertz range*, Nat. Mater. **8**, 803 (2009).
- [210] H. Bruus and K. Flensberg, *Many-body quantum theory in condensed matter physics: An introduction* (Oxford University Press, Oxford, 2004).
- [211] K. E. Miller, D. Krause, and L. R. Hunter, *Precise measurement of the Stark shift of the Rubidium and Potassium D1 lines*, Phys. Rev. A **49**, 5128 (1994).
- [212] B. Arora, M. S. Safranova, and C. W. Clark, *Magic wavelengths for the np-ns transitions in alkali-metal atoms*, Phys. Rev. A **76**, 052509 (2007).
- [213] B. Arora, M. S. Safranova, and C. W. Clark, *Determination of electric-dipole matrix elements in K and Rb from Stark shift measurements*, Phys. Rev. A **76**, 052516 (2007).
- [214] J. Ye, D. W. Vernoy, and H. J. Kimble, *Trapping of single atoms in cavity QED*, Phys. Rev. Lett. **83**, 4987 (1999).